

2024-01-17

# Influence of Development on Peri-urban Headwater Streams in Calgary, Alberta

Johnson, Samuel Douglas

---

Johnson, S. D. (2024). Influence of development on peri-urban headwater streams in Calgary, Alberta (Master's thesis, University of Calgary, Calgary, Canada). Retrieved from <https://prism.ucalgary.ca.https://hdl.handle.net/1880/118013>

*Downloaded from PRISM Repository, University of Calgary*

UNIVERSITY OF CALGARY

Influence of Development on Peri-urban Headwater Streams in Calgary, Alberta

by

Samuel Douglas Johnson

A THESIS

SUBMITTED TO THE FACULTY OF GRADUATE STUDIES  
IN PARTIAL FULFILMENT OF THE REQUIREMENTS FOR THE  
DEGREE OF MASTER OF SCIENCE

GRADUATE PROGRAM IN GEOSCIENCE

CALGARY, ALBERTA

JANUARY, 2024

© Samuel Douglas Johnson 2024

## **Abstract**

The natural connection between surface water and groundwater is inevitably altered by urban development. However, the degree of alteration is dependent on the physical and climatic characteristics of a watershed as well as the development characteristics. The goal of this study was to compare a developed and an undeveloped headwater catchment in Calgary, Alberta, to understand the influence of urbanization on streamflow response to precipitation, groundwater contributions to streamflow, and the spatial and temporal variability of streamflow in a low relief, semi-arid landscape. Hydrometric measurements of streamflow, groundwater, and precipitation were used in conjunction with electrical conductivity and stable water isotopes to compare streamflow regimes and assess the impact of development. The developed Sage Hill ravine (SHR) stream had significantly smaller runoff ratios and smaller maximum event water fractions than the undeveloped Glacier Ridge ravine (GRR) stream, which was attributed to the capture and re-routing of urban stormwater away from the stream. Groundwater was shown to be an essential source of flow to both streams. Baseflow separation and stable water isotopes showed that 95% and 86% of the cumulative streamflow volume in SHR and GRR, respectively, was from baseflow sourced from shallow groundwater. Additionally, spatial and temporal differences in streamflow between SHR and GRR were attributed to the geologic heterogeneity of the shallow subsurface. Although this study did not directly identify cause-and-effect relationships of streamflow characteristics and urban development, it did identify the importance of effective area, groundwater, and geologic heterogeneity on the generation of streamflow. These findings will be useful for improving our understanding of how future development might impact streamflow, informing urban water resource management, and protecting valuable urban ecosystems.

## **Preface**

This thesis is an original, unpublished, independent work by the author, Samuel Johnson.

## Acknowledgments

First and foremost, I would like to thank my supervisor Dr. Edwin Cey. Thank you for the opportunity to be a researcher, for supporting me throughout this process, and for providing me with excellent mentorship. I am forever grateful for everything you've done for me.

Thank you to Dr. Masaki Hayashi for all your support during this project as well. I'm grateful for the opportunity to work with you and your lab group. Thank you for providing valuable mentorship and including me in lab activities.

Thank you to Bert van Duin and the City of Calgary for supporting this project and for providing guidance and resources along the way. Thank you Alberta Innovates for funding this project and many others like it. Thank you to Anthem, for permission to access Glacier Ridge and install monitoring equipment. Thank you to Dean Tuttle and Stantec for allowing us to safely access the Glacier Ridge site and for providing updates on the construction at the site.

Sean, it was a pleasure to share the grad school experience with you. Thank you for the long hours in the field and being there every step of the way. Thank you to Glenn, Sama, Teddi, Lucas, Stu, Blair, Jess, and Dan for the friendship, the amazing office banter, and help in the field. Special thank you to Quinn. The field work for this project would not have been possible without you. Thank you to Sophie and Eric for your help in the field and lab as well.

Thank you to Stephen Taylor and Michael Nightingale for your help with the water quality analysis and all the hard work you do.

Finally, I'd like to thank Taylor for being my rock. Thank you for your patience and for supporting me on this journey.

# Table of Contents

<b>Abstract.....</b>	<b>ii</b>
<b>Preface.....</b>	<b>iii</b>
<b>Acknowledgments .....</b>	<b>iv</b>
<b>Table of Contents .....</b>	<b>v</b>
<b>List of Tables .....</b>	<b>vii</b>
<b>List of Figures.....</b>	<b>viii</b>
<b>List of Abbreviations .....</b>	<b>x</b>
<b>Chapter 1: Introduction .....</b>	<b>1</b>
1.1 Motivation .....	1
1.2 Urban Streamflow .....	4
1.3 Streamflow Contributions .....	6
1.3.1 Seasonal Flow.....	6
1.3.2 Event Flow.....	11
1.4 Objectives and Study Design .....	15
1.5 Thesis Organization .....	17
<b>Chapter 2: Influence of Development on Peri-urban Streams in Calgary, Alberta.....</b>	<b>18</b>
2.1 Introduction.....	18
2.2 Site Description.....	20
2.3 Methods.....	26
2.3.1 Precipitation Monitoring .....	26
2.3.2 Groundwater Monitoring.....	27
2.3.3 Streamflow Monitoring .....	29
2.3.4 Differential Gauging and Flow Duration Curves .....	31
2.3.5 Streamflow Electrical Conductivity .....	32
2.3.6 Water Sampling.....	33

2.3.7 Hydrograph Separation.....	34
2.4 Results and Discussion.....	38
2.4.1 Streamflow Season 2022 .....	38
2.4.2 Streamflow Response to Precipitation Events.....	40
2.4.2.1 Cumulative Streamflow, Peak Flow, and Runoff Ratios.....	40
2.4.2.2 Tracer-based Hydrograph Separation .....	48
2.4.3 Seasonal Streamflow Regime.....	55
2.4.3.1 Surface Water – Groundwater Relationship.....	55
2.4.3.2 Spatial and Temporal Streamflow Characteristics.....	66
2.5 Conclusions.....	75
<b>Chapter 3: Conclusion and Recommendations.....</b>	<b>78</b>
3.1 Summary and Implications .....	78
3.2 Limitations .....	80
3.3 Future Work .....	83
<b>References.....</b>	<b>87</b>
<b>Appendix A: Catchment Delineation .....</b>	<b>96</b>
<b>Appendix B: Site Photographs.....</b>	<b>98</b>
<b>Appendix C: Borehole Logs and Well Completions .....</b>	<b>102</b>
<b>Appendix D: Hydraulic Conductivity Tests .....</b>	<b>109</b>
<b>Appendix E: Rating Curves .....</b>	<b>112</b>
<b>Appendix F: Stable Water Isotope Sampling.....</b>	<b>117</b>
<b>Appendix G: Event Breakdown 2022.....</b>	<b>118</b>
<b>Appendix H: Hydrograph separation tracer comparison.....</b>	<b>124</b>

## List of Tables

Table 2.1. Summary of catchment properties used in this study. ....	25
Table 2.2. Summary of well lithologies and hydraulic conductivity (K). ....	28
Table 2.3. Monthly breakdown of the total monthly precipitation for each catchment. SHR-TB and GRR-TB not deployed until April 7, 2022, however no significant precipitation occurred between April 1 and April 7. ....	40
Table 2.4. Hydrograph separation values for events 27 and 28. ....	50
Table 2.5. Summary of stable water isotope analysis. n = number of samples. SD = Standard deviation. ....	63

# List of Figures

- Figure 1.1. Map of the study area showing the location of the Sage Hill ravine (SHR) catchment, the Glacier Ridge ravine (GRR) catchment, and the West Nose Creek (WNC) catchment relative to northwest Calgary (red line) and the regional topography. The inset maps in the top-left show the location of the study area in relation to the City of Calgary and West Nose Creek. The inset map of Alberta (AB) shows the position of Calgary (red dot) relative to the northern prairie pothole region. mASL: meters above sea level. .... 3
- Figure 1.2. Schematic representation of hydrograph separation using graphical and tracer-based techniques. a) Stream discharge ( $Q_s$ ) is separated into flow associated with precipitation events (quick flow) and baseflow ( $Q_b$ ) using a straight-line graphical method to estimate seasonal baseflow contributions. b) Comparison of graphical and tracer-based hydrograph separation of event streamflow with relevant parameters used in this study. .... 8
- Figure 2.1. Map of SHR (blue) and GRR (orange) relative to WNC (green) and City of Calgary (red). Main map and inset maps show the locations of monitoring equipment, important groundwater springs, and relevant land use for SHR and GRR. Land use is representative of conditions circa July 2022 and was delineated manually by the author using satellite imagery (ESRI Inc., 2021). The top right hand corner map shows SHR, GRR, and WNC relative to the regional topography. mASL: meters above sea level. .... 24
- Figure 2.2. Hydrograph and daily precipitation for SHR-SW5, GRR-SW4, and WNC in 2022. Daily precipitation was recorded for each individual catchment at SHR-TB, GRR-TB, and SpH-TB. Spring is defined by the months of April-May, Early-summer is June, Late-summer is July-August, and Fall is September-October. Precipitation data starts on April 7, due to instrument deployment timing. .... 39
- Figure 2.3. Streamflow response to rainfall events at SHR-SW5, GRR-SW4, and WNC in 2022. a) Cumulative streamflow ( $V_s$ ) vs. total event precipitation ( $P_E$ ), b) Peak flow ( $Q_{peak}$ ) vs.  $P_E$ . Dashed lines are the best fit lines for each data set and are described with a linear equation for each watershed. Each data set has a magnified plot to better represent smaller events. Note that the magnified plots have differing axis limits. .... 42
- Figure 2.4. Comparison of runoff ratios from SHR-SW5, GRR-SW4, and WNC for 2022. Each runoff ratio was calculated using the contributing area to the stream gauging station used in this analysis. .... 45
- Figure 2.5. Hydrograph separation in SHR and GRR using EC for events 27 and 28. a) Hydrograph separation for SHR-SW5. b) Hydrograph separation for GRR-SW4. c) 15-minute EC measurements for events 27 and 28 period. The colored portions of the hydrograph denote the contributions from event water. .... 49

- Figure 2.6. Maximum event water fraction ( $MEF$ ) contributing to streamflow relative to total event precipitation ( $P_E$ ) for 2022. The equations and coefficients of determination describe the linear best fit lines (dashed lines) for each catchment. The red inset within plot a) denotes the limits of the zoomed in plot labelled b). ..... 51
- Figure 2.7. Comparison of daily average stream discharge ( $Q_s$ ) to daily average groundwater level fluctuations. a) Daily average baseflow ( $Q_b$ ) (solid lines) separated from the daily average streamflow ( $Q_s$ ) (dotted lines) for SHR and GRR in 2022. b) Daily average local groundwater levels from shallow wells (light colors) in the glacial overburden and deep wells (dark colors) completed at the overburden-bedrock interface. Groundwater levels are reported relative to an arbitrary datum to compare relative fluctuations. .... 56
- Figure 2.8. Streamflow-groundwater relationship in July 2022 for a) SHR-SW5 vs SHR-MW2B and b) GRR-SW4 vs. GRR-MW3. Streamflow is taken from the most downstream gauging station in each catchment and groundwater levels are from shallow monitoring wells near groundwater discharge areas in the drainages. Groundwater levels are reported relative to arbitrary values. Small, color-coded arrows indicate timing of E23 data points. .... 59
- Figure 2.9. Comparison of stable water isotope values from surface water (SW) and groundwater (GW) in SHR and GRR. Samples were taken over a timespan from June 2021 to October 2022. The local meteoric water line (LMWL) and mean annual precipitation value is from Peng *et al.* (2004). The average composition of groundwater recharge for WNC is from Hayashi and Farrow (2014). The LMWL from Hayashi & Farrow (2014) is  $\delta^2H = 7.74 \delta^{18}O - 0.06$ . One GRR SW outlier sample ( $\delta^{18}O = -18.6\text{‰}$ ,  $\delta^2H = -147\text{‰}$ ) was not included in the linear best fit line. .... 62
- Figure 2.10. Differential gauging plot for SHR and GRR in 2022. Each data point is the mean of the daily flows for a 9–11-day period representative of the Spring, Early-summer, Late-summer, and Fall phases of the flow season. The dotted lines are straight line interpretations of the gaining and losing fluxes and represent the net change in streamflow for a given reach. The exact locations of the gaining and losing fluxes require higher resolution streamflow measurements. Error bars are the standard deviation of the daily average flows used to calculate the mean for that given period. .... 68
- Figure 2.11. Flow duration curve for each streamflow monitoring station within the study sites. All flow duration curves use 15-minute discharge data for the time period of 2022-05-13 to 2022-10-28. \*SHR-SW1 is from 2022-05-13 to 2022-10-05 due to data logger issues. .... 74

## List of Abbreviations

Abbreviation	Definition
SHR	Sage Hill ravine
GRR	Glacier Ridge ravine
WNC	West Nose Creek watershed
SpH	Spy Hill
ET	Evapotranspiration
FDC	Flow duration curve
EC	Electrical conductivity
SW	Surface water
GW	Groundwater
MW	Groundwater monitoring well
TB	Tipping bucket rain gauge
$Q_s$	Stream discharge
$Q_b$	Baseflow discharge
$Q_e$	Event water discharge
$Q_p$	Pre-event water discharge
$C_s$	Stream water tracer concentration
$C_e$	Event water tracer concentration
$C_p$	Pre-event water tracer concentration
$MEF$	Maximum event water fraction
$P_E$	Total event precipitation
$V_s$	Cumulative streamflow discharge
$V_p$	Cumulative pre-event discharge
$V_e$	Cumulative event water discharge
$Q_{peak}$	Peak flow discharge

# Chapter 1: Introduction

## 1.1 Motivation

Urban sprawl and mounting pressure on freshwater resources has increased the need to further understand how streamflow is influenced by the urban environment. Alterations to the land surface and shallow subsurface by urban development have been shown to impact the conveyance of surface and subsurface water to streams (Oswald *et al.*, 2023). Impermeable surfaces, subsurface infrastructure, and landscape modifications alter the connection between surface water and groundwater, leading to changes in storm response and baseflow behavior (Smith *et al.*, 2013; Bhaskar *et al.*, 2016). Thus, urban development has impacts on both the high flows during precipitation events and sustained streamflow during dry periods, which has implications for evaluating flood risks and drought resiliency of streams. Urban streams sustain critical urban ecosystems and provide value to communities in the form of recreation space and aesthetic appeal. Therefore, it is important to further understand how development influences surface and subsurface streamflow generation to promote the natural hydrologic function of urban streams and protect these areas from the negative effects of increased flooding and drought, such as water quantity and quality degradation, ecosystem degradation, and increased erosional potential (Paul and Meyer, 2001).

Development of small headwater catchments in northwest Calgary, Alberta has spurred interest in streamflow generating processes in order to protect valuable urban greenspace and surrounding urban infrastructure. These catchments are located on the western edge of the Canadian prairies within city limits (Figure 1.1) and contain small streams flowing through shallow ravines that vary in permanency from intermittent to perennial. The ravines that these

streams flow through provide valuable habitat for flora and fauna, and greenspace for residents to recreate. In order to understand the influence of development on these catchments, both the surface and subsurface contributions to streamflow need to be evaluated. Previous research in this region has identified the semi-arid climate and glacially deposited terrain as important controls on hydrologic processes (van der Kamp and Hayashi, 2009; Hayashi and Farrow, 2014), however the influence of urban development on these prairie ravine streams is not well understood. In addition, urban hydrology research in semi-arid climates is underrepresented in the literature (Jefferson *et al.*, 2017; McPhillips *et al.*, 2019). The low relief undulating topography of this region coupled with the semi-arid climate create a unique situation to evaluate the influence of development on streamflow response to precipitation, and groundwater contributions to streamflow.

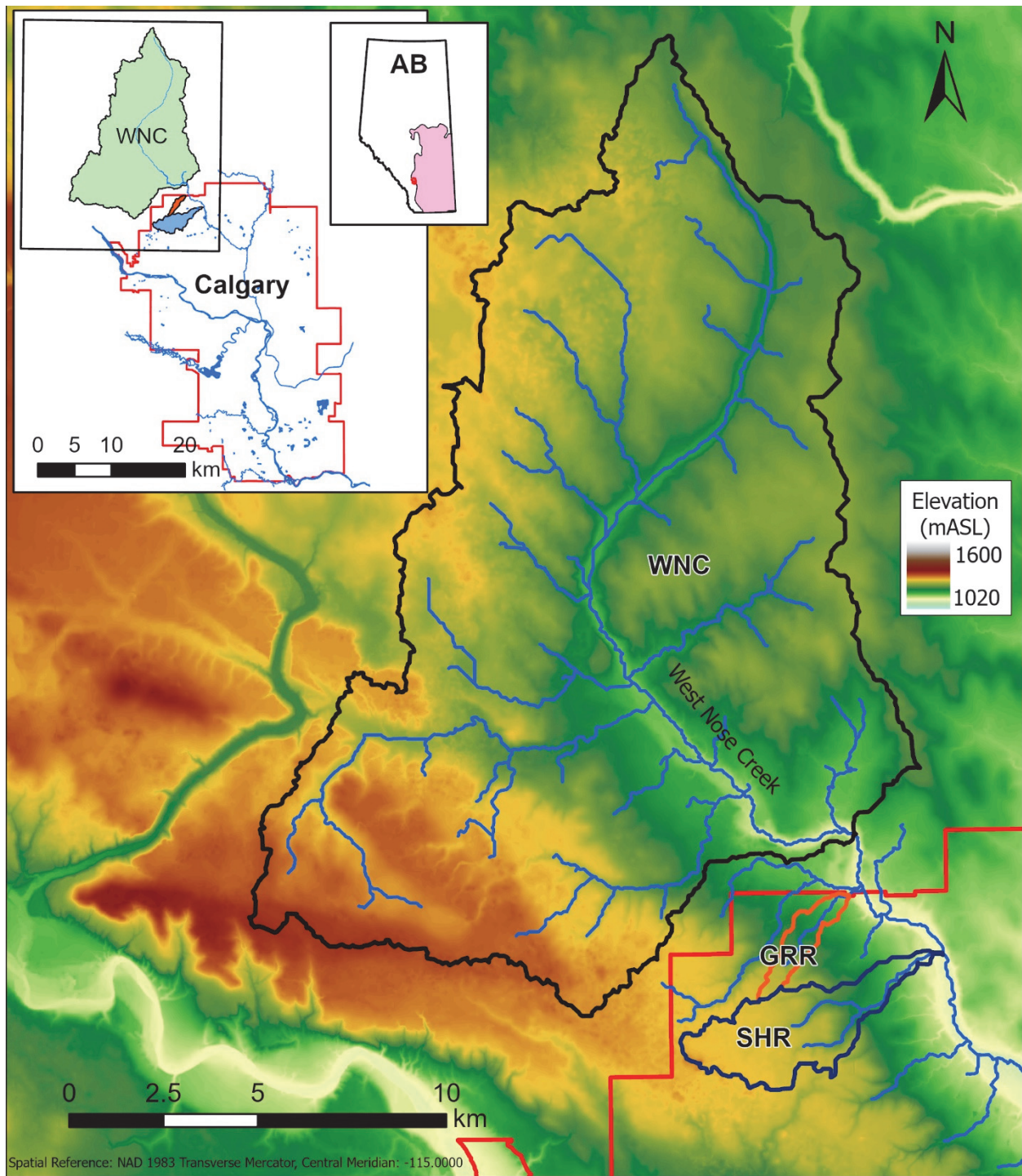


Figure 1.1. Map of the study area showing the location of the Sage Hill ravine (SHR) catchment, the Glacier Ridge ravine (GRR) catchment, and the West Nose Creek (WNC) catchment relative to northwest Calgary (red line) and the regional topography. The inset maps in the top-left show the location of the study area in relation to the City of Calgary and West Nose Creek. The inset map of Alberta (AB) shows the position of Calgary (red dot) relative to the northern prairie pothole region. mASL: meters above sea level.

## 1.2 Urban Streamflow

The urban landscape is a complex environment that inevitably alters naturally occurring hydrologic processes governing streamflow. Understanding the impacted hydrologic processes and the magnitude of those impacts has important implications for water resource management, healthy ecosystems, and hazard assessment (Walsh *et al.*, 2012; Bhaskar *et al.*, 2016). The introduction of impermeable surfaces, such as rooftops and pavement, removal of vegetation, alteration of soils and topography, and re-routing of stormwater are known to result in altered flow paths and reduced infiltration (Leopold, 1968; Oswald *et al.*, 2023). Among other consequences, these alterations are known to lead to higher and more rapid stormflow responses, also known as “flashiness”, altered baseflow, and reduced water quality in streams, which has been described as “urban stream syndrome” (Meyer *et al.*, 2005; Walsh *et al.*, 2005). Urban stream syndrome is generally thought to occur when the impervious surface cover in a catchment is directly connected to receiving streams via highly efficient stormwater systems (Walsh *et al.*, 2005). However, not all impervious surfaces are equally connected to stormwater systems and not all streams receive stormwater directly from stormwater outfalls (Sulam, 1979; Booth and Jackson, 1997; Sultana *et al.*, 2020; Ariano and Oswald, 2022a). The variability in stormwater system design and the subsequent variability in hydrologic responses (Smith *et al.*, 2013) highlights the continued need to evaluate the hydrologic processes contributing to streamflow in urban environments.

In addition to variable urban landscape design, the physical and climatic characteristics of a catchment determine the naturally occurring streamflow generating processes, which will in turn impact how streamflow processes respond to urban development (Hopkins *et al.*, 2015; Bhaskar *et al.*, 2016; Ross *et al.*, 2019). Low relief catchment topography and highly permeable soils have

been shown to reduce stormflow flashiness in urbanized catchments relative to steeply sloping and lower permeable counterparts (Hopkins *et al.*, 2015). McPhillips *et al.* (2019) also showed that in arid Arizona, stream flashiness decreased as development increased compared to streams in humid environments. In terms of baseflow, not only did Bhaskar *et al.* (2016) observe an overall rise in baseflow in response to urban development in Perth, Australia and an overall decrease in baseflow in Baltimore, USA, they also observed that baseflow response to urban development varied spatially within each catchment due to water-table height, geologic substrate, and subsurface infrastructure. Understanding and assessing the spatially variable characteristics of a catchment is important for identifying areas of high vulnerability, reducing damage to ecosystems and infrastructure, and planning mitigation strategies (Bhaskar *et al.*, 2016).

Arid and semi-arid landscapes in particular are typically not well represented in urban hydrology, and the influence of urban development on hydrologic processes appears to be difficult to predict (Jefferson *et al.*, 2017; McPhillips *et al.*, 2019). One such landscape is the cold, semi-arid Canadian prairies that have unique conditions for evaluating urban streamflow processes. The low relief, undulating terrain that is characteristic of the prairie landscape (Ehsanzadeh *et al.*, 2012; Hayashi and Farrow, 2014) can form portions of a catchment that are unconnected from the main streamflow (Fang *et al.*, 2007). Therefore, there are areas within catchments on the Canadian prairies that do not contribute to the production of runoff because they are isolated from the catchment outlet and drain internally. The portion of the catchment that does facilitate streamflow generation during a precipitation event is known as the effective drainage area (Ehsanzadeh *et al.*, 2012; Shaw *et al.*, 2013). The effective drainage area will be smaller than the total drainage area under natural conditions, but is dynamic and may evolve as a function of rainfall and antecedent moisture on event and seasonal time-scales (Shaw *et al.*, 2013). The dynamic nature of contributing

areas in this undulating landscape make this a challenging environment to determine contributions to streamflow (Ehsanzadeh *et al.*, 2012; Ross *et al.*, 2017). With the addition of development, the drainage characteristics of a catchment are inevitably altered by changing topography, impervious surfaces, and stormwater management systems. In response, the effective area of a catchment could increase if development connects previously unconnected areas of the catchment to the stream, or the effective area could decrease if development results in higher capture and routing of stormwater away from the catchment outlet. Therefore, it is important to determine if and how the effective drainage area of a catchment is altered to better understand the hydrologic response to development.

## **1.3 Streamflow Contributions**

### **1.3.1 Seasonal Flow**

In the absence of precipitation, streamflow is sustained by its baseflow, which is defined by Hall (1968) as “the proportion of flow that comes from groundwater storage or other delayed sources.” For the purposes of this discussion, groundwater is defined as all water derived from the saturated zone below the water table (Freeze and Cherry, 1979), and all waters below ground surface will be referred to as subsurface water. Other delayed sources include, but are not limited to, lakes, shallow subsurface storage, and glacial melt; however, groundwater and shallow subsurface water are generally considered the main contributors to baseflow (Smakhtin, 2001; Price, 2011). A hydrograph is a representation of stream discharge as a function of time, and on a seasonal scale, the baseflow portion of the hydrograph can be separated from the total flow rate (Arnold *et al.*, 1995). The goal of baseflow separation is to separate the portion of streamflow generated by surface and subsurface processes responding rapidly to precipitation inputs, known

as “quick flow,” from the slower baseflow portion released from storage (Figure 1.2a). The result is a representation of the long-term streamflow regime associated with the discharge, recharge, and storage properties of the catchment (Smakhtin, 2001). Therefore, baseflow can provide insight into the groundwater contributions to streamflow as well as the processes that impact discharge, recharge, and storage, such as evapotranspiration (ET) and groundwater extraction (Wittenberg, 2003). Hayashi & Farrow (2014) used baseflow to understand the meteorological conditions controlling recharge and how long-term shifts in precipitation could impact the amount of groundwater available for extraction. In an urban environment, characterizing baseflow may be a useful tool for understanding how impervious cover and subsurface infrastructure may impact groundwater contributions to streamflow (Hamel *et al.*, 2013).

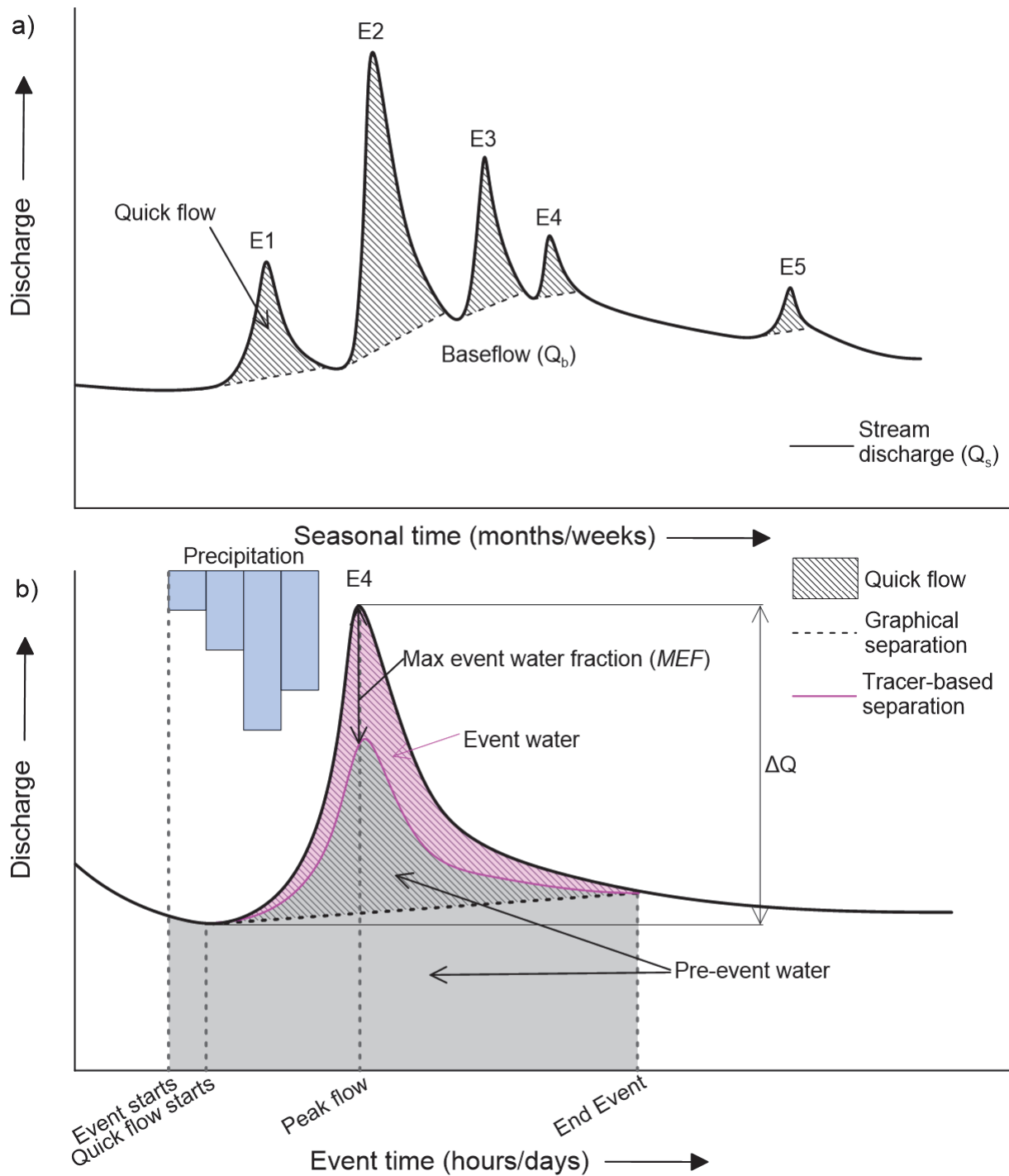


Figure 1.2. Schematic representation of hydrograph separation using graphical and tracer-based techniques. a) Stream discharge ( $Q_s$ ) is separated into flow associated with precipitation events (quick flow) and baseflow ( $Q_b$ ) using a straight-line graphical method to estimate seasonal baseflow contributions. b) Comparison of graphical and tracer-based hydrograph separation of event streamflow with relevant parameters used in this study.

Stable water isotopes  $^{18}\text{O}/^{16}\text{O}$  and  $^2\text{H}/^1\text{H}$  are useful tools to further understand the recharge processes within a catchment by tracing the source of groundwater discharge. Due to isotopic fractionation, the isotopic signature of precipitation varies depending on temperature, elevation, and latitude, and the isotopic signature of surface water can be altered by evaporative processes (Clark and Fritz, 1997). Since groundwater is a mix of precipitation and surface water that percolates through the vadose zone to the water table, the isotopic signature of groundwater can be used to trace the contributing sources of groundwater recharge (Clark and Fritz, 1997). The climatic or physical characteristics of a catchment, such as undulating terrain, may favor recharge during a particular season, which is then reflected in the isotopic signature of the groundwater (Maule *et al.*, 1994; Hayashi and Farrow, 2014). In an urban environment, impervious cover and altered vegetation could influence infiltration, and subsurface infrastructure could reduce mixing of subsurface water and introduce water from leaky pipes (Bonneau *et al.*, 2018). Furthermore, the groundwater recharge area for a catchment is often different than the catchment boundaries determined using topography (Winter *et al.*, 2003), which makes understanding the main sources of groundwater recharge important for identifying important recharge areas.

Another way to characterize streamflow on a seasonal scale is by using a flow duration curve (FDC). An FDC is a statistical representation of streamflow over a given time-frame that does not consider the sequence of flow (Searcy, 1959). Stream discharge is plotted relative to its exceedance probability, which is the frequency, in percent, during a specified time span that a given magnitude of discharge was met or exceeded (Searcy, 1959; Vogel and Fennessey, 1994). Because of its simplicity, FDCs have been used in hydrology as a graphical analysis tool for engineering purposes and water resource management for nearly a century (Searcy, 1959; Vogel and Fennessey, 1995). The guiding principle of FDCs is that a curve with a long shallow slope

represents a stable flow regime, as opposed to a steep slope that represents a highly variable flow regime (Searcy, 1959). Each curve is a representation of the upstream conditions influencing streamflow, such as geology, topography, vegetation, climate, etc. (Searcy, 1959; Cheng *et al.*, 2012). For example, groundwater contributions from high hydraulic conductivity aquifers tend to produce flat curves, and streams associated with low hydraulic conductivity substrate tend to produce steeply sloping curves (Winter, 2007). FDCs have also been used to understand regional streamflow regimes (Ye *et al.*, 2012), the impacts of deforestation (Brown *et al.*, 2013), and urban stormwater management (Petrucci *et al.*, 2014). Petrucci *et al.* (2014) modelled different stormwater management scenarios and used FDCs to compare the resulting flow regimes of receiving waters. FDCs may also prove to be useful for comparing the flow regimes of urban and non-urban watersheds. Despite their utility, FDCs are a simplification of streamflow data, and only provide insight into the integrated properties of flow upstream from a given gauging location (Vogel and Fennessey, 1995). FDCs need to be used in conjunction with other data to understand the spatial variation of streamflow along a stream's length.

Certain reaches of a stream may gain water in the form of groundwater discharge, or lose flow to groundwater, and these relationships can vary both spatially and temporally depending on the geologic substrate, topography, ET, and the rise and fall of groundwater levels within a given system (Anderson and Burt, 1978; Winter *et al.*, 1998; Payn *et al.*, 2012). The interconnection between groundwater and surface water means that changes to the factors that influence groundwater processes also impact streamflow and vice-versa (Winter *et al.*, 1998; Price, 2011). Differential gauging is a technique that can delineate gaining and losing reaches of stream to help understand the spatial and temporal variability of a streamflow regime. Differential gauging, also known as a “seepage run”, is a calculation of the net difference in streamflow between two stream

gauging locations that define a reach or section of a stream (Rosenberry and LaBaugh, 2008). The gains and losses for defined reaches of stream can then be quantified, and the controlling processes may be identified. Groundwater discharge is usually the main natural process contributing to streamflow gains, which is strongly linked to the geologic characteristics of a catchment (Smakhtin, 2001). Payn *et al.* (2012) used differential gauging to identify multiple structural mechanisms controlling the spatial patterns of baseflow generation, such as bedrock transitions, valley floor substrate, and large-scale hydraulic gradients. Streamflow losses, also known as transmission losses, are generally attributed to direct evaporation from the stream surface and infiltration into surrounding substrate (McMahon and Nathan, 2021), which can have important implications in terms of aquifer recharge and water management (Ruehl *et al.*, 2006). When differential gauging is performed at different times of the year, the temporal variability of gaining and losing reaches can be characterized, such as the impact of irrigation on groundwater gradients and subsequent streamflow gains (Donato, 1998). In an urban catchment, differential gauging may help identify both natural and anthropogenic influences on streamflow gains and losses. Understanding where the main contributions to streamflow occur in an urban catchment is important for identifying sensitive or vulnerable areas, and to help protect these areas from degradation (Bhaskar *et al.*, 2016).

### **1.3.2 Event Flow**

Streamflow response to precipitation is the product of the streamflow generating processes activated by precipitation during an event. For the purposes of this study, an “event” refers to the streamflow response to rainfall or snow melt and a “precipitation event” refers to the rainfall or snowmelt causing the streamflow response. A hydrograph detailing streamflow response to precipitation is referred to as an event hydrograph. The quick flow portion of the event hydrograph

that is derived from the quick conveyance of water to a stream can be separated from the portion of flow, considered baseflow, that would have continued in the absence of the event (Blume *et al.*, 2007) (Figure 1.2b). Separating a hydrograph into quick flow and baseflow components using only the streamflow response is known as graphical hydrograph separation (McNamara *et al.*, 1997; Guillemette *et al.*, 2005). The quick flow portion of the hydrograph isolates the streamflow response to precipitation, whereas characterizing the total streamflow over the course of the event incorporates the streamflow response with the flow conditions preceding the event (Blume *et al.*, 2007). Since quick flow is determined using only discharge data, it is therefore a representation of both surface and subsurface streamflow generating processes during an event because there is no definitive way to determine the flow path of water to the stream using this method (Blume *et al.*, 2007). Quick flow is an overall streamflow response to precipitation that can be used to characterize the timing and magnitude of streamflow response. For example, a “flashier” streamflow response is often associated with higher peak flow and a faster rate of change (Baker *et al.*, 2004; Roodsari and Chandler, 2017). Stream flashiness is often correlated with urban land use, due to alteration of soils and impervious cover (Oswald *et al.*, 2023). The total volume of quick flow can then be used as a ratio of the total volume of precipitation to quantify a catchment’s ability to translate precipitation into runoff (Blume *et al.*, 2007). This ratio is also known as a “runoff ratio.” Although rainfall characteristics and antecedent wetness influence the amount of runoff produced (Boyd *et al.*, 1993; Ross *et al.*, 2019), impervious cover and leaky subsurface infrastructure have been linked to increased runoff production in urban catchments (Smith *et al.*, 2013; Ariano and Oswald, 2022a; Forgrave *et al.*, 2022). Quick flow characteristics and runoff ratios provide useful information on streamflow response to precipitation; however, pathways such as overland flow, unsaturated throughflow, and groundwater are not easily identified (Freeze and

Cherry, 1979; von Freyberg *et al.*, 2018). Further separation of the hydrograph is needed to understand streamflow generating processes in more detail.

One of the ways to classify contributions to streamflow during an event is to consider all existing water within a catchment prior to the onset of precipitation as "pre-event" water, and any water added to the catchment by precipitation as "event" water (Sklash and Farvolden, 1979). As surface and subsurface processes convey event and pre-event water to a stream, the resulting streamflow during an event becomes a mixture of the water derived from pre-event and event water producing processes. Environmental tracers such as electrical conductivity (EC),  $^{18}\text{O}$ ,  $^2\text{H}$ , and silica have been used to characterize the geochemical signature of event and pre-event water and quantify the proportion of event and pre-event water contributing to streamflow (Laudon and Slaymaker, 1997; Cey *et al.*, 1998; Pellerin *et al.*, 2008). The process of separating an event hydrograph into pre-event and event water is known as 2-component tracer-based hydrograph separation, referred to as tracer-based hydrograph separation in this study. The proportion of event and pre-event water contributing to streamflow can be used to identify dominant runoff pathways during a precipitation event. In general, surface runoff produced by overland flow will convey precipitation (event water) and its distinct geochemical signature to a stream with minimal mixing (Buttle, 1994). Precipitation also percolates into the subsurface and interacts with subsurface water (pre-event) to generate subsurface runoff, which also has a distinct geochemical signature. The proportion of event and pre-event water can then be determined by combining and solving the mass balance equations (Sklash and Farvolden, 1979):

$$Q_s = Q_e + Q_p \quad (1.1)$$

$$Q_s C_s = Q_e C_e + Q_p C_p \quad (1.2)$$

$$\frac{Q_p}{Q_s} = \frac{(C_s - C_e)}{(C_p - C_e)} \quad (1.3)$$

where  $Q_s$  is the stream discharge ( $L^3/T$ ),  $Q_e$  is the event component of discharge, and  $Q_p$  ( $L^3/T$ ) is the pre-event component of discharge ( $L^3/T$ ).  $C_s$ ,  $C_e$ , and  $C_p$  are the tracer concentrations of the stream, event, and pre-event components. The assumptions of 2-component tracer-based hydrograph separation are (Sklash and Farvolden, 1979; Buttle, 1994):

1. There are only two components, and the mixing of the components is complete.
2. The endmembers have sufficiently different compositions.
3. The composition of each member is constant in space and time, or variations can be accounted for.

The distinction of only two components (pre-event and event water) is often a simplification of many systems since vadose water can contribute a significant amount of water to streamflow during an event and often has a distinct chemical signature (McDonnell *et al.*, 1991). Stored surface water may also contribute to streamflow (Klaus and McDonnell, 2013). The composition of precipitation (event) and groundwater (pre-event) are often not constant and can be difficult to constrain because their geochemical signatures may vary spatially throughout a catchment and temporally over the duration of an event (Klaus and McDonnell, 2013). That being said, 2-component tracer-based hydrograph separation can still provide valuable information about the flow paths of water contributing to event streamflow.

The use of tracer-based hydrograph separation has brought to light the importance of pre-event water to streamflow generation during events. Many studies have calculated pre-event water contributions greater than 50% (Buttle, 1994) and even up to 97% (Pearce *et al.*, 1986). On the

Canadian prairies, Ross *et al.* (2017) calculated a median pre-event water contribution of 55% for rainfall events. Large pre-event water contributions to streamflow have been observed in urban environments as well, such as, 25-63% in the Greater Toronto Area in Ontario, Canada (Ariano and Oswald, 2022b) and 22-82% in Massachusetts, USA (Pellerin *et al.*, 2008). Large proportions of pre-event water observed in urban catchment studies challenges the long-held belief that runoff from impervious surfaces (event water) dominates the urban hydrograph, highlighting the need to understand streamflow contributions in the unique climatic and physical conditions of a given catchment (Bhaskar *et al.*, 2016; Ariano and Oswald, 2022b). However, in both natural and urban catchments, the precise mechanisms for conveying large amounts of subsurface water rapidly to a stream during an event are difficult to identify and may vary depending on the climatic and physical characteristics of a catchment (Weiler and McDonnell, 2004; Ariano and Oswald, 2022b). Nonetheless, hydrograph separation is an important tool for understanding the surface and subsurface contributions to streamflow and is valuable for identifying the possible influences of urban development on streamflow generating processes during events.

## 1.4 Objectives and Study Design

The objective of this study was to compare pre- and post-developed headwater catchments in northwest Calgary (Figure 1.1) that have similar climatic and physical characteristics to understand the influence of urban development on streamflow generating processes. The specific questions this thesis addresses are:

1. Does urban development influence streamflow response to rainfall?
2. Does urban development influence groundwater contributions to streamflow?

3. How do surface water-groundwater interactions vary spatially and temporally within catchments at different stages of development?

To achieve these goals, streamflow and groundwater were monitored and sampled using a paired catchment study design. The paired catchment approach takes two catchments with similar properties such as topography, geology, and climate to compare and associate hydrologic differences to a key variable of interest such as development (Petrakis *et al.*, 2021). A calibration period is often used to determine a baseline relationship between the catchments before changes occur within one of the catchment (Clausen and Spooner, 1993). Paired catchment studies have previously been used to study hydrologic processes in forested catchments and the impacts of land disturbances such as fire and logging (Neary, 2016). For example, Burton, (1997) used paired catchments in Utah to show the impacts of clearcut logging on peak flow and annual water yields. Paired catchment studies have also been used in urban settings. Bonneau *et al.*, (2018) demonstrated the differences in shallow groundwater flow paths in an urbanized catchment compared to forested catchment using stable isotopes. Paired catchment studies also provide a way to assess hydrologic processes under the same meteorological conditions, opposed to a long-term study in a single catchment where the influence of meteorologic conditions needs to be factored into the results (Hewlett *et al.*, 1969).

In this study, a developed and an undeveloped catchment were chosen to assess the influence of development on the hydrologic function of prairie catchments in northwest Calgary. The first catchment, which is considered developed, is in the community of Sage Hill, referred to as the Sage Hill ravine (SHR). The second catchment, which is in the early stages of development but considered undeveloped, is the community of Glacier Ridge, referred to as the Glacier Ridge

ravine (GRR). Obtaining a baseline relationship for the catchments in this study was not possible due to a lack of pre-development data in SHR and the lengthy process of developing a catchment. Without a calibrated baseline relationship, this study assumes that the paired catchments would have behaved similarly under pre-development conditions. Therefore, the catchments were selected adjacent to each other to minimize hydrologic differences associated with topography, geology, and climate. Streamflow data was then collected from both catchments and analyzed using hydrograph separation to determine relative contributions of surface and subsurface water at the event and seasonal scale. Stable water isotopes were used to evaluate the sources of groundwater, and differential gauging was used in conjunction with FDCs to characterize surface-water groundwater interactions within each catchment.

## **1.5 Thesis Organization**

Chapter 1 is an introductory chapter summarizing the primary concepts and objectives of the thesis. The goal of Chapter 1 is to provide important background information pertaining to catchment hydrology and surface water-groundwater interactions. Chapter 2 is presented as a stand-alone manuscript for potential submission to a scientific journal in the future. In this chapter the study sites, methods, results, and discussion are detailed along with the primary conclusions. Since Chapter 2 is meant to be a stand-alone manuscript, some information from Chapters 1 and 3 may be repeated. Chapter 3 is a summary of the first two chapters with further discussion of the implications and limitations of the study, and the opportunities for future work.

## Chapter 2: Influence of Development on Peri-urban Streams in Calgary, Alberta

### 2.1 Introduction

Natural streamflow generating processes are a product of the climatic and physical characteristics of a catchment. The influence that urban development has on streamflow generating processes also depends on those same physical and climatic characteristics (Hopkins *et al.*, 2015; Bhaskar *et al.*, 2016). Traditionally, the introduction of impermeable surfaces, removal of vegetation, and alteration of topography are thought to increase stream flashiness, increase peak flow, and alter baseflow, which is known as “urban stream syndrome” (Leopold, 1968; Meyer *et al.*, 2005; Walsh *et al.*, 2005; Oswald *et al.*, 2023). However, much of what is known about urban hydrology is focused in humid climates (Hopkins *et al.*, 2015; Bhaskar *et al.*, 2016; Jefferson *et al.*, 2017; McPhillips *et al.*, 2019). Depending on the connectedness of the impervious surfaces and design of the stormwater system, the hydrologic response to development may vary considerably (Sulam, 1979; Booth and Jackson, 1997; Smith *et al.*, 2013; Ariano and Oswald, 2022a). Urban hydrology research is also limited in arid and semi-arid climates including the semi-arid Canadian prairies. The influence of development on streamflow in the Canadian prairies where low relief, undulating topography, glacially deposited overburden, and hot, dry summers control hydrologic process is relatively unknown (Fang *et al.*, 2007; van der Kamp and Hayashi, 2009; Ehsanzadeh *et al.*, 2012; Ross *et al.*, 2017).

Understanding the surface and subsurface contributions to streamflow are important for identifying hydrologic processes controlling streamflow (Bonneau *et al.*, 2018; von Freyberg *et al.*, 2018). This knowledge can be used to help mitigate undesirable impacts of urban development

(Jefferson *et al.*, 2015; Bhaskar *et al.*, 2016; Fanelli *et al.*, 2017). In the absence of precipitation, streamflow is maintained by baseflow, which is contributions from groundwater or other delayed sources (Hall, 1968). Depending on topography, geology, and the height of the water table, stream reaches may gain flow from groundwater discharge or lose flow to groundwater (Winter *et al.*, 1998). Previous studies have shown the importance of geology on the spatial and temporal variability of groundwater discharge using tools such as differential gauging (Donato, 1998; Payn *et al.*, 2012) and flow duration curves (FDCs) (Winter, 2007). Additionally, urban development has also been shown to have spatially variable impacts on baseflow within catchments (Bhaskar *et al.*, 2016). Understanding the spatial and temporal variability of losing and gaining reaches of stream is important for understanding controls on groundwater discharge and to identify areas of vulnerability, as different reaches of stream may respond differently to urban development (Payn *et al.*, 2012; Bhaskar *et al.*, 2016).

Runoff generating processes are also altered by urban development during precipitation events (Ariano and Oswald, 2022a). The timing and magnitude of the quick flow portion of the hydrograph may be influenced by impervious cover, stormwater systems, and altered soils (Baker *et al.*, 2004; Oswald *et al.*, 2023). When quick flow is taken as a ratio of total event precipitation, also known as the runoff ratio, it represents a catchment's ability to turn precipitation into streamflow (Blume *et al.*, 2007; Forgrave *et al.*, 2022). However, the quick flow portion of the hydrograph does not identify the processes that are translating precipitation into streamflow. Tracer-based hydrograph separation can be used to distinguish between contributions to streamflow from pre-existing water in the catchment (pre-event water) and contributions from precipitation (event water) to better understand subsurface and surface flow paths. In both natural and urban catchments, tracer-based hydrograph separation has been used to identify large

contributions of pre-event water to streamflow during precipitation events (Buttle, 1994; Pellerin *et al.*, 2008; Ariano and Oswald, 2022b). This means the commonly held belief that urban event streamflow is dominated by runoff from impervious cover may not hold true in all situations. Knowledge of how urban development influences surface and subsurface contributions to streamflow can help inform better stormwater management strategies (Jefferson *et al.*, 2015; Bonneau *et al.*, 2018).

The City of Calgary is located on the western edge of the Canadian prairies, and recent development within small headwater catchments in the city's northwest has garnered interest into the impact of urban land use on streamflow. This study uses a paired catchment approach to understand the influence of urban development on streamflow regimes by comparing pre- and post-developed catchments with similar climate and physical characteristics. The research questions considered for this study were: 1) How does development impact streamflow response during a precipitation event? 2) Are groundwater contributions influenced by urban development? 3) Is the spatial and temporal variability of surface water-groundwater interactions different within catchments at different stages of development? Hydrograph separation, stable water isotopes, differential gauging, and FDCs were used to evaluate the relative contributions of surface and subsurface water to streamflow, to determine the sources of groundwater discharge, and to characterize surface water-groundwater interactions within each catchment.

## **2.2 Site Description**

Lying on the western edge of the Canadian prairies, the climate of Calgary is semi-arid, with hot, dry summers and cold winters. From 1961-2011 the average summer temperature was 15.4°C, with an average annual rainfall of 342mm (ECCC, 2023) The average winter temperature

was -7.0°C, with an average annual snowfall of 140mm (ECCC, 2023). This semi-arid climate results in high potential evaporation that surpasses precipitation (van der Kamp and Hayashi, 2009).

Two headwater catchments in northwest Calgary with perennial streams were selected for this study (Figure 2.1). The first catchment is located in the community of Sage Hill, referred to as the Sage Hill ravine (SHR). The total catchment area of SHR is 10.1km<sup>2</sup> with an estimated impervious cover of 20% (Table 2.1) (City of Calgary, 2023). Based on air photos of northwest Calgary (City of Calgary, n.d.), development in Sage Hill began around 2003, with the exception of landfill and gravel extraction operations. The catchment boundaries for this study were delineated from a digital elevation model (AltaLIS n.d.) that pre-dates the majority of development in the area with the intention of capturing the most unaltered catchment boundaries as possible. See Appendix A for catchment boundaries and the delineation process. Development has taken place throughout the catchment except for the hillslopes and riparian areas of the ravines that are preserved as greenspace (Appendix B). The preserved ravine area is estimated to account for 8% of the total catchment area in the SHR catchment. All land use area estimates for this study were derived manually using satellite imagery circa July 2022 on ArcGIS Pro (ESRI Inc., 2021). These ravine greenspaces are not only important hydrologically, but they provide refuge for flora and fauna within the urban landscape and are important recreational and aesthetic areas for the people living in these communities. Urban land use within the SHR catchment consists of residential, commercial, and industrial use. There are no known free-flowing stormwater outfalls discharging stormwater to the SHR stream (B. van Duin, personal communication, July 27, 2020). Two noteworthy land uses within the SHR catchment are the landfill and gravel extraction operations

that account for 50% of the total catchment area and may play a unique role in the hydrologic function of the small headwater catchments in northwest Calgary.

The landfill operation accounted for 19% of the SHR catchment area in 2022 and is located in the headwater portion of the catchment (Figure 2.1). Stormwater is managed on the landfill site and is retained in stormwater ponds on the property. Stormwater from some ponds can be released into the south tributary of the SHR stream, but these releases are controlled and infrequent. Evidence of such a release did occur during this study's monitoring period and this will be discussed in more detail in section 2.4.

Gravel extraction that also occurs in the headwater portion of the SHR catchment is prevalent in this region and was estimated to take up 31% of the catchment area in 2022 (Figure 2.1). Gravel extraction activities that could potentially impact streamflow in the area are discharges to the streams, stormwater capture and storage, and dewatering of the gravel pits. Surface discharge was not observed during this study and does not likely influence streamflow in the study catchments. The nature of the stormwater management systems in the gravel operations area is unknown, but if stormwater is captured and stored on site, this could influence the effective runoff area of the catchment and ponding could promote local recharge. Dewatering of the pits could influence the shallow groundwater levels in the area and in turn alter groundwater discharge with the ravines. However, an environmental report from the western part of the study area claimed that the pre-Pleistocene gravels in the proposed mining area were generally unsaturated, that dewatering should not be necessary, and that new mining activities should have minimal impact on the hydrogeology of the area except for increased recharge to the underlying bedrock aquifer due to the removal of vegetation and the glacial overburden (EBA, 2003). It is unclear though,

how pre-existing gravel operations adjacent to the area may have influenced the conditions at the time of the report. Additionally, topographic changes from the mining operations likely alter the drainage properties of this part of the SHR catchment, which could impact the effective runoff area. Also, groundwater contributing areas are often different than the surface drainage area increasing the uncertainty of the role the gravel operations play in the hydrologic function within these catchments (Winter *et al.*, 2003). Nevertheless, without access to the headwater portions of these streams it is unclear how gravel operations influence streamflow in this area.

The second catchment is located in the community of Glacier Ridge, referred to as the Glacier Ridge ravine (GRR). The total catchment area of GRR is 2.03km<sup>2</sup> with an estimated impervious cover of 5% (City of Calgary, 2023). Impervious cover in GRR consists of a paved highway that crosses the stream, gravel and paved roads, a school, and a farmhouse on the downstream end of the catchment. Current land use in GRR is primarily agricultural, including actively farmed cropland, actively grazed pastureland, and non-grazed grasslands. The same gravel extraction operation occurring in the headwater portion of SHR also extends into the headwater portion of the GRR catchment and accounts for 29% of the total catchment area. GRR is currently considered undeveloped but is rapidly being developed in a similar fashion to SHR, with urban development occurring throughout the catchment while leaving the ravines as greenspace (Appendix B). Construction of the new development began in 2021 on the lands east of the catchment and by the end of 2022 construction crept into the study area affecting 6% of the total catchment area.

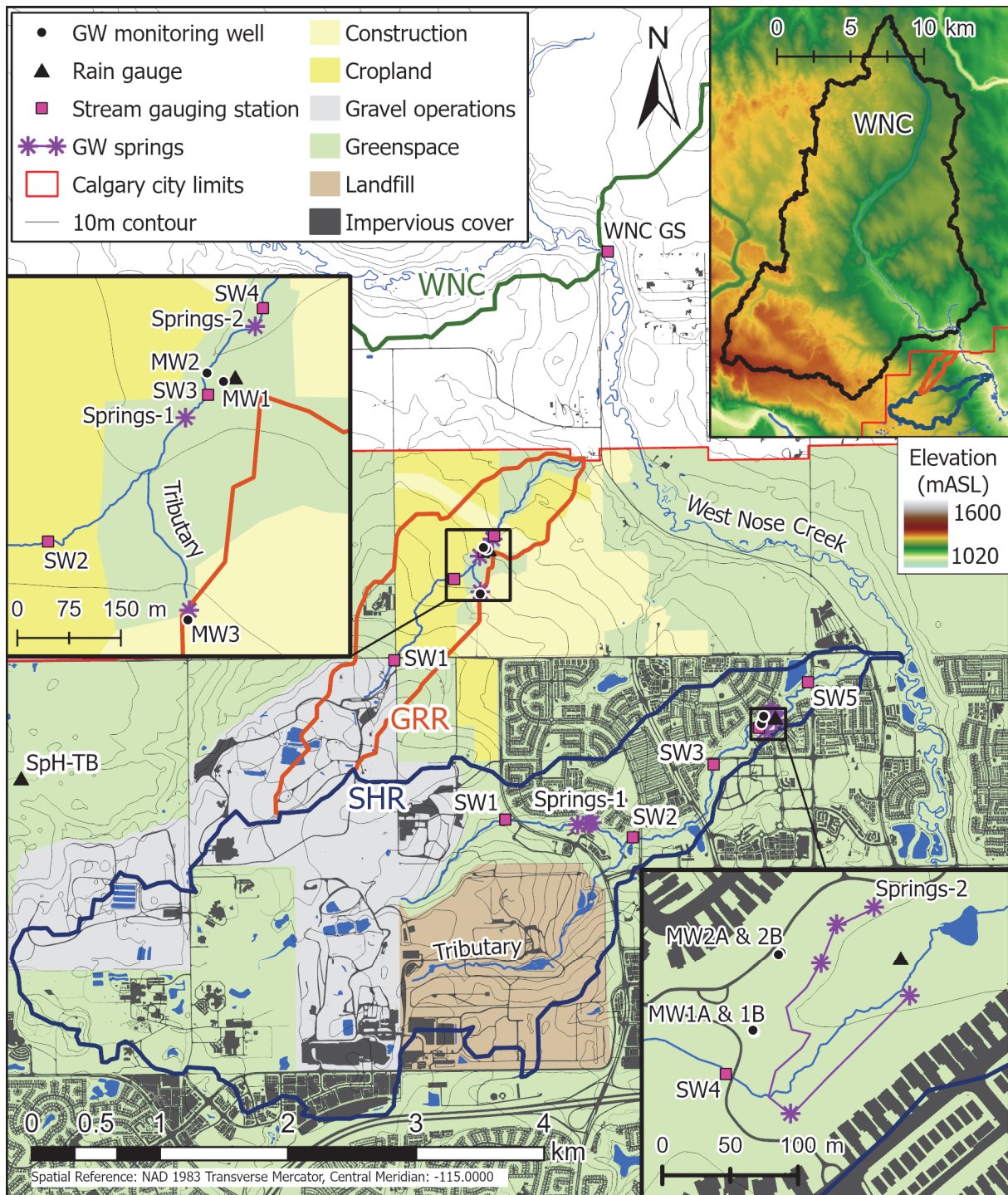


Figure 2.1. Map of SHR (blue) and GRR (orange) relative to WNC (green) and City of Calgary (red). Main map and inset maps show the locations of monitoring equipment, important groundwater springs, and relevant land use for SHR and GRR. Land use is representative of conditions circa July 2022 and was delineated manually by the author using satellite imagery (ESRI Inc., 2021). The top right hand corner map shows SHR, GRR, and WNC relative to the regional topography. mASL: meters above sea level.

Table 2.1. Summary of catchment properties used in this study.

	SHR	GRR	WNC
Total catchment area (km <sup>2</sup> )	10.1	2.03	244
Stream length (m)	5,800	3,000	-
Impervious cover (%)	20.1	5.4	-

Both catchments feature small streams that originate from the same topographic high to the southwest. The topographic high is characterized by pre-Pleistocene gravel deposits that were deposited by rivers coming off the Rockies and later incised by glacial activity (Moran, 1986). The pre-Pleistocene gravel deposits are the target of the gravel extraction operations in the area. The streams in this area, including the SHR and GRR streams, generally flow from the southwest to the northeast, eventually contributing to West Nose Creek. Both SHR and GRR have permanent and semi-permanent reaches fed by prominent groundwater discharge areas. The groundwater discharge areas, also referred to as springs, were identified by walking the entire length of accessible stream in each catchment. The springs were surveyed visually and with an infrared camera (FLIR P20) along some reaches. In general, groundwater discharge areas in SHR and GRR appear to emerge at similar elevations (Figure 2.1). The overburden in this area is comprised of the Lochend Drift and Balzac Formations that were deposited in the Quaternary period (Moran, 1986). Both the Lochend and Balzac Formations are silty glacial tills with the inclusion of clay, sand, and stones (Moran, 1986). Bedrock of the Paskapoo Formation underlies both catchments and consists of Paleocene non-marine deposits of siltstone, mudstone, and sandstone (Hamblin, 2004) that represent an important water bearing unit for the region (Barker *et al.*, 2011).

West Nose Creek (WNC) was also utilized in this study because it is a prairie watershed that is close in proximity to the SHR and GRR catchments, and has long-term streamflow and groundwater data that served as a useful comparator for results from SHR and GRR (Hayashi and

Farrow, 2014). The stream gauging station that defines the WNC catchment is located upstream (northwest) on WNC from the confluences of the SHR and GRR streams (Figure 2.1). The area of the WNC catchment is much larger than SHR and GRR (244km<sup>2</sup>) but shares similar geologic and climatic characteristics. No impervious cover data was available for WNC; however, farmed cropland and grazed pasturelands are the primary land uses within the catchment (Hayashi and Farrow, 2014).

## **2.3 Methods**

Within the SHR and GRR catchments, streamflow gauging stations were installed at multiple locations along each stream, groundwater monitoring wells were installed near prominent groundwater discharge locations, and rain gauges were installed, within each catchment (Figure 2.1). Water samples were collected from all stream gauging and groundwater monitoring well locations. The data used in this study was collected during the ice-free months of 2022 (April – October), also known as the 2022 streamflow season. Hydrograph separation was used to analyze streamflow data at the event and seasonal scale. An “event” is defined as the streamflow response to precipitation, and a “precipitation event” refers to the rainfall leading to a streamflow response.

### **2.3.1 Precipitation Monitoring**

Rainfall at each site was measured using a tipping bucket rain gauge (Hydrological Services P/L, model TB4/0.2mm) and recorded hourly (Campbell Scientific CR10x) during the 2022 streamflow season. Tipping buckets were centrally located within each catchment near the streams (Figure 2.1). The rainfall data for WNC was collected from the University of Calgary’s Spy Hill tipping bucket rain gauge (SpH-TB). Although the Spy Hill site is not located within the

WNC catchment (Figure 2.1), it has been used historically for meteorological monitoring of the WNC area (Hayashi and Farrow, 2014).

A small rain collector was also placed in the SHR and GRR catchments to sample event water. The rain collectors funnel precipitation through a small opening in a capped bottle to limit evaporation. After each rain event, the electrical conductivity (EC) of the collected precipitation was manually recorded (Oakton CON400).

### **2.3.2 Groundwater Monitoring**

Seven new boreholes were drilled and outfitted with groundwater monitoring wells for this project. The boreholes drilled in SHR (Figure 2.1) were completed as vertically nested pairs near a prominent groundwater discharge area. One pair of wells is located in the ravine bottom (SHR-MW1A and MW1B) and the second pair is located on the ravine uplands (SHR-MW2A and MW2B). The SHR boreholes were drilled using overburden drilling excentric (ODEX) technology, which is an air rotary down-hole hammering method. This method was necessary due to the coarse gravel deposits encountered at the site; however, this meant that borehole logging and sampling were limited to fragments of overburden brought to surface by the rig. One well of each pair was completed in the upper 1.5m of bedrock (SHR-MW1A and MW2A), and the second well in each pair was completed in the thick gravel deposit found at the drilling location (SHR-MW1B and MW2B). The boreholes in GRR were drilled using a combination of hollow stem and solid stem augers. The boreholes were logged and sampled as the augers were brought to the surface. GRR-MW1 is located on the uplands of the ravine and completed at the overburden-bedrock interface. GRR-MW2 is located at the ravine bottom and completed within the till overburden. GRR-MW3 is located upgradient of a prominent groundwater discharge area and

completed in the till overburden. All the wells in this study were completed using 50mm (2”) diameter PVC and 0.03mm (10 slot) PVC screen. Borehole logs and completion details for all seven wells can be found in Appendix C.

All wells were developed using a submersible pump to purge and agitate fine sediments. GRR-MW2 did not recover any water until 3-months after completion and water levels did not stabilize during the study period. Therefore, the hydraulic conductivity of GRR-MW2 has not been tested. Hydraulic conductivity was tested using slug and bail tests, and estimated using the Hvorslev method (Hvorslev, 1951) (Table 2.2). Due to extremely rapid recovery of the shallow wells in SHR (SHR-MW1B and SHR-MW2B), the hydraulic conductivity was tested using a constant flow test and interpreted using the Hvorslev shape factor (Hvorslev, 1951). The hydraulic conductivity analysis and estimate details are found in Appendix D.

Table 2.2. Summary of well lithologies and hydraulic conductivity (K).

Well ID	Well Depth (mbgs)	Screened Lithology	K Test type	K (m/s)
SHR-MW1A	9.1	Shale	Slug test	$8 \times 10^{-6}$
SHR-MW1B	4.6	Gravel	CFT	$2 \times 10^{-3}$
SHR-MW2A	14.0	Shale	Slug test	$2 \times 10^{-5}$
SHR-MW2B	8.5	Gavel	CFT	$2 \times 10^{-3}$
GRR-MW1	11.9	Silty-Clay	Slug test	$6 \times 10^{-6}$
GRR-MW2	7.6	Clay	n/a	-*
GRR-MW3	6.1	Gravelly-Clay	Slug test	$6 \times 10^{-5}$

\*GRR-MW2 did not recover during study, therefore there was no hydraulic conductivity test.

CFT: Constant flow test

mbgs: meters below ground surface.

Absolute pressure transducers (Solinst Levelogger,  $\pm 3$  mm) were used to record water level every 15-minutes in each well. The water level data was compensated using a Solinst Barologger, ( $\pm 0.05$ kPa) located in SHR-MW2A and Solinst Levelogger software V4.6.2. The compensated

water levels were then corrected to water elevations using manual water level readings and surveyed elevation details from the monitoring wells. All groundwater level data for 2022 can be found in the supplementary data folder.

### **2.3.3 Streamflow Monitoring**

Streamflow was monitored at multiple locations in SHR and GRR to capture spatial and temporal variability (Figure 2.1). In the SHR catchment, five stream gauging stations were established at culvert inlets. In Glacier Ridge, four stream gauging stations were established: one culvert inlet and three v-notch weirs (Appendix B). At all nine locations, a stilling well was constructed from 51mm PVC pipe and outfitted with an absolute pressure transducer (Solinst Levelogger,  $\pm 3\text{mm}$ ) that was programmed to measure water levels at 15-minute intervals. The absolute pressure data was compensated for barometric pressure using a barometer (Solinst Barologger,  $\pm 0.05\text{kPa}$ ) in SHR-MW2A. The compensated water level data were then calibrated to a fixed point at each location using manual measurements from a ruler taken weekly during the study period.

At each culvert location, manual discharge measurements were taken using a horizontal-axis propeller flow meter (Global Water, FP111,  $\pm 0.03\text{m/s}$ ) and the velocity-area method (Turnipseed and Sauer, 2010). At the v-notch weir locations, a bucket and stop-watch were used to calculate the flow rate over the weir by taking multiple consecutive tests and then averaging the tests to determine the discharge for that time. A stage-discharge rating curve was then established for each location using the equation:

$$Q_s = C(h - a)^n \quad (2.1)$$

where  $Q_s$  (L/s) is the stream discharge,  $C$ ,  $a$  (m), and  $n$  are constants, and  $h$  (m) is the height of water above the fixed point. The least squares method was used to determine the constants for each rating curve by minimizing the error between the calculated discharge from Equation 2.1 and the manually measured discharge for the corresponding stage measurement. See Appendix E for rating curves and uncertainty details. The transducer data was then applied to the rating curves to create a continuous stream discharge record at each location. The calculated flows were then be expressed volumetrically ( $L^3/T$ ) or as depth normalized to the catchment area ( $L/T$ ). Stream discharge data for all gauging stations in 2022 can be found in the supplementary data folder.

Uncertainty for individual stream gauging measurements using the velocity-area method was estimated using the method outlined in Sauer & Meyer (1992). The average standard error of the 78 total measurements taken was 16%. Of the 78 measurements, 91% of the measurements had a standard error less than 20%. Uncertainty for stream gauging measurements using the bucket and stop-watch method was estimated by calculating the standard error of the group of tests taken to calculate discharge for a given time. The average standard error of the 35 discharge measurements using the bucket and stop-watch method was 5%. Of the 35 measurements, 91% of the measurements had a standard error less than 10%. The root mean squared error of the stage-discharge rating curve for all gauging stations were below 2.2 L/s, with the largest error occurring at SHR-SW4 (Appendix E).

Another source of uncertainty in the streamflow data appears to arise from rapid temperature fluctuations that occur in shallow water that impact the strain gauge of the pressure transducers (Liu and Higgins, 2015). This phenomenon is believed to have impacted all pressure transducers in the study to varying degrees and at different times. The monitoring stations located

at culverts seem to be the most impacted, likely because of the higher exposure to sun during the day. The weirs located in GRR are tucked within a deeply incised channel and do not seem to be as impacted by fluctuating temperatures. This phenomenon is estimated to have increased the error of pressure transducers from  $\pm 3\text{mm}$  to  $\pm 15\text{--}25\text{mm}$ .

Streamflow at the WNC gauging station was also monitored using a stage-discharge relationship. Manual discharge measurements were estimated using the velocity-area method to produce a rating curve that was fit using the least squares method. The rating curve was then used to convert stage measured by an absolute pressure transducer (Solinst Levelogger  $\pm 3\text{mm}$ ) every 30-minutes to discharge. The root mean squared error for the 2022 WNC rating curve was 25 L/s. The absolute pressure data at WNC was compensated using a barometer (Solinst Barologger  $\pm 0.05\text{kPa}$ ) at Big Hill Creek roughly 20km west of the WNC gauging station.

### **2.3.4 Differential Gauging and Flow Duration Curves**

Differential gauging was used to understand how streamflow varies along the length of the stream and throughout the flow season. The mean of the daily average flows for a 9–11-day period was chosen to represent the overall streamflow behavior at each gauging station during different phases of the 2022 flow season. The standard deviation of the daily average flows for the 9-11 - day period was used to determine the uncertainty. Average net gains or losses of streamflow can then be estimated by the difference in flow between two stations. Representative time periods vary slightly in length to avoid days with significant precipitation events, and to account for data gaps at some gauging stations.

FDCs for all SHR and GRR stream gauging stations were created using 15-minute discharge data. In order to compare high resolution data for the same time period, all FDCs

represent the time from May 13 to October 28, 2022. The discharge was then ranked in descending order for the given time frame and the exceedance probability ( $EP$ ) was calculated and expressed in percent (%) for each data point using the equation (Risley *et al.*, 2008):

$$EP = \left( \frac{m}{n + 1} \right) \cdot 100 \quad (2.2)$$

where  $m$  is the rank of the flow measurement for the given time period, and  $n$  is the total number of flow measurements used in the FDC.

### 2.3.5 Streamflow Electrical Conductivity

In 2022, EC was monitored at 15-minute intervals at the most downstream flow monitoring station in each catchment, SHR21-SW5 (Solinst Levellogger 5 LTC) and GRR21-SW4 (HOBO U24-001). Drift in the EC data was corrected using manual measurements (Oakton CON400) and the equation:

$$C = m + \left( \frac{t}{\sum t} \right) \cdot (S_i - S_f) \quad (2.3)$$

where  $C$  is the corrected value,  $m$  is the uncorrected value,  $t$  is the time since the beginning of the test,  $\sum t$  is the time interval of the entire test,  $S_i$  is calibration value, and  $S_f$  is the measured value at the time of calibration (Shaughnessy *et al.*, 2019). For this application  $C$ ,  $m$ , and  $S$  have units of  $\mu\text{S/cm}$ . After calibration, EC was temperature corrected using the equation:

$$EC_{25} = \frac{EC}{\left( 1 - \left( (25 - T) \cdot \frac{a}{100} \right) \right)} \quad (2.4)$$

where  $EC_{25}$  ( $\mu\text{S/cm}$ ) is the temperature corrected EC,  $EC$  ( $\mu\text{S/cm}$ ) is the measured EC, 25 ( $^{\circ}\text{C}$ ) is the is the temperature of normalization,  $T$  ( $^{\circ}\text{C}$ ) is the measured temperature, and  $a$  (1.9  $\%/^{\circ}\text{C}$ ) is

the linear temperature coefficient of the calibration tool. See the supplementary data folder for complete EC results in 2022.

### **2.3.6 Water Sampling**

Stream water, groundwater, and precipitation samples were collected for isotopic analysis of oxygen ( $^{18}\text{O}/^{16}\text{O}$ ) and hydrogen ( $^2\text{H}/^1\text{H}$ ). Samples were collected from all stream gauging stations (if flow was present) and groundwater monitoring stations (except GRR-MW2) in SHR and GRR every 4-6 weeks from February 2022 to October 2022. Sampling also occurred in June of 2021 and September 2021. All streamflow and groundwater samples were taken during baseflow conditions. Precipitation samples were collected using a clean syringe from the rainfall collectors after select events in 2022. Stream samples were collected by hand by submerging the sample bottle in the flowing portion of the stream. Groundwater samples were collected using a submersible pump to pump water into a flow through cell measuring the pH and EC of the well water. Groundwater samples were collected after the pH and EC stabilized.

All samples were collected in polyethylene bottles, filtered through a  $0.45\mu\text{m}$  membrane, and refrigerated until laboratory analysis. The processed samples were submitted to the University of Calgary Isotope Laboratory and analyzed using laser spectroscopy (LosGatosResearch DLT-100). The results are reported relative to the Vienna Standard Mean Ocean Water (VSMOW) in per mil (‰) delta notation ( $\delta$ ). The analytical error of the results is 0.2‰ for  $\delta^{18}\text{O}$  and 1.0‰ for  $\delta^2\text{H}$ . Separate duplicate samples were taken throughout the sampling program for quality control to test for consistency. Of the 10 duplicate samples taken, three  $\delta^{18}\text{O}$  analyses were outside the analytical error and zero  $\delta^2\text{H}$  analyses were outside the analytical error when compared to the original sample. The average difference between duplicate samples and the original samples was

0.11‰ for  $\delta^{18}\text{O}$  and 0.3‰ for  $\delta^2\text{H}$ . See Appendix F for sample list and quality assurance/quality control (QA/QC) results.

### 2.3.7 Hydrograph Separation

During the 2022 streamflow season, 41 separate events were identified; however, some events were not captured in all catchments due to logger deployment, data loss, and station failure. For a complete breakdown of the events in each catchment and how events were delineated, see Appendix G. Two hydrograph separation techniques were utilized in this study. Graphical hydrograph separation was used to characterize the streamflow response to precipitation and 2-component tracer-based hydrograph separation, referred to as tracer-based hydrograph separation throughout this study, was used to characterize the surface and subsurface flow paths of event streamflow generation.

Graphical hydrograph separation was used to separate the quick flow portion of the hydrograph from the baseflow portion using a modified straight line technique (Dingman, 2002). The quick flow portion of the hydrograph was determined by calculating the area under the  $Q_s$  curve bound by a straight line connecting the lowest flow before the rising limb of the event to the flow at the end event. The end of event for was determined when the falling limb of the hydrograph was 95% recovered from peak flow (Figure 1.2b) (Appendix G). Runoff ratios ( $RR$ ) were calculated using quick flow ( $QF$ ) and total event precipitation ( $P_E$ ) as follows:

$$RR = \frac{QF}{P_E} \quad (2.5)$$

where the units for  $QF$  and  $P_E$  can be expressed in terms of depth (L) or volume (L<sup>3</sup>) as long as both variables have the same units. The runoff ratios in this study were calculated using the total

or gross drainage area for the corresponding stream gauging locations since there are a variety of land uses within the study catchments that could potentially impact the effective area. Based on the current understanding of the urban land uses within the study catchments, the stormwater management systems generally capture and re-route runoff likely reducing the effective area. Without knowing the effective areas in each catchment, the total drainage area is used to get a better understanding of how the effective area may be influenced. Assuming the naturally occurring effective area within the catchments in this region are proportionally the same when compared to total drainage area, the total drainage area is used to calculate the runoff ratio and is intended to identify if artificial alterations to landscape impacts the efficacy of runoff production.

For events that had corresponding EC data, tracer-based hydrograph separation was used to determine the pre-event and event water contributions to streamflow. The following mass balance equations (Sklash and Farvolden, 1979) were used to determine the proportions of pre-event and event water:

$$Q_s = Q_e + Q_p \quad (2.6)$$

$$Q_s C_s = Q_e C_e + Q_p C_p \quad (2.7)$$

$$\frac{Q_p}{Q_s} = \frac{(C_s - C_e)}{(C_p - C_e)} \quad (2.8)$$

$$\frac{Q_e}{Q_s} = 1 - \frac{Q_p}{Q_s} \quad (2.9)$$

where  $Q$  is discharge ( $L^3/T$ ),  $C$  is the tracer concentration,  $s$  is the stream,  $e$  is event water,  $p$  is pre-event water. EC ( $\mu S/cm$ ) was the primary tracer used to characterize event and pre-event water in this study and although EC is not a direct measure of concentration, it is a proxy for total

dissolved solids (TDS) and is therefore a suitable substitute. It is important to note that the calculations of equations (2.8) and (2.9) are taken at instantaneous timesteps during an event. A metric used in this study is the “maximum event water fraction” (*MEF*), which is defined at the time step when  $Q_e/Q_s$  is largest during an event. The discharge values  $Q_s$ ,  $Q_p$ , and  $Q_e$  can also be integrated over the duration of the event to determine the cumulative stream discharge ( $V_s$ ), cumulative pre-event water ( $V_p$ ), and cumulative event water ( $V_e$ ) in units of  $L^3$ . The concentration of the stream water was measured continuously by the EC loggers at SHR-SW5 and GRR-SW4. The pre-event concentration used for each event was the EC of streamflow before the onset of precipitation. The event water concentration was measured from each catchment’s respective rainfall collector after each event as soon after each event as possible. Since the collected water is the cumulative rainfall, the measured value is considered representative of the average composition for that event.

Traditionally, isotopic tracers such as  $\delta^{18}O$  and  $\delta^2H$  have been used in tracer-based hydrograph separation (Sklash and Farvolden, 1979; Jefferson *et al.*, 2015); however, non-conservative tracers such as EC and silica have also been used successfully (Laudon and Slaymaker, 1997; Pellerin *et al.*, 2008). EC was chosen as the tracer for this study due to the significant difference in pre-event and event values, and the ability to collect high-resolution data during events. It is important to recognize that the terms event water and pre-event water refer to the time-source of storm runoff, where pre-event water is the water that existed in the catchment before the precipitation event and event water is the runoff derived directly from the precipitation event (Sklash and Farvolden, 1979). By this definition environmental isotopes such as  $^{18}O$  and  $^2H$  are thought to best represent time-source components because they are conservative and do not react when in contact with surface and subsurface materials (Buttle, 1994). By that same definition,

the terms pre-event water and event water may not apply directly to hydrograph components determined using EC as a tracer. EC is a non-conservative tracer and is influenced by the amount of time runoff is in contact with surrounding sediments and therefore may overestimate contributions from pre-event water (Pilgrim *et al.*, 1979). Because of the non-conservative nature of EC, the components of hydrograph separation are better described as water that has reacted with surface or subsurface materials and water that has not reacted. That being said, the terms pre-event water and event water are still used in the literature to describe the components of hydrograph separation using EC (Pellerin *et al.*, 2008) and will be used in this study for consistency.

Additionally, two events were sampled for stable water isotopes  $\delta^{18}\text{O}$  and  $\delta^2\text{H}$  to evaluate the use of EC as a tracer for hydrograph separation in this study. For events 22 and 33, EC consistently yielded the highest values of pre-event water,  $\delta^2\text{H}$  the second highest and  $\delta^{18}\text{O}$  the lowest. In terms of  $V_p/V_s$ , EC differed from  $\delta^2\text{H}$  by 2-12% and from  $\delta^{18}\text{O}$  by 5-16%. In terms of individual samples, EC had an average difference of 8% from  $\delta^2\text{H}$  and 14% from  $\delta^{18}\text{O}$  however, the largest individual differences occurred near the peak of the events. For peak  $Q_p$ , EC differed from  $\delta^2\text{H}$  by 6-31% and from  $\delta^{18}\text{O}$  by 12-55%. When EC was at the *MEF* (Minimum EC  $Q_p/Q_s$ ), EC differed 6-20% from  $\delta^2\text{H}$  and 14-29% from  $\delta^{18}\text{O}$ . Hooper & Shoemaker (1986) estimated a precision of  $\pm 10\%$  using stable isotopes for hydrograph separation. Although some of the individual samples in this comparison are outside of the precision estimated by Hooper & Shoemaker (1986), EC,  $\delta^{18}\text{O}$ , and  $\delta^2\text{H}$  followed consistent trends and the overall and average differences are within reason. Based on this comparison, EC will be relied on for tracer-based hydrograph separations throughout this study using the terms pre-event water and event water to describe the components. See Appendix H for the event 22 and event 33 comparison.

## **2.4 Results and Discussion**

### **2.4.1 Streamflow Season 2022**

The streamflow season in 2022 spanned from the beginning of April to the end of October and was determined by the ice-free time window within the catchments. The hydrographs for the farthest downstream monitoring stations in SHR and GRR are compared to the hydrograph for WNC in Figure 2.2. Daily average flow rates calculated for the 2022 flow season at each of these stations highlight the difference in overall catchment size with 11 L/s, 2 L/s, and 114 L/s for SHR-SW5, GRR-SW4, and WNC, respectively.

In general, the 2022 streamflow season can be separated into four phases: Spring, Early-summer, Late-summer, and Fall (Figure 2.2). These phases were defined by monthly precipitation (Table 2.3) and the coinciding streamflow trends. Flows in the Spring phase (April and May) were relatively low and consistent with a moderate amount of precipitation. June defines the Early-summer phase and had the highest monthly rainfall for each catchment and the highest peak flows. July and August define the Late-summer phase, with moderate to high amounts of precipitation and an overall recession in streamflow. The Fall phase was from September to October and had the lowest precipitation with consistently low streamflow similar to flows in the Spring. Overall, the streamflow regime of the SHR stream was different than GRR and WNC. This trend is highlighted by the relatively small rise in flows in June compared to GRR and WNC, and by the lack of a recession limb in July and August. The streamflow response to precipitation events also appears to be less prominent in SHR compared to GRR and WNC.

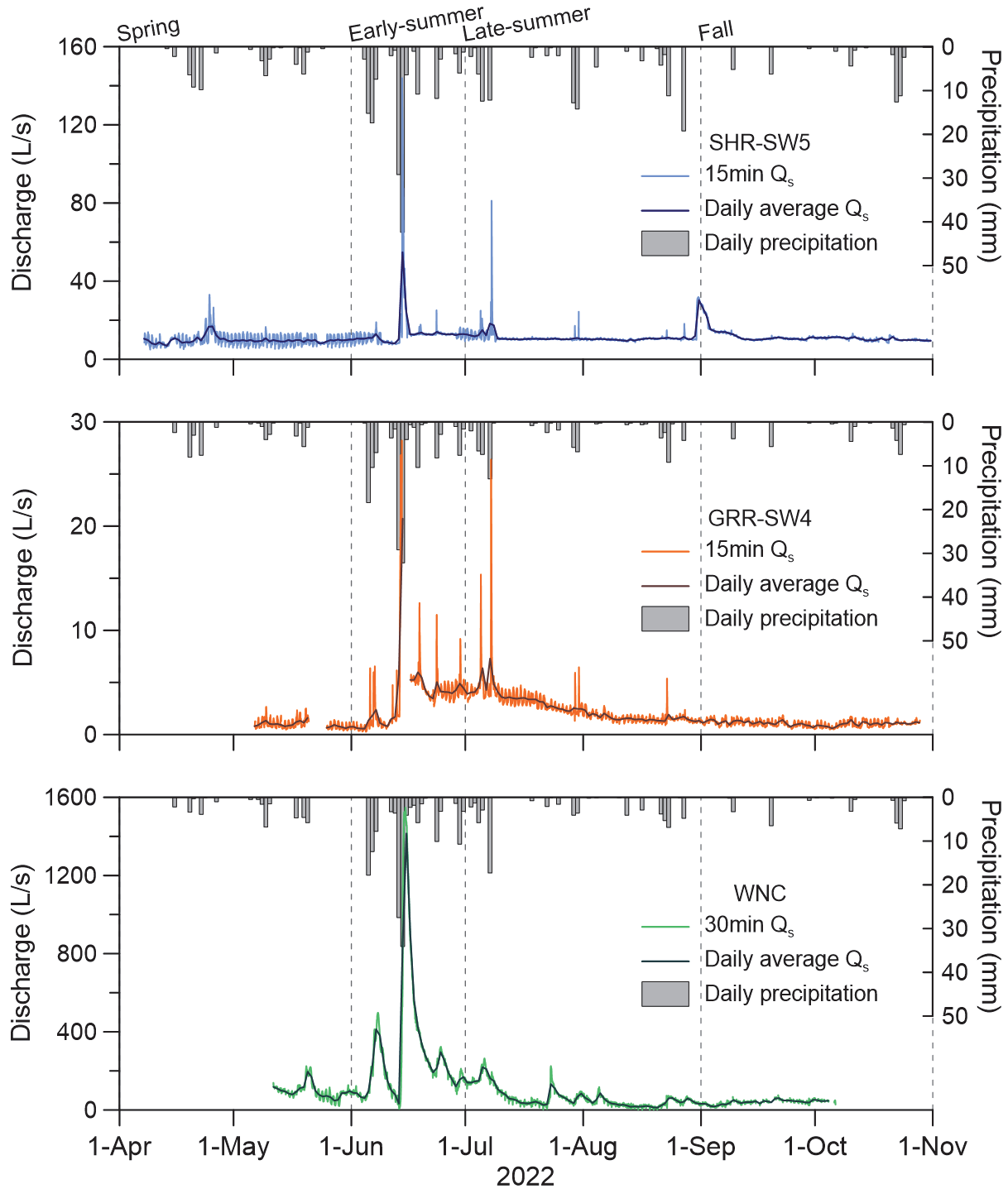


Figure 2.2. Hydrograph and daily precipitation for SHR-SW5, GRR-SW4, and WNC in 2022. Daily precipitation was recorded for each individual catchment at SHR-TB, GRR-TB, and SpH-TB. Spring is defined by the months of April-May, Early-summer is June, Late-summer is July-August, and Fall is September-October. Precipitation data starts on April 7, due to instrument deployment timing.

Table 2.3. Monthly breakdown of the total monthly precipitation for each catchment. SHR-TB and GRR-TB not deployed until April 7, 2022, however no significant precipitation occurred between April 1 and April 7.

Month	SHR-TB $P$ (mm)	GRR-TB $P$ (mm)	SpH-TB (WNC) $P$ (mm)
April	29.4	22.2	10.9
May	25.6	18.8	26.1
June	158.8	140.8	150.8
July	67.0	47.2	41.8
August	45.6	22.2	28.3
September	11.8	9.6	10.7
October	34.4	19.8	18.6

Two anomalies in the streamflow data are of note. The first is the large daily fluctuations in streamflow in SHR that occur from April to the beginning of June, and briefly at the beginning of July. These fluctuations are suspected to be an artifact of rapid daily temperature fluctuations that can occur in shallow water and impact the strain gauge of the pressure transducer, which is described in section 2.3.3. At SHR-SW5, the stilling well was deepened at the beginning of June, which appears to have resolved the issue other than the brief occurrence in July. The second anomaly is the large increase in flow rate in SHR starting on August 30 that was not clearly associated with a corresponding rainfall event. This event is a confirmed release from the landfill stormwater pond into the south tributary of the SHR stream (City of Calgary, personal communication, May 15, 2023)

## 2.4.2 Streamflow Response to Precipitation Events

### 2.4.2.1 Cumulative Streamflow, Peak Flow, and Runoff Ratios

Figure 2.3 shows the relationship between common streamflow metrics and  $P_E$  in SHR, GRR, and WNC. The total catchment area for each monitoring station was used to normalize the

$V_s$  and peak flow ( $Q_{peak}$ ) in this analysis. The stations used were the farthest downstream monitoring stations (SHR-SW5 and GRR-SW4) to capture the behavior of the largest fraction of each catchment possible. In all cases  $V_s$  (Figure 2.3a) and  $Q_{peak}$  (Figure 2.3b) increased with  $P_E$ . The SHR catchment showed less total runoff generation in proportion to  $P_E$  (Figure 2.3a) compared to the GRR and WNC catchments. For  $V_s$  (Figure 2.3a), both GRR (slope = 0.019) and WNC (slope = 0.022) had normalized flows relative to  $P_E$  that were more than double compared to SHR (slope = 0.009), suggesting that less runoff is generated per unit area in SHR even when considering the flow conditions preceding the event. In contrast,  $Q_{peak}$  relative to  $P_E$  were highest in GRR compared to SHR and WNC (Figure 2.3b). GRR is the smallest stream with the smallest catchment area and has the highest  $Q_{peak}$  relative to  $P_E$ , in contrast with WNC that has the lowest  $Q_{peak}$  in proportion to  $P_E$ , but the largest area and stream volume. Assuming peak flow as a proxy for stream flashiness, other studies have also observed increased peak flow with decreasing catchment size and attributed this to fewer flow paths for flood waters within the catchment (Baker *et al.*, 2004; Ariano and Oswald, 2022a). However, Brown *et al.* (1999) observed the opposite, as peak runoff increased as a function of drainage size.

It is important to note that the best fit lines in Figure 2.3 are strongly influenced by the highest values of  $P_E$ . This is clear when comparing the relatively high coefficients of determination ( $R^2$ ) for GRR with those of SHR and WNC, where the higher precipitation events were lost due to weir failure and as a result, the  $R^2$  values are significantly lower. Also, the majority of the data points are for events less than 25mm, which creates uncertainty of the trends for events of larger magnitudes.

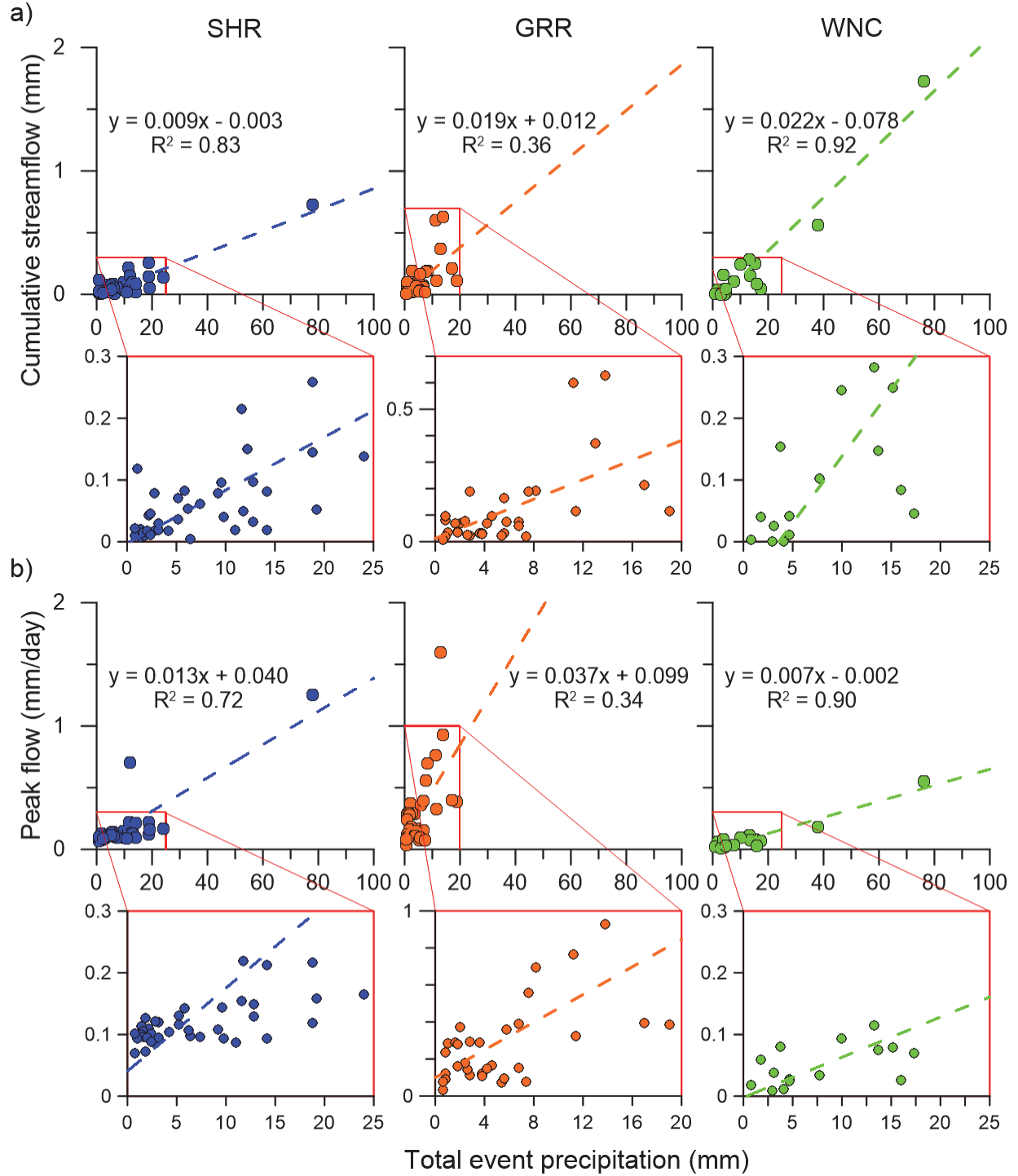


Figure 2.3. Streamflow response to rainfall events at SHR-SW5, GRR-SW4, and WNC in 2022. a) Cumulative streamflow ( $V_s$ ) vs. total event precipitation ( $P_E$ ), b) Peak flow ( $Q_{peak}$ ) vs.  $P_E$ . Dashed lines are the best fit lines for each data set and are described with a linear equation for each watershed. Each data set has a magnified plot to better represent smaller events. Note that the magnified plots have differing axis limits.

Linear best fit lines are useful for interpreting and comparing the general trends of event streamflow in the study catchments. However, other studies have shown that streamflow response to increasing precipitation inputs may not necessarily be linear (Ali *et al.*, 2013). The relationship between event streamflow and precipitation within a given catchment may change due to the interplay of storage and rainfall properties (Mcgrath *et al.*, 2007). The point at which the relationship between event streamflow and precipitation changes is known as a “threshold” (Ali *et al.*, 2013). In the context of this study, a threshold for event streamflow response would be in terms of the amount of precipitation however, thresholds in hydrology have also been identified in terms of rainfall intensity, antecedent rainfall, and antecedent evapotranspiration (Ross *et al.*, 2021). Identifying a threshold for event streamflow behavior is thought to signify the triggering of runoff processes such as saturation or infiltration excess flow (Mcgrath *et al.*, 2007). Thresholds have been used in the past as a tool for characterizing the impact of urban land use on runoff responses (Gwenzi and Nyamadzawo, 2014; Fanelli *et al.*, 2017). The general hypothesis being that increased impervious cover reduces the storage capacity of the watershed and therefore decreases the amount of rainfall needed to invoke a change in the streamflow response. Threshold behaviors are generally not observed in the streamflow-precipitation relationships in Figure 2.3. This is likely due to the lack of rainfall events for  $P_E$  values greater than 25mm. However, one exception may exist in the SHR peak flow data (Figure 2.3b). The best fit line does not fit the values below 25mm, and it is possible that a threshold exists at 10mm total precipitation. Without more data points though, it is difficult to definitively define a threshold for this data.

Overall, the runoff ratios in all catchments were small ( $< 3\%$ ); however, the SHR catchment had the smallest runoff ratios and the smallest variation compared to GRR and WNC (Figure 2.4). Few studies have reported runoff ratios less than 3%, but one example is a study by

Blume *et al.* (2007) for a small forested catchment in Chile. Small runoff ratios indicate that the majority of precipitation in this area does not contribute to quick flow, which in a prairie setting is likely due to the capture of precipitation by low relief, undulating terrain and subsequent loss to evapotranspiration (ET) (van der Kamp and Hayashi, 2009; Ehsanzadeh *et al.*, 2016). Despite the low overall runoff ratios, the SHR catchment demonstrated considerably lower runoff ratios than GRR and WNC as well as a smaller interquartile range. SHR runoff ratios had a mean of 0.13% and median of 0.05%, compared to GRR with a mean of 0.56% and a median of 0.36%, and WNC with a mean of 0.56% and a median of 0.31%. An interquartile range of 0.10% in SHR demonstrates much less variability in runoff ratios compared to interquartile ranges of 0.68% in GRR and 0.64% in WNC. Similar means and interquartile ranges for runoff ratio at GRR and WNC suggest that the mostly natural landscapes in these watersheds have similar capabilities of transforming precipitation into runoff. The runoff ratio similarities between GRR and WNC in contrast to SHR points to the presence of urban development leading to a reduction in runoff generated in these prairie catchments.

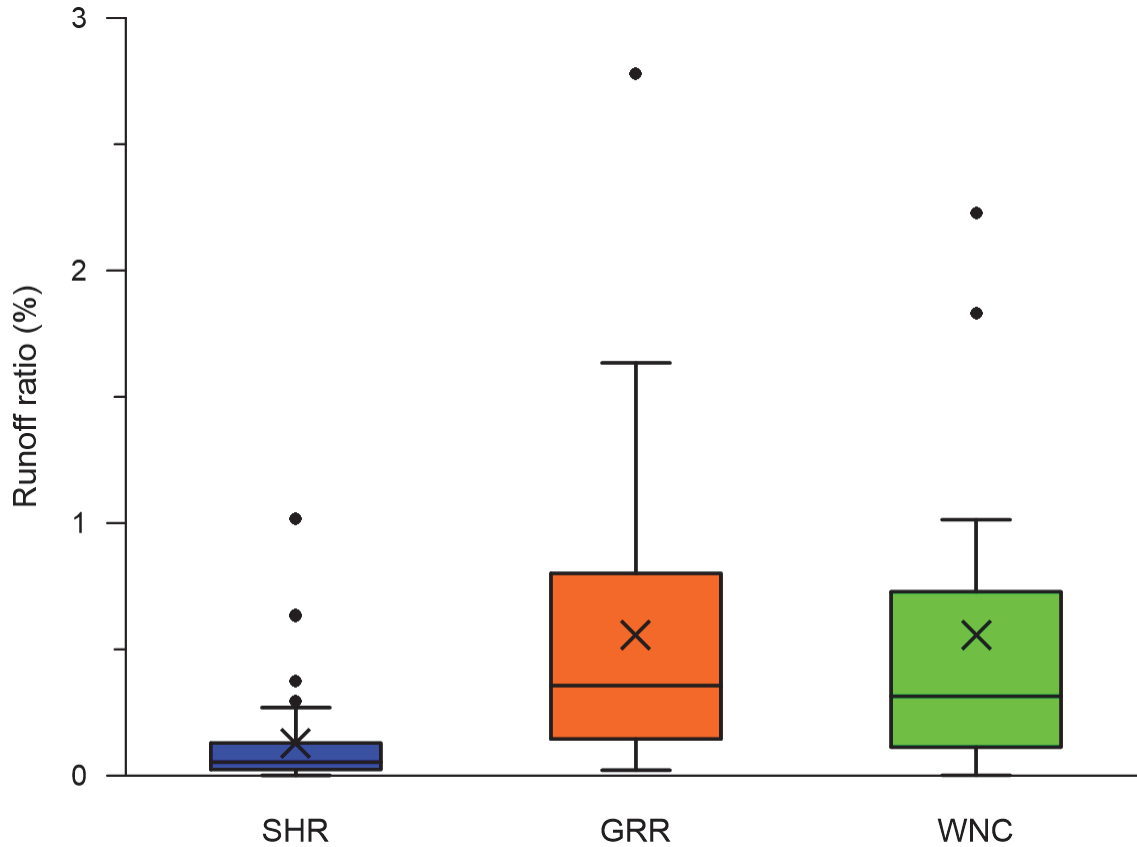


Figure 2.4. Comparison of runoff ratios from SHR-SW5, GRR-SW4, and WNC for 2022. Each runoff ratio was calculated using the contributing area to the stream gauging station used in this analysis.

In the prairies, the effective area of a catchment is dynamic and changes due to precipitation characteristics, soil moisture, topography, and land cover (Spence, 2007; Shaw *et al.*, 2013). Due to the proximity of each catchment, it is reasonable to assume that the natural state of these catchments would have similar ET and soil moisture conditions. Differences in runoff characteristics may then be attributed to differences in effective areas. Both the streamflow-precipitation relationships (Figure 2.3a) and the smaller runoff ratios (Figure 2.4) in SHR suggest that the SHR catchment does not transform rainfall into runoff as effectively as GRR or WNC. Less runoff production within the catchment may be due to a proportionally smaller effective drainage area compared to GRR and WNC (Ehsanzadeh *et al.*, 2012). Based on satellite data,

approximately 93% of the SHR-SW5 drainage area represents land uses that are drained by some sort of stormwater management system, including roadways, industrial operations (e.g., landfill, gravel extraction), and other residential or commercial properties. These stormwater management systems capture or re-route the majority of stormwater, resulting in a reduction in effective area in the SHR catchment relative to the GRR and WNC catchments. Therefore, the difference in runoff response at SHR-SW5 compared to GRR-SW4 and WNC is likely due to the large portion of the SHR-SW5 drainage area altered by development and stormwater management systems that reduce the effective drainage area. The low variability in runoff ratios for SHR also suggests that the effective area is less dynamic and that  $P_E$  has not reached the threshold for runoff generating processes (Shaw *et al.*, 2013). Unfortunately, the data in this study for larger precipitation events is sparse, meaning this behavior has only been observed for events less than 25mm.

Other studies comparing urban and rural stormflow responses demonstrate mixed results. Increased impervious cover is generally associated with more runoff, higher peaks and flashier flows (Boyd *et al.*, 1993; Bell *et al.*, 2016; Ariano and Oswald, 2022a). Smith *et al.* (2013) showed an increase in runoff and peak flow from rural to urban land cover; however, significant variation was observed within the urbanized catchments due to storm system design and the presence of detention ponds. In contrast, results from arid Arizona showed an overall decrease in flashiness as development increased (McPhillips *et al.*, 2019). This decrease in flashiness is attributed to the urban landscape improving the retention of water compared to the natural landscape in this arid region (McPhillips *et al.*, 2019). The mixed results across different regions demonstrates the need for more understanding of urban streamflow processes across a variety of environments (Hopkins *et al.*, 2015).

In addition, runoff ratios from other urban hydrology studies also demonstrate mixed results. Median runoff ratios from nine catchments in the Baltimore metropolitan area ranged from 9-58%, with the highest median runoff ratios associated with large amounts of connected impervious cover and the presence of stormwater detention basins (Smith *et al.*, 2013). This appears to be contradictory to runoff ratios calculated in this study where runoff ratios are less than 3% and are smaller in the urban SHR catchment. The overall discrepancy in runoff ratios is likely due to differences in physical and climatic settings. The impervious cover in the SHR catchment is also not connected to the stream by stormwater infrastructure, which might explain why runoff ratios decreased with urbanization in this study and increased in the study by Smith *et al.* (2013). In another example, the average runoff ratio calculated for a watershed in Pittsburgh was 48%; however, runoff ratios greater than 100% were observed and were attributed to water subsidies from urban infrastructure such as leaky water mains and sewer outflows (Forgrave *et al.*, 2022). Based on the low runoff ratios, it seems unlikely that leaky infrastructure is a major factor on runoff ratios in the SHR catchment. The variability in runoff ratios between these studies highlights the importance of stormwater routing and connected impervious cover in urban environments (Roodsari and Chandler, 2017; Kayembe and Mitchell, 2018; Ariano and Oswald, 2022a).

#### 2.4.2.2 Tracer-based Hydrograph Separation

Tracer-based hydrograph separation using EC<sub>25</sub> was performed for all events in SHR and GRR during the monitoring period that had supporting EC data (SHR: n=32, GRR: n=26). Events 27 and 28 are small to medium sized events that were chosen as representative examples of the event behavior observed throughout the 2022 streamflow season (Figure 2.5). Table 2.4 breaks down the values used to separate each event hydrograph. At GRR-SW4,  $Q_s$  increases roughly 3-times between  $Q_{peak}$  and discharge at the beginning of the event ( $\Delta Q$ ) for events 27 and 28, as opposed to SHR-SW5, which had increases of 1.7-times for event 27, and 2.4-times for event 28. In both instances, GRR-SW4 demonstrated a greater contribution of event water: a 17.3% greater  $MEF$  and a 12.0% greater  $V_e$  during event 27, and a 6.4% greater  $MEF$  and 4.4% greater  $V_e$  during event 28, despite lower precipitation measured in GRR for both events (Table 2.4). Smaller relative increases in peak flow coupled with relatively smaller contributions from event water in SHR suggest that the conveyance of event water to the stream in this catchment is less effective than in GRR.

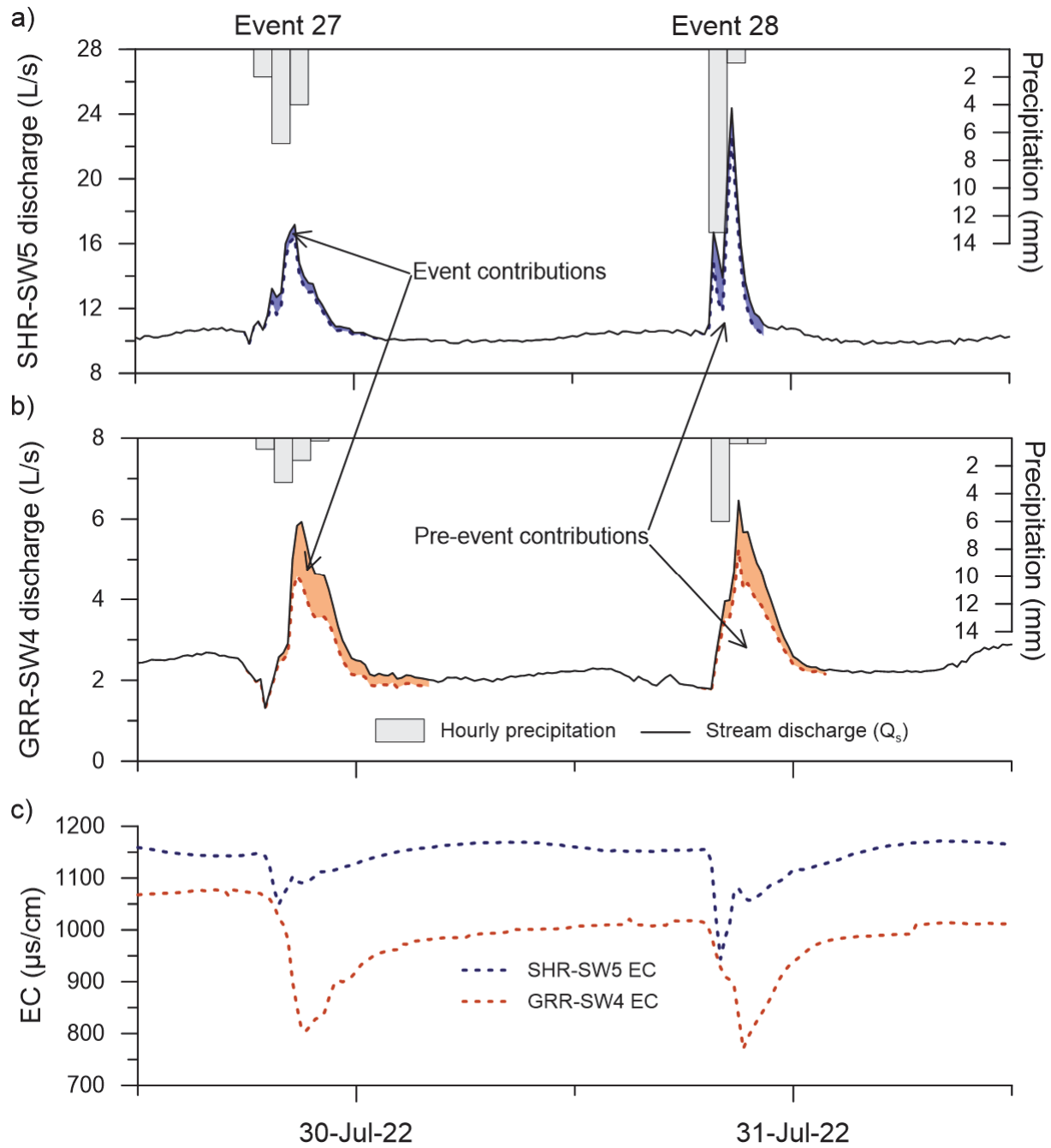


Figure 2.5. Hydrograph separation in SHR and GRR using EC for events 27 and 28. a) Hydrograph separation for SHR-SW5. b) Hydrograph separation for GRR-SW4. c) 15-minute EC measurements for events 27 and 28 period. The colored portions of the hydrograph denote the contributions from event water.

Table 2.4. Hydrograph separation values for events 27 and 28.

Event 27	$P_E$ (mm)	$Q_{peak}$ (L/s)	EC <sub>pre-event</sub> ( $\mu\text{S/cm}$ )	EC <sub>event</sub> ( $\mu\text{S/cm}$ )	$MEF$ (%)	$V_e/V_s$ (%)
SHR	12.8	17.2	1145	18	8.4	2.9
GRR	5.8	5.9	1073	34	25.7	14.9
Event 28	$P_E$ (mm)	$Q_{peak}$ (L/s)	EC <sub>pre-event</sub> ( $\mu\text{S/cm}$ )	EC <sub>event</sub> ( $\mu\text{S/cm}$ )	$MEF$ (%)	$V_e/V_s$ (%)
SHR	14.2	24.4	1155	18	18.6	8.8
GRR	6.8	6.5	1016	34	25.0	13.2

$MEF$ : Maximum event water fraction

$V_e/V_s$ : Cumulative event water fraction

Using data from all available events, hydrograph separations reveal how event water contributes to streamflow with varying amounts of precipitation (Figure 2.6). A linear fit to the  $MEF$  vs  $P_E$  data sets for both the SHR and GRR demonstrates a positive correlation between the  $MEF$  and  $P_E$  in both catchments. Similar positive correlations of event water fractions to  $P_E$  and storm characteristics have been observed in other studies. von Freyberg *et al.* (2018) demonstrated a positive correlation between storm size and  $V_e/V_s$ . Cumulative event water fractions were also calculated and compared to  $P_E$  for SHR and GRR events and showed similar trends to  $MEF$  vs  $P_E$ . The  $MEF$  was chosen in order to represent the upper limit of event water contributions for a given event size. The relationship between  $MEF$  and  $P_E$  in SHR (slope = 0.67) indicates that a smaller proportion of event water contributes to streamflow with increasing amounts of precipitation in SHR compared to GRR (slope = 2.12). Although the clustering of data points below 25mm total precipitation creates uncertainty for prediction of event water contributions of larger rainfall events from this study.

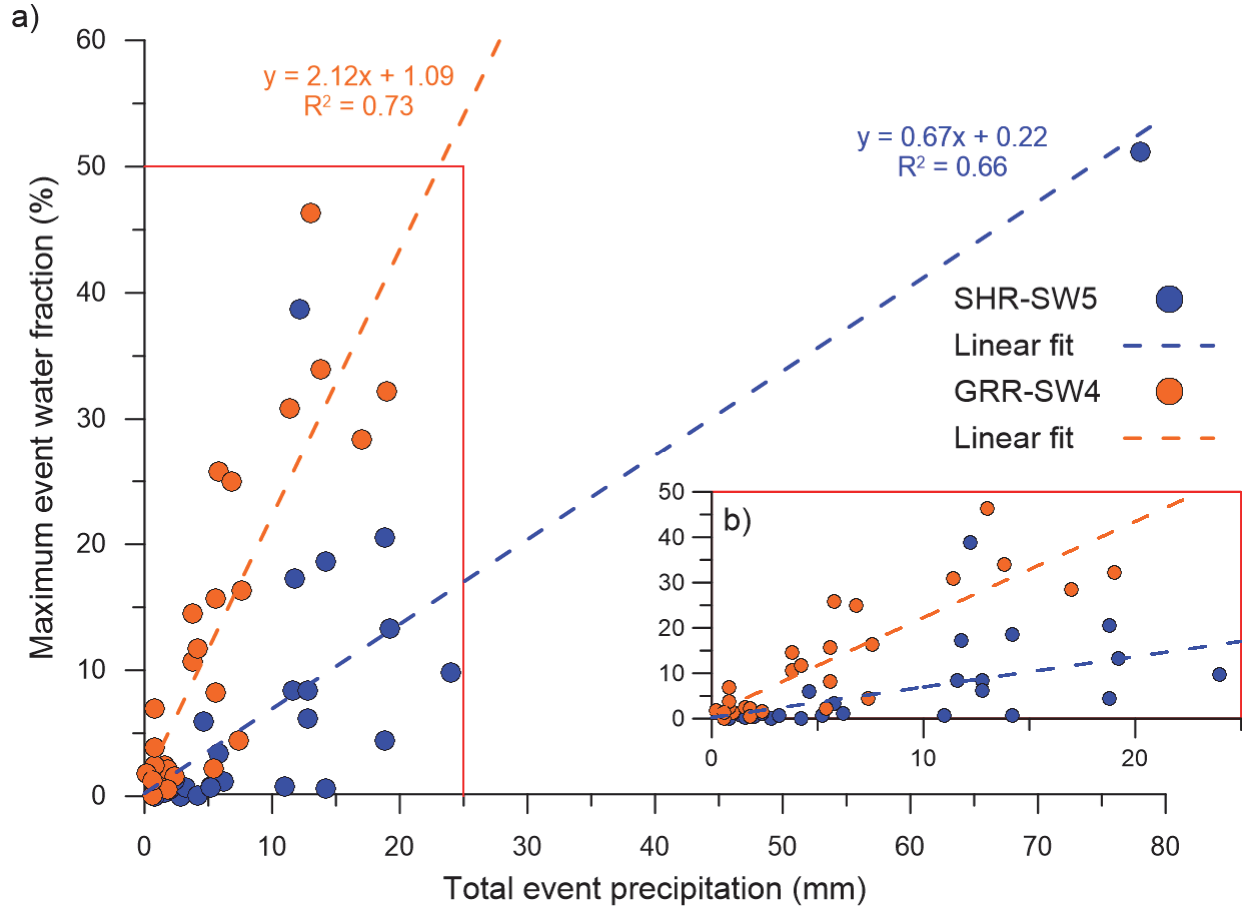


Figure 2.6. Maximum event water fraction ( $MEF$ ) contributing to streamflow relative to total event precipitation ( $P_E$ ) for 2022. The equations and coefficients of determination describe the linear best fit lines (dashed lines) for each catchment. The red inset within plot a) denotes the limits of the zoomed in plot labelled b).

The proportionally smaller contributions from event water in SHR (Figure 2.6) in conjunction with smaller runoff ratios (Figure 2.4) suggests that reduced event water contributions is a factor in the SHR catchment's reduced ability to transform precipitation into surficial runoff relative to GRR. If the stream size to catchment area ratio is similar for the compared gauging stations (SHR-SW5 and GRR-SW4), then it is reasonable to assume that for similar sized rainfall events, any differences in the event water contributions may be attributed to catchment characteristics such as size, antecedent moisture, and land use. The catchment area for SHR-SW5

is larger than GRR-SW4 and catchment size has been shown to be negatively correlated to the fraction of event water contributions (Brown *et al.*, 1999). However, other studies on the effect of catchment size on event water contributions to streamflow show mixed results with the general consensus being that there is no established relationship (McGlynn *et al.*, 2004). Thus, difference in catchment size between SHR and GRR is likely not driving the difference in event water contribution. von Freyberg *et al.* (2018) showed the event water fractions are negatively correlated to antecedent moisture conditions due to corresponding increases in total discharge and pre-event water. von Freyberg *et al.* (2018) then used the ratio  $V_e/P_E$  to show that event water is more closely associated with storm size than with antecedent moisture because wetter conditions favor the mobilization of pre-event water. In this study, antecedent moisture was determined using 5-day antecedent precipitation ( $AP_5$ ) and was not correlated to event water fractions in SHR but showed a positive correlation in GRR (data not shown), which is contrary to the findings by von Freyberg *et al.* (2018). Although the influence of antecedent moisture on event water contributions is unclear, given the proximity of SHR to GRR, the pre-development antecedent moisture conditions should be similar in these catchments. Therefore, if antecedent moisture does influence event water contributions, then in theory, differences in antecedent moisture conditions leading to reduced event water contributions should be linked to development.

A number of other factors also influence hydrologic stream response, including topography, geology, and vegetation, but the paired catchment concept used in this study was designed to minimize these differences. Therefore, the degree of urban land use within the SHR catchment is considered to have a major impact on the contributions of event water during storm events. Stormwater capture and re-routing are ubiquitous within the urban landscape, whether in residential or industrial settings, and could provide an explanation for reduced event streamflow

generation in SHR since stormwater is routed away from the stream. Previous studies indicate the importance of understanding the hydrologically connected impervious cover to the stream versus the total impervious cover in the catchment (Pellerin *et al.*, 2008; Ariano and Oswald, 2022a). Although Pellerin *et al.* (2008) observed much larger event water contributions (18-78%) than this study, they found that less than half of the rainfall that fell on impervious cover was transferred rapidly to the stream and highlight that precipitation that falls on hydrologically disconnected portions of impervious cover either evaporates, infiltrates, or enters the stormwater system. Since there are no stormwater outfalls freely discharging to the SHR stream, then rainfall within the urban environment that is drained by the stormwater system would not be expected to contribute to streamflow. Therefore, stormwater infrastructure in the SHR catchment likely plays a role in the relative reduction of surficial runoff compared to GRR, demonstrated by smaller runoff ratios and *MEF* contributions to streamflow.

In addition, only the largest event recorded in either catchment reached a *MEF* higher than 50%, indicating that pre-event water is the primary contributor to streamflow during most events, and that the mobilization of pre-event water is an important process for event streamflow generation in both catchments. Pre-event water has been observed in many contexts as the primary driver of stormflow, although identifying the precise mechanisms for subsurface stormflow contributions can be difficult (Buttle, 1994; Weiler *et al.*, 2005). A study by Sklash *et al.* (1986) calculated total pre-event contributions of greater than 75% for a forested catchment in New Zealand, and a study by Cey *et al.* (1998) calculated total pre-event water contributions of 64-80% for a small agricultural stream in southern Ontario. A study on the Canadian prairies using hydrograph separation and tracers also identified subsurface water as a significant contributor to stormflow (Ross *et al.*, 2017). Ross *et al.* (2017) went a step further and speculated that macropore

flow and saturation excess flow are dominant subsurface stormflow mechanisms during rainfall events and that transmissivity feedback was important during snowmelt events. These could also be plausible mechanisms for subsurface stormflow in SHR and GRR due to near surface water tables in groundwater discharge areas similar to those observed by Ross *et al.* (2017).

Urban hydrology studies using tracer-based hydrograph separation techniques have also observed varying degrees of pre-event stormflow contributions. Pellerin *et al.* (2008) highlights the complex nature of urban runoff generation by calculating a range of 22-82% pre-event water contributions (18-78% event water). In the Greater Toronto Area, Ariano & Oswald (2022b) calculated pre-event contributions of 25-63% and speculated that flood wave propagation, groundwater ridging, and urban karst may explain the pre-event water contributions. Ariano & Oswald (2022b) propose that recharge in undeveloped headwater area and greenspaces in the urban landscape could account for the continued mobilization of pre-event water after development. The importance of undeveloped headwaters and greenspaces on pre-event water generation can be applied to SHR since the majority of the catchment surface area is pervious, and the ravine portion of the catchment is preserved as greenspace. Since many of the proposed mechanisms for the rapid mobilization of pre-event water, such as groundwater ridging, return flow, and transmissivity feedback (Buttle, 1994; Weiler and McDonnell, 2004) are near-stream processes that would occur within the ravine of SHR, it is possible that pre-event contributions are less impacted by the development on the uplands and more dependent on the depth to water table within the ravine. However, more data is needed to fully understand these processes.

## 2.4.3 Seasonal Streamflow Regime

### 2.4.3.1 *Surface Water – Groundwater Relationship*

To explore the relationship between streamflow and groundwater on a seasonal timescale, the baseflow contributions to streamflow were separated from the stream hydrographs for SHR-SW5 and GRR-SW4 and then compared to local groundwater fluctuations (Figure 2.7). Baseflow for each catchment was estimated by removing the graphically determined quick flow portion (streamflow associated with precipitation) of each event hydrograph from the total stream discharge (Figure 2.7a). The seasonal baseflow fraction was calculated between May 6 and October 28, 2022, to compare the SHR and GRR catchments over the same period. Therefore, the characteristic peak in the SHR-SW5 baseflow from April 23-26, 2022, due to snowmelt was not included in the baseflow fraction calculation. Also, the SHR-SW5 baseflow peak from August 30 to September 12, 2022, due to the storm pond release discussed in section 2.4.1, was not associated with a particular precipitation event, and therefore was included in the baseflow calculation. On a daily average basis, baseflow constituted 95% of the total flow volume at SHR-SW5 and 86% of the total flow volume at GRR-SW4. Although baseflow at SHR-SW5 is 9% higher than at GRR-SW4, long-term streamflow data is needed to determine if baseflow contributions have changed in response to development in SHR. However, it is clear that both stations get large contributions of seasonal streamflow from baseflow demonstrating that groundwater is an important source of flow these streams. Conversely, seasonal baseflow separation also shows that only 5% of streamflow is from event-based runoff at SHR-SW5 compared to 14% event-based runoff at GRR-SW4. This 3-fold difference between SHR-SW5 and GRR-SW4 in event-based contributions at the seasonal timescale may be the cumulative result of the relative reductions in runoff (Figure 2.4) and event water contributions (Figure 2.6) at the event timescale.

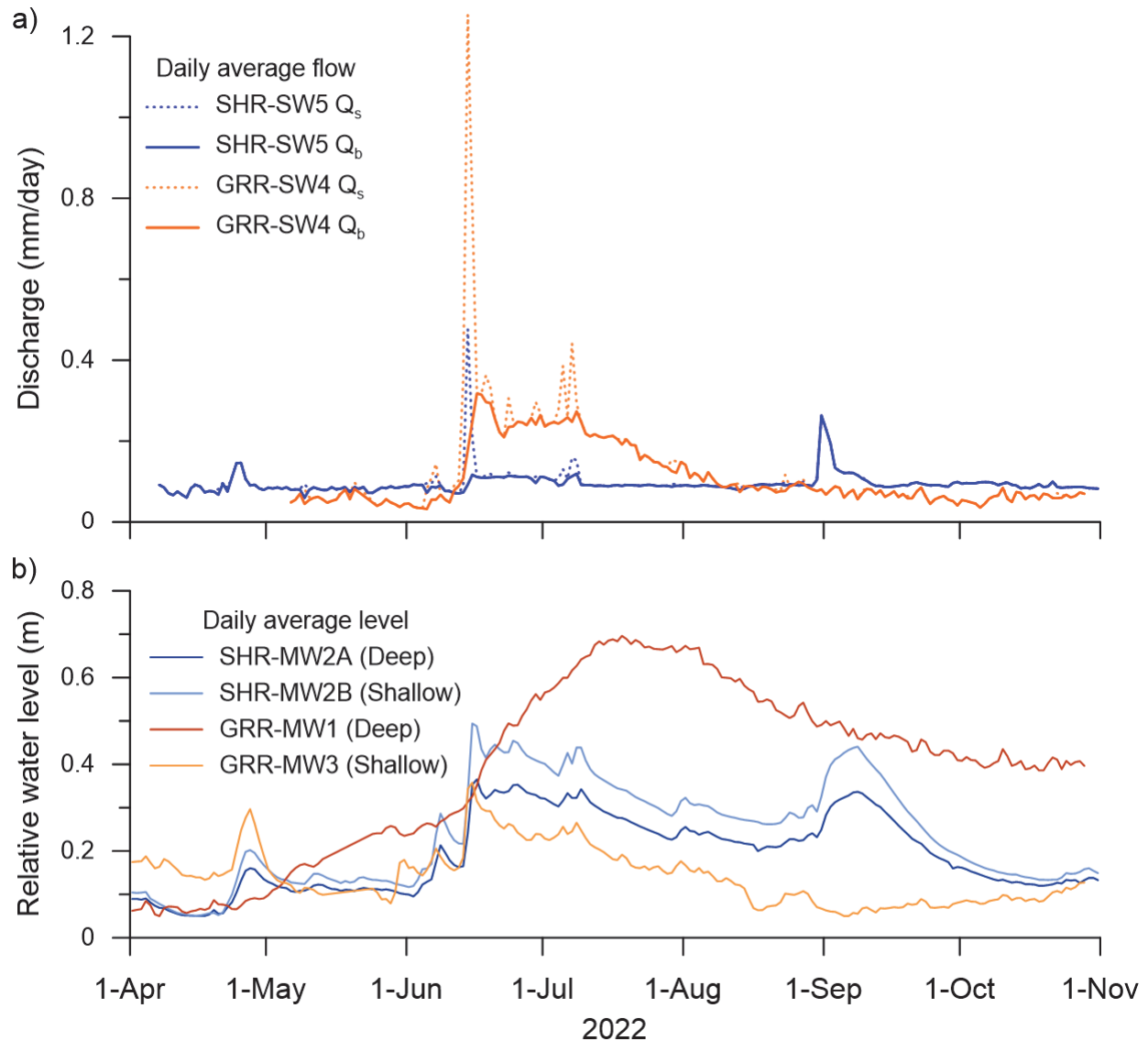


Figure 2.7. Comparison of daily average stream discharge ( $Q_s$ ) to daily average groundwater level fluctuations. a) Daily average baseflow ( $Q_b$ ) (solid lines) separated from the daily average streamflow ( $Q_s$ ) (dotted lines) for SHR and GRR in 2022. b) Daily average local groundwater levels from shallow wells (light colors) in the glacial overburden and deep wells (dark colors) completed at the overburden-bedrock interface. Groundwater levels are reported relative to an arbitrary datum to compare relative fluctuations.

In terms of normalized streamflow, SHR-SW5 shows a consistent baseflow pattern averaging 0.09mm/day, reaching a maximum baseflow of 0.26mm/day during the stormwater release in early September. GRR-SW4 on the other hand, averages 0.11mm/day and reaches a maximum contribution of 0.32mm/day in mid-June, eventually decaying back to pre-June flow

rates by September (Figure 2.7). The difference in baseflow variability is also demonstrated by the coefficient of variation of 22% for SHR-SW5 and 67% for GRR-SW4. Although baseflow makes a larger contribution by volume to SHR-SW5, GRR-SW4 has a larger contribution per catchment area. SHR-SW5 exhibits a more stable flow throughout the season compared to GRR, which has a more pronounced rise and fall of baseflow during the flow season.

Since groundwater is considered the main contributor to stream baseflow, the baseflow trends were compared to relative groundwater levels near prominent groundwater discharge areas within the catchments (Figure 2.7b). An arbitrary datum is used to reference the relative groundwater levels for comparison purposes. All groundwater levels demonstrate a seasonal fluctuation. SHR-MW2A, SHR-MW2B, and GRR-MW3 have sharp responses to precipitation throughout the season due to higher local hydraulic conductivities, whereas GRR-MW1 is completed in a lower conductivity unit causing water levels to respond slower and remain higher throughout the season. Streamflow in GRR appear to follow a similar trend to groundwater in GRR, with groundwater highs occurring in June and July and then decaying from August to November (Figure 2.7). In contrast, streamflow and groundwater trends do not appear to correlate as well in the SHR catchment, as groundwater follows a similar seasonal fluctuation to that seen in the GRR catchment, yet streamflow remains consistent.

To better understand the relationship between streamflow and groundwater, streamflow measurements from stations SHR-SW5 and GRR-SW4 were plotted against the corresponding groundwater levels from shallow monitoring wells near known groundwater discharge locations within each catchment (SHR-MW2B and GRR-MW3) for the month of July (Figure 2.8). During the non-event times, groundwater and streamflow at GRR-SW4 were positively correlated ( $R^2 =$

0.50) with a stronger correlation than SHR-SW5, where streamflow was slightly positively correlated to groundwater ( $R^2 = 0.17$ ). In contrast, the relationships between streamflow and groundwater appear to be more complex during precipitation events. Event 23 (E23) is used as a representative example of the streamflow-groundwater relationship in each catchment and has been outlined with arrows to delineate the sequence of the data points (Figure 2.8). During precipitation events, streamflow appears to be driving groundwater at SHR-SW5, while groundwater continues to drive streamflow at GRR-SW4.

The hysteretic relationship for SHR is clockwise meaning streamflow responds quicker to precipitation than groundwater (Gelmini *et al.*, 2022). Gelmini *et al.* (2022) found that clockwise hysteresis loops of streamflow and groundwater level were correlated to dry antecedent moisture and low runoff coefficients, which are typical of the prairie landscape. Streamflow reaches its peak flow with almost no increase in groundwater levels; however, as streamflow decreases, groundwater levels then rise and reach the peak at the end of the event (E23). This suggests that at this location streamflow is driving groundwater levels during events and that a large amount of bank storage is occurring in the conductive gravels found within the ravine near the SHR monitoring wells. SHR-MW2B is also a short distance from the stream, which amplifies the bank storage response. When a linear line is fit to the non-event points for SHR-SW5 (Figure 2.8a), there is a positive correlation of streamflow to groundwater levels that suggests groundwater becomes the driver of streamflow during non-event periods. The stability of baseflow (Figure 2.7a) and non-event streamflow (Figure 2.8a) may be explained by the highly conductive gravel unit found at SHR-MW2B, as Winter (2007) has also associated high hydraulic conductivity substrate with stable streamflow.

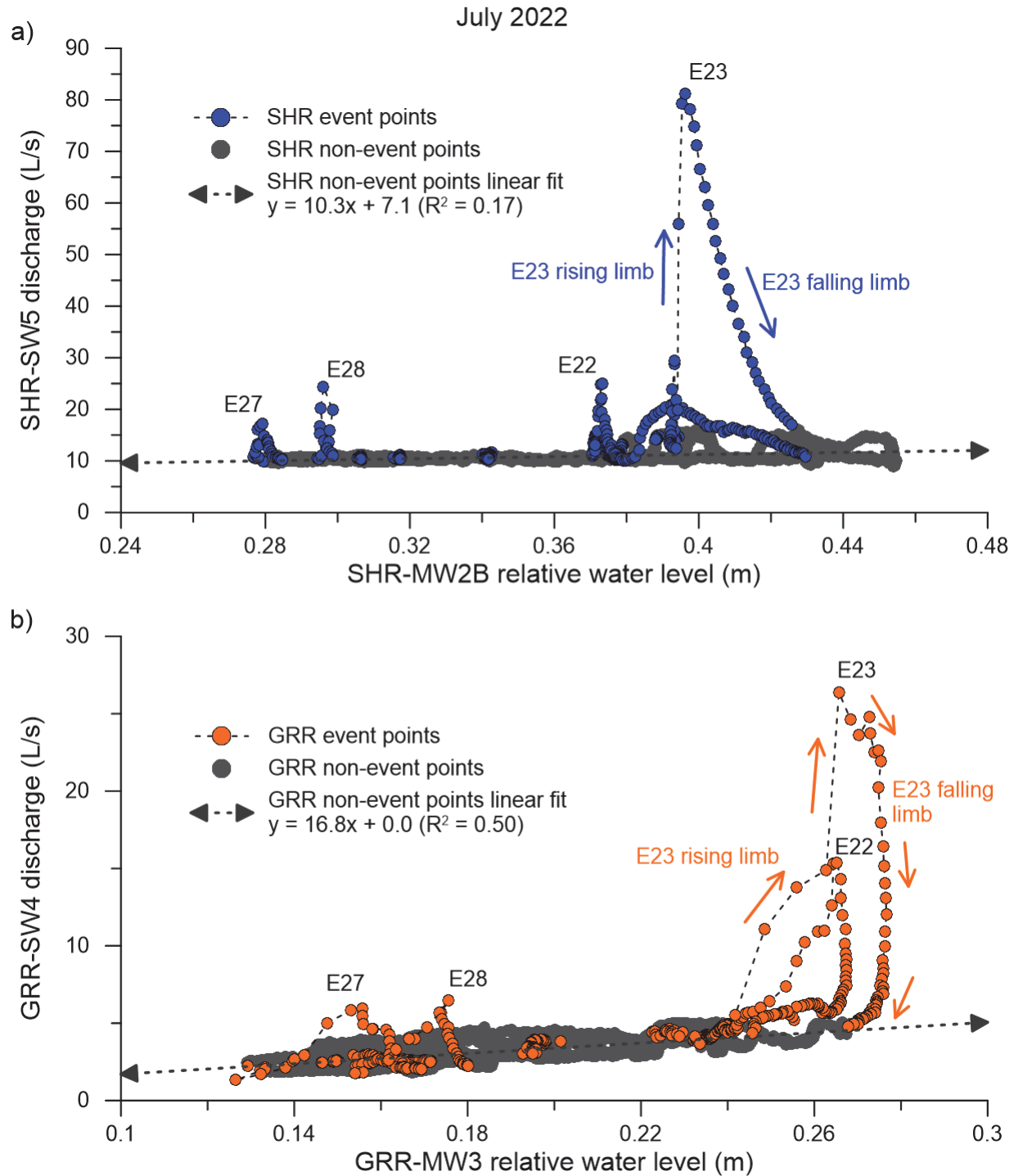


Figure 2.8. Streamflow-groundwater relationship in July 2022 for a) SHR-SW5 vs SHR-MW2B and b) GRR-SW4 vs. GRR-MW3. Streamflow is taken from the most downstream gauging station in each catchment and groundwater levels are from shallow monitoring wells near groundwater discharge areas in the drainages. Groundwater levels are reported relative to arbitrary values. Small, color-coded arrows indicate timing of E23 data points.

At GRR-SW4 (Figure 2.8b), the hysteric relationship during events is also clockwise however, streamflow and groundwater rise nearly simultaneously to peak flow, followed by a steep decrease in streamflow. Peak groundwater level is near the middle of the falling limb, followed by a simultaneous decrease in streamflow and groundwater until the end of the event. The negative correlation of streamflow and groundwater at the beginning of the falling limb indicates that bank storage is occurring at this location. However, this portion of the falling limb is small, reflecting the low hydraulic conductivity at GRR-MW3. A dampened bank storage response also reflects the distance a well is located from the stream since the bank storage response will take longer to reach a well further from the stream. The simultaneous decrease in both streamflow and groundwater at the end of E23 indicates that groundwater is a driver of streamflow during events at GRR-SW4. The linear fit to the non-event data points for GRR-SW4 (Figure 2.8b) also shows a positive relationship with groundwater, indicating that groundwater drives streamflow at GRR-SW4 during non-event periods. Streams fed by substrate with low hydraulic conductivity, like that found at GRR-MW3, have been associated with greater variability, which reflects the trends shown in baseflow (Figure 2.7b) and in July non-event periods (Figure 2.8b). The differences in the streamflow-groundwater relationship at SHR-SW5 and GRR-SW4 highlight the geologic heterogeneity of the region. Although the paired watershed concept is designed to minimize differences in geology, based on the borehole geology and the streamflow-groundwater relationships, it is clear that geologic heterogeneity is influencing the streamflow regimes in these catchments regardless of development status.

To explore potential sources of baseflow, stable water isotopes  $\delta^{18}\text{O}$  and  $\delta^2\text{H}$  were sampled from each streamflow monitoring station and each groundwater monitoring well in the SHR and GRR catchments during baseflow conditions (Figure 2.9). Overall, stable water isotopes suggest

that streamflow is derived from shallow groundwater and that snowmelt and summer precipitation are both important contributors to groundwater recharge. The surface water (SW) and groundwater (GW) samples for both the SHR and GRR catchments were plotted alongside the local meteoric water line (LMWL), ( $\delta^2\text{H} = 7.68 \delta^{18}\text{O} - 0.21$ ) and the amount-weighted annual average ( $\delta^{18}\text{O} = -17.9\text{‰}$ ,  $\delta^2\text{H} = -136.1\text{‰}$ ) for Calgary, AB, (Peng *et al.*, 2004) (Figure 2.9). The SW and GW samples formed distinct clusters with respect to their individual catchments. However, there was no discernable difference between SW and GW samples in either case. This is demonstrated by comparing the mean values for all surface water-groundwater (SW-GW) samples to only the SW samples and only the GW samples of each catchment, which are all similar within the analytical error for each catchment (Table 2.5). No obvious trends related to sample timing or location were observed. The close clustering of means for SW-GW, SW, and GW within the individual catchments supports the observation that these streams are groundwater dominated and that groundwater and surface water are closely connected.

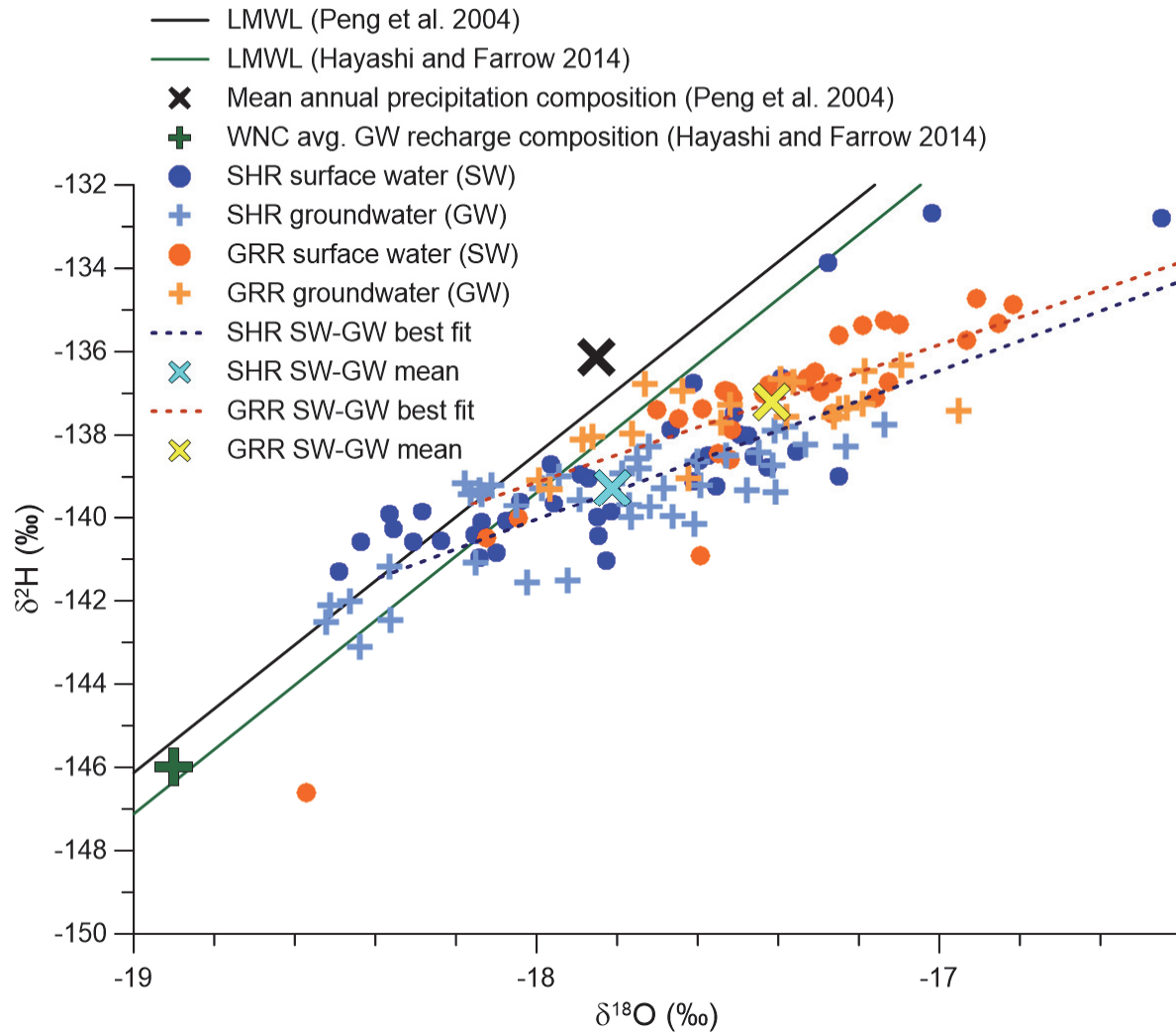


Figure 2.9. Comparison of stable water isotope values from surface water (SW) and groundwater (GW) in SHR and GRR. Samples were taken over a timespan from June 2021 to October 2022. The local meteoric water line (LMWL) and mean annual precipitation value is from Peng *et al.* (2004). The average composition of groundwater recharge for WNC is from Hayashi and Farrow (2014). The LMWL from Hayashi & Farrow (2014) is  $\delta^2\text{H} = 7.74 \delta^{18}\text{O} - 0.06$ . One GRR SW outlier sample ( $\delta^{18}\text{O} = -18.6\text{‰}$ ,  $\delta^2\text{H} = -147\text{‰}$ ) was not included in the linear best fit line.

Table 2.5. Summary of stable water isotope analysis. n = number of samples. SD = Standard deviation.

	Mean		n	SD		Slope	Intercept	r <sup>2</sup>	LMWL intersect	
	δ <sup>18</sup> O	δ <sup>2</sup> H		δ <sup>18</sup> O	δ <sup>2</sup> H				δ <sup>18</sup> O	δ <sup>2</sup> H
	(‰)	(‰)		(‰)	(‰)				(‰)	(‰)
SHR										
SW-GW	-17.8	-139.3	78	0.4	1.8	3.6	-75.4	0.65	-18.4	-141.4
SW	-17.8	-138.9	38	0.4	2.0					
GW	-17.8	-139.7	40	0.4	1.4					
GRR										
SW-GW	-17.4	-137.4	53	0.3	1.8	3.3	-79.8	0.60	-18.2	-139.7
SW	-17.4	-137.3	33	0.4	2.2					
GW	-17.5	-137.5	20	0.3	0.8					

However, the SW-GW means do demonstrate differences between the catchment clusters (SHR:  $\delta^{18}\text{O} = -17.8\text{‰}$ ,  $\delta^2\text{H} = -139.3\text{‰}$ ), (GRR:  $\delta^{18}\text{O} = -17.4\text{‰}$ ,  $\delta^2\text{H} = -137.4\text{‰}$ ). The difference in clustering is likely a product of the amount of evaporation the stream experiences and the average composition of the precipitation recharging the aquifer. The best fit line for each SW-GW sample set can be considered the evaporation line for each catchment. The slope of the best fit lines for SHR and GRR are similar (SHR = 3.6 and GRR = 3.3), suggesting that the evaporative processes after precipitation are similar in each catchment. This is expected since these catchments are located in the same climate. However, GRR-SW samples do tend to be slightly more positive, plotting further away from the LMWL on the evaporation trend line. The GRR stream is smaller than the SHR stream, and flows through an open agricultural field, which could lead to increased effects of evaporation on the stream. Increased evaporation of stream water in GRR appears to be one of the reasons why the GRR and SHR clusters are slightly different. Due to sampling conditions, one GRR-SW sample ( $\delta^{18}\text{O} = -18.6\text{‰}$ ,  $\delta^2\text{H} = -147\text{‰}$ ) is considered an outlier because it consists of mostly snowmelt and is not considered a representative stream sample for this location, therefore was not included in the SW-GW best fit line for GRR (Figure 2.9).

The intersection of the evaporation line and the LMWL can be used to estimate the average composition of groundwater recharge (Maule *et al.*, 1994). An average recharge composition occurring at more negative values than the annual mean precipitation suggests that snowmelt makes a greater contribution to recharge than rainfall (Hayashi and Farrow, 2014). The average recharge compositions of both SHR and GRR are more negative than the mean annual precipitation value, indicating that snowmelt is the dominant source of recharge for both catchments however, the proximity to the annual mean suggests that rainfall is an important source of recharge as well. However, the SW-GW best fit lines for SHR and GRR have different intersections with the LMWL (SHR:  $\delta^{18}\text{O} = -18.4\text{‰}$ ,  $\delta^2\text{H} = -141.4\text{‰}$ ), (GRR:  $\delta^{18}\text{O} = -18.2\text{‰}$ ,  $\delta^2\text{H} = -139.7\text{‰}$ ), suggesting that snowmelt is preferentially recharged in SHR compared to GRR, which is another factor in the difference between the SHR and GRR isotope clusters (Figure 2.9).

Hayashi and Farrow (2014) also found that recharge to the bedrock aquifer in the WNC catchment was primarily from snowmelt with important contributions from summer precipitation. However, the average recharge composition of the bedrock aquifer is different than the recharge compositions in GRR and SHR. Groundwater from the bedrock aquifer underlying the WNC watershed was sampled by Grieff (2006) and reported by Hayashi & Farrow (2014). The average composition of groundwater recharge ( $\delta^{18}\text{O} = -18.9\text{‰}$ ,  $\delta^2\text{H} = -146\text{‰}$ ) reported by Hayashi & Farrow (2014) is plotted on Figure 2.9. The average recharge composition from the WNC bedrock aquifer is more negative than the shallow overburden groundwater sampled in both SHR and GRR. Since SW samples are similar to the GW samples in both SHR and GRR, the difference in average recharge composition between the overburden groundwater and bedrock groundwater indicates that streamflow in SHR and GRR is primarily sourced from shallow overburden groundwater.

Mixing with bedrock groundwater could also provide another explanation for the slightly more negative average recharge composition of SHR groundwater compared to GRR groundwater.

Stable water isotopes were also used to compare the baseflow of an urban and rural stream in Melbourne, Australia (Bonneau *et al.*, 2018). They found that the urban catchment demonstrated more variation along the LMWL and larger short-term fluctuations in isotopic composition. They showed that groundwater transit was quicker in the urban catchment and had more diversified groundwater pathways (possibly urban karst); however, without supporting data, the results could not be attributed to urban land use alone (Bonneau *et al.*, 2018). Both SHR and GRR demonstrate similar isotopic variability, suggesting that impacts from subsurface infrastructure, such as urban karst and leaky pipes in SHR are unlikely. However, SW-GW samples from SHR and GRR do exhibit slightly different isotopic signatures. Considering the importance of the shallow groundwater from the glacial overburden, one might hypothesize that the interception of precipitation by impervious cover could lead to less recharge derived from summer rainfall. SHR does exhibit a slightly more negative average recharge value than GRR, which would support this hypothesis, however, given the average composition of the regional bedrock aquifer and the differences in geology at the groundwater sampling locations, it is difficult to determine if this difference is due to land use or mixing with deeper bedrock groundwater. This suggests that the groundwater contributing areas may be more regional than the SHR and GRR catchment boundaries determined by topography, which is typical of small headwater catchments (Winter *et al.*, 2003). Groundwater contributing areas can be difficult to define due to layered groundwater flow systems and fluctuating flow divides (Winter *et al.*, 2003). The differences in baseflow behavior between SHR and GRR can be further understood by assessing spatial and temporal variability in groundwater discharge in each catchment.

#### ***2.4.3.2 Spatial and Temporal Streamflow Characteristics***

In SHR, streamflow exhibits significant losses and gains along the length of the stream (Figure 2.10). However, the gaining and losing reaches of stream are consistent throughout the season. The stream reach between SHR-SW1 and SHR-SW2 shows net gains throughout the flow season ranging from 3.6 – 5.1 L/s of net gains. The upstream springs in SHR (SHR-Springs-1) are the primary origin of streamflow in SHR (Appendix B). Significant flow was only observed at SHR-SW1 in June and early July. Although the tributary to SHR was not gauged during the study, very little flow was observed during the 2022 season except for between August 30 and September 8, when a release from an upstream stormwater pond occurred (Figure 2.2). This release occurred outside of the selected time periods for Figure 2.10, however, discharge at SHR-SW3, SHR-SW4, and SHR-SW5 recovered to slightly higher flows for the remainder of the flow season after the end of the release. The streamflow at SHR-SW2 remained relatively stable throughout the entire flow season, with a low 4.3 L/s in Spring to a high of 5.8 L/s in Early-summer. The stability of flow at SHR-SW2 is interesting because without stable inputs from the tributary, streamflow at this station is assumed to be completely sourced from discharge at SHR-Springs-1. However, one might expect seasonal fluctuations of streamflow to resemble the rise and fall of groundwater more closely. Groundwater data for this study is limited to the wells completed downstream at SHR-Springs-2, therefore, it is possible that groundwater behavior varies spatially throughout the catchment, which has been observed in other differential gauging studies (Donato, 1998). Geologic heterogeneity would be the likely explanation for spatial variability in groundwater behavior, but the role of urban infrastructure, such as near-stream stormwater detention ponds on local groundwater levels is also an interesting topic for future research. Higher resolution streamflow

and groundwater monitoring is necessary to fully understand streamflow dynamics between SHR-Springs-1 and SHR-SW2.

Both the SHR-SW2 to SHR-SW3 reach and the SHR-SW3 to SHR-SW4 reach exhibit net losses throughout the flow season. Interestingly, the flow at SHR-SW3 increases throughout the season, starting at 0.0 L/s in the Spring and reaching 2.8 L/s by the Fall (Figure 2.10). Groundwater discharge was not observed between SHR-SW2 and SHR-SW3 suggesting this reach is losing less streamflow as the season progresses, or that there is unidentified seasonal groundwater discharge. Flow at SHR-SW4 is non-existent for most of the season except for during Early-summer events (not represented in Figure 2.10), and during the Fall, where sustained baseflow was observed after the stormwater release. Streamflow losses, or transmission losses as described by McMahon and Nathan (2021), are primarily attributed to the infiltration of water into the stream channel and evaporation from the stream surface, which can vary both spatially and temporally. Winter (2007) also notes that in arid climates, streamflow may disappear as it flows over high conductivity substrate but may remain hydrologically connected to downstream surface waters via groundwater, and that ET is capable of noticeably decreasing streamflow. The observations of streamflow losses between SHR-SW2 and SHR-SW4 are consistent with the literature considering the high hydraulic conductivity gravels observed in SHR and that the study sites are located on the semi-arid Canadian prairies where evaporative demands are high (van der Kamp and Hayashi, 2009).

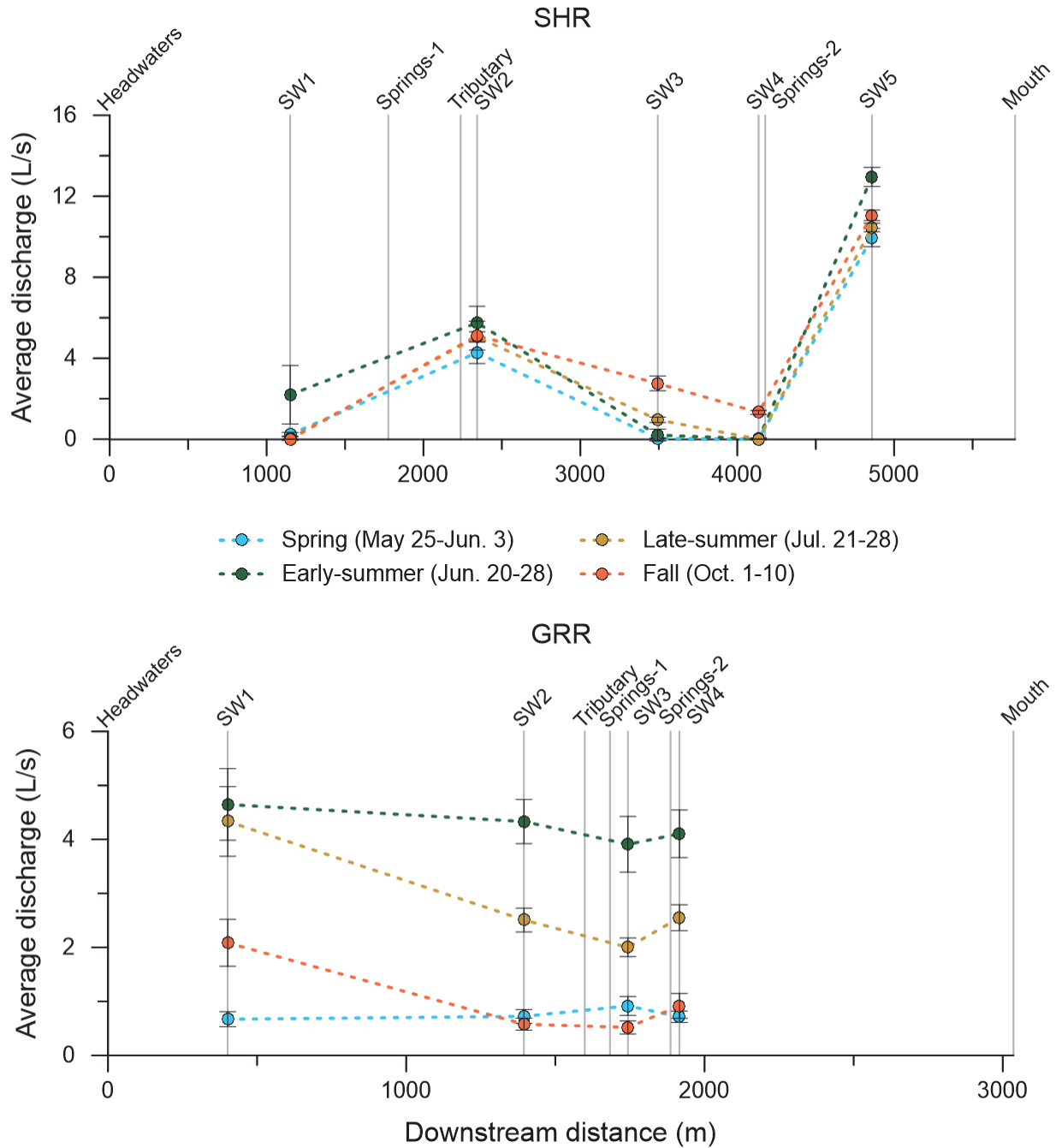


Figure 2.10. Differential gauging plot for SHR and GRR in 2022. Each data point is the mean of the daily flows for a 9–11-day period representative of the Spring, Early-summer, Late-summer, and Fall phases of the flow season. The dotted lines are straight line interpretations of the gaining and losing fluxes and represent the net change in streamflow for a given reach. The exact locations of the gaining and losing fluxes require higher resolution streamflow measurements. Error bars are the standard deviation of the daily average flows used to calculate the mean for that given period.

The reach between SHR-SW4 and SHR-SW5 shows the greatest flow gains due to the contributions from SHR-Springs-2. The gains in this reach range from 9.7 L/s to 12.9 L/s and, at times, are fully sourced from SHR-Springs-2 due to zero flow at SHR-SW4. The disappearance and reappearance of streamflow between SHR-SW2 and SHR-SW5 suggests that significant groundwater underflow is occurring and although flow may not be observed, there is a hydraulic connection due to the highly conductive substrate observed in the boreholes near SHR-SW4 (Appendix C). The stable flows at SHR-SW5 appear to be correlated to the gravels located at SHR-Springs-2, which is consistent with Winter (2007), who observed streams receiving discharge from highly conductive aquifers tended to have stable streamflow regimes. Correlating the differential gauging results with current knowledge of the geologic substrate from geotechnical reports and boreholes drilled for this study reveals that significant spatial variation in streamflow in SHR is likely due to geologic heterogeneity along the length of the stream and that highly conductive gravels play a role in maintaining streamflow throughout the year.

Unlike SHR, the GRR catchment demonstrated considerable temporal variability throughout the streamflow season, with relatively consistent flows between gauging stations indicating much less spatial variability (Figure 2.10). The original source of streamflow in GRR is not well understood because flow emanates from private property that was not accessible during this study. The reach between GRR-SW1 and GRR-SW2 generally shows net losses throughout the flow season except for the Spring, where a small net gain of 0.1L/s was observed. No groundwater discharge was observed over this stretch and the small gain could be due to uncertainty in the data. The reversal from streamflow gains in Spring to losses the rest of the season may be due to the ramping up of ET that occurs during the Summer and Fall growing season. Much of this reach is channelized and flows through open agricultural cropland that would subject

this reach to increased temperatures of Summer and Fall (Appendix B). Geotechnical reports from the area show that high hydraulic conductivity sand and gravels are found in the GRR catchment, however, the substrate of monitored stream length is mostly low hydraulic conductivity tills. Low hydraulic conductivity substrate likely limits infiltration into the streambed, making evaporation the primary transmission loss process. A similar trend occurs from GRR-SW2 to GRR-SW3, where streamflow experiences net gains in the Spring season and net losses for the rest of the year. However, there are known groundwater discharge areas along this reach that contribute to streamflow, and much of this reach is not channelized and meanders through topographically low relief grassland that slows down streamflow and likely promotes evaporation, infiltration and subsequent ET during the summer months.

Between GRR-SW3 and GRR-SW4, net gains occur for all phases except for during the Spring season. The stream has cut a roughly 1m deep narrow channel for most of this reach providing shade and reducing direct evaporation from the stream surface (Appendix B). The net losses that occur during the Spring season may be due to lower groundwater levels at this time of year (Figure 2.7b) resulting in smaller contributions to streamflow. Overall, streamflow at all four gauging stations in GRR follows the same temporal trend, which is consistent with the rise and fall of groundwater: low flows in the Spring, followed by seasonal high flows in Early-summer, followed by a decrease in flows through Late-summer and Fall (Figure 2.7b; Figure 2.10). Differential gauging in GRR suggests that transmission loss is less prominent between gauging stations and that low conductivity substrate promotes temporal variation of streamflow over spatial variation.

Spatial and temporal baseflow trends not only vary within each individual catchment, but the SHR and GRR catchments showed considerable differences in spatial and temporal baseflow trends, even for catchments in close proximity to each other. Baseflow in SHR varied along the length of the stream, but showed little temporal variation at each gauging station, in contrast to baseflow in GRR, which varied temporally at each gauging station, but showed little variation along the length of the stream. However, differences in the spatial and temporal baseflow trends between the SHR and GRR catchments were not attributed to urban land use. Differential gauging used in conjunction with the current knowledge of the subsurface suggests that geologic heterogeneity is impacting the spatial and temporal variability of streamflow. Other studies have also attributed changes in subsurface structure to spatial and temporal streamflow variability, such as underflow emerging at valley pinch points (Payn *et al.*, 2012), and changes in hydraulic conductivity of channel substrate leading to streamflow losses (Winter, 2007). The geologic heterogeneity of the glacial overburden in this region appears to be a major factor determining the spatial and temporal variability of baseflow within these catchments, with ET also playing a role. Although there were no obvious spatial or temporal trends associated with urban land use, characterizing the spatial and temporal trends of individual catchments is useful for predicting and testing the impacts of future development and making water resource management decisions.

For further insight into the temporal characteristics of streamflow within the SHR and GRR catchments, stream discharge at each gauging station is plotted as an FDC (Figure 2.11). FDCs characterize the variability in streamflow conditions observed in each catchment, but also underscore the importance of groundwater for maintaining streamflow. In the SHR catchment (Figure 2.11a), an inflection point for all gauging stations is observed between  $EP = 4\%$  (SHR-SW5) and  $EP = 9\%$  (SHR-SW4). Discharge above this inflection point usually represents the

elevated flows during precipitation events (Searcy, 1959), but also includes the flows from the stormwater release observed at SHR-SW2, SW3, SW4, and SW5. Only SHR-SW2 and SHR-SW5 had continuous flow over the analysis timeframe, remaining relatively stable 92% (SHR-SW2) and 96% (SHR-SW5) of the time. Stable flows represented by the flat portion of the FDC, demonstrate the direct influence of groundwater discharge on flows at SHR-SW2 and SHR-SW5 (Winter, 2007), which are located directly downstream from SHR-Springs-1 and SHR-Springs-2 respectively (Figure 2.10). The remaining three stations demonstrated varying degrees of intermittency. SHR-SW1 has the least prominent inflection point ( $EP = 9\%$ ) and only flowed for 43% of the flow season. A steep slope throughout the entire FDC for SHR-SW1 suggests that flow at this location is mostly runoff based with little contributions from storage (Searcy, 1959; Winter, 2007). SHR-SW3 and SHR-SW4 have similar inflection points ( $EP = 8\%$ ) with nearly parallel slopes to the middle portion of the FDC, and steep drop-offs at the end of the curve. However, SHR-SW3 was only dry 19% of the time, while SHR-SW4 was dry 61% of the time. The decrease in flow duration from SHR-SW2 to SHR-SW4 further demonstrates the losing nature of these stream reaches. Similar to the differential gauging results (Figure 2.10), FDCs show that streamflow behavior varies along the length of the SHR stream. Streamflow at gauging stations directly downstream from groundwater discharge locations showed stable flows during the flow season and flow duration decreased with downstream distance from the groundwater discharge locations.

Compared to SHR, the FDCs for the GRR streamflow monitoring stations are more consistent (Figure 2.11b). All four curves demonstrate relatively flat slopes throughout with a prominent inflection point between 1% and 3%, suggesting that streamflow remained consistent throughout the monitoring period due to sustained groundwater discharge, and that event flows

contributed significant amounts of water to streamflow 1%-3% of the time (Searcy, 1959). During the established time frame, none of the monitoring stations went dry and the fact that GRR-SW2, SW3, and SW4 curves show little deviation suggests that minimal transmission loss occurred between these stations. The GRR-SW1 curve appears to deviate from the other three stations, which might be explained by a few factors. The deviation of the middle of the curve, or flat part, may be due to issues with the stage-discharge relationship (Appendix E). The high flows at the upper end of the curve may be due to the stage-discharge relationship as well as contributions of stormwater from the highway ditches that drain the immediate area. Overall, FDCs show stable flows at all four gauging stations that are sustained by groundwater discharge. Similar to SHR, it is clear that groundwater is important for sustaining flows in these small streams throughout the year.

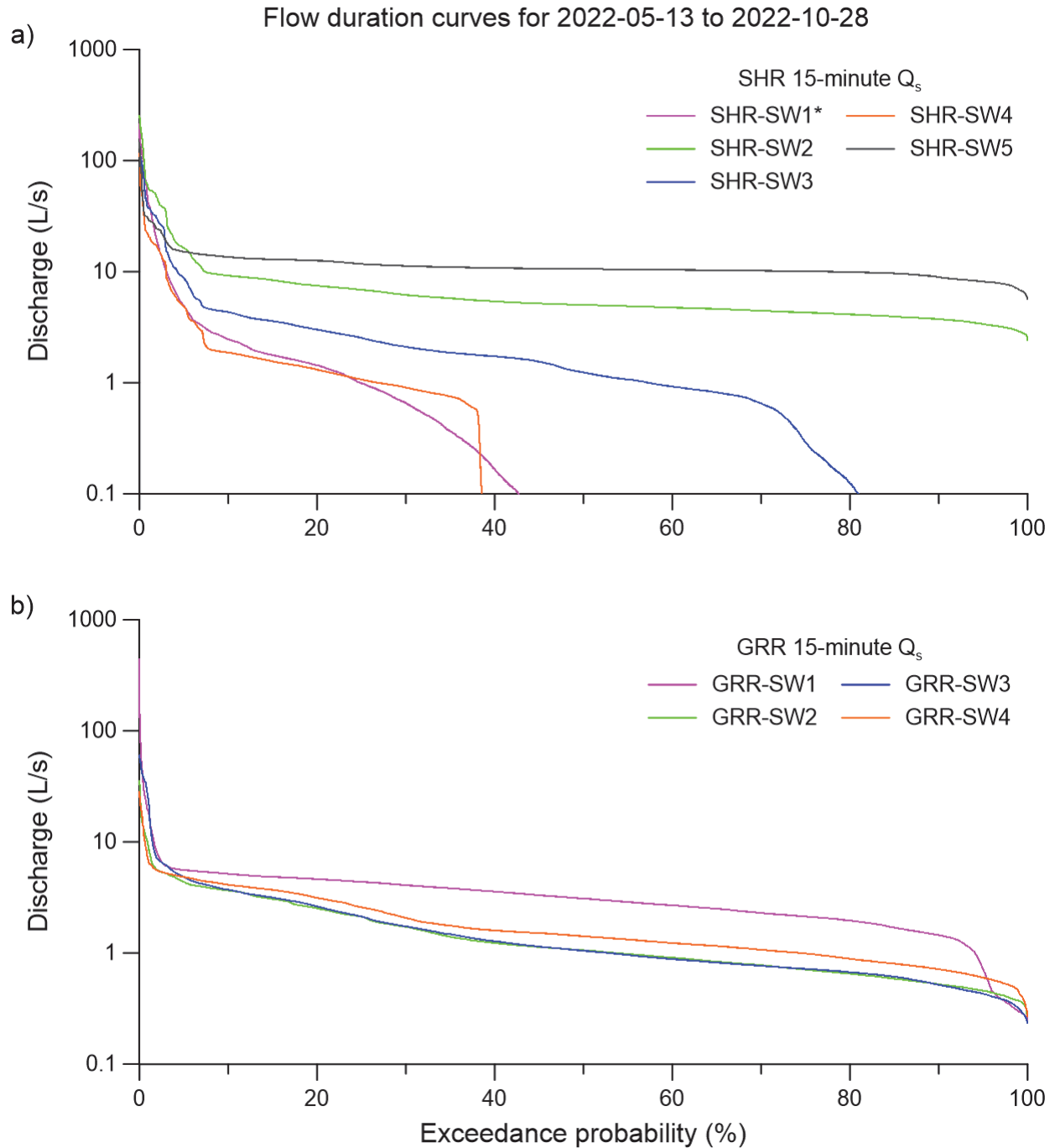


Figure 2.11. Flow duration curve for each streamflow monitoring station within the study sites. All flow duration curves use 15-minute discharge data for the time period of 2022-05-13 to 2022-10-28. \*SHR-SW1 is from 2022-05-13 to 2022-10-05 due to data logger issues.

## 2.5 Conclusions

The objective of this study was to use paired pre- and post-developed catchments to understand the influence of development on streamflow processes in northwest Calgary. The results show differences in the pre- and post-developed streamflow regimes that suggest the influence of urban land use on streamflow generating processes, but also highlight the influence of natural catchment characteristics.

Precipitation is not translated into surficial runoff as effectively in the SHR catchment compared to the GRR or WNC catchments. Runoff ratios for all catchments were relatively small, as even the largest runoff ratios in the study were less than 3%, meaning the vast majority of precipitation during events is lost to internal drainage within the catchments and ET, which is typical of this region's low hummocky terrain and high ET to precipitation ratios. That being said, runoff ratios for SHR were significantly lower and less variable than GRR and WNC, suggesting that the effective area of the SHR catchment has been reduced in proportion to the effective areas of GRR and WNC. Furthermore, proportionally smaller *MEFs* relative to  $P_E$  in the SHR catchment compared to the GRR catchment point to reduced overland flow contributions during events. Stormwater infrastructure in the SHR catchment designed to capture, divert, and store stormwater could explain a reduction in effective area and overland flow leading to consistently small runoff responses even as precipitation increases.

Groundwater is the primary contributor to streamflow in both the SHR and GRR catchments at the event and seasonal timescale. During events, pre-event water was the primary contributor to streamflow in both catchments, with all but one event having a *MEF* greater than 50%. The continued rapid mobilization of pre-event water in SHR is attributed to most of the

catchment remaining as pervious surface cover, especially the ravine greenspace that remains largely undeveloped creating a buffer for near stream processes that generate pre-event runoff water. Seasonal baseflow separation also showed that groundwater contributed 95% of the flow volume at SHR-SW5 and 86% of the flow volume at GRR-SW4. Stable water isotopes confirmed that streamflow in both catchments is derived from groundwater discharge and that the shallow overburden is the primary source of groundwater for both catchments. However, the isotopic signatures of surface water and groundwater from SHR and GRR were different. Stable water isotopes suggest that groundwater is preferentially recharged by snowmelt in both SHR and GRR, but to a greater degree in SHR. Stormwater infrastructure in SHR could reduce the recharge of summer precipitation relative to GRR, thereby leading to the recharge of proportionately more snowmelt in SHR. However, groundwater mixing with the regional bedrock aquifer could also explain differences in the average recharge composition between SHR and GRR.

The SHR and GRR catchments demonstrated different spatial and temporal streamflow characteristics. The SHR catchment showed high spatial variations in streamflow with consistent temporal trends, opposed to GRR, which demonstrated consistent spatial trends, but high temporal variability. Differential gauging and FDCs showed that reaches of the SHR stream directly downstream from groundwater discharge locations had stable flows, but that other reaches were intermittent, and were dry up to 61% of the monitoring period. In contrast, FDCs from the GRR catchment demonstrated stable flows at all the stream gauging stations. Based on the data collected, geology is a primary driver of the surface water-groundwater connections within the study catchments. However, other factors like urban development may still play an important role. Therefore, understanding the surface water-groundwater connectivity and how it is altered by urbanization is important for managing key sources of streamflow within these prairie catchments.

Although this study could not conclusively identify cause and effect relationships between urban land use and streamflow regime, development was more associated with changes to surficial contributions to streamflow than subsurface contributions. However, the results from this study also underscore the importance of groundwater for maintaining streamflow in these small headwater catchments of northwest Calgary. Knowing that the shallow overburden is the primary source of groundwater, and that streamflow can vary in time and space has important implications for decisions regarding urban water management and development planning. Shallow groundwater is more vulnerable to water quality degradation and groundwater discharge areas are important for maintaining flows to larger streams and for flora and fauna that reside in the urban greenspace. Strategies for maintaining natural flow regimes and to mitigate the impacts of development in this area should therefore consider management of groundwater and surface water in a holistic manner.

## **Chapter 3: Conclusion and Recommendations**

### **3.1 Summary and Implications**

Comparing pre- and post-developed headwater catchments in northwest Calgary revealed differences in streamflow regimes that could be explained by urban land use as well as streamflow regime differences attributed to natural catchment characteristics. In the end, this study highlights the importance of groundwater for generating streamflow in these catchments. Knowing that groundwater is important for streamflow generation has important implications for future development and water resource management decisions in this region.

Streamflow event responses characterized using graphical and tracer-based hydrograph separation showed that the SHR stream had a reduced ability to translate precipitation into runoff. Small runoff ratios in conjunction with smaller maximum event water contributions suggest that overland flow processes convey proportionately less water to the stream in SHR compared to GRR, which is attributed to impervious cover and stormwater systems that are disconnected from the stream channel reducing the effective area of the catchment. A reduction in overland flow contributions to streamflow in this situation has interesting implications for stormwater management planning and reducing the impact of development on urban ecosystems. More focus might shift to the drying out of hillslopes, which could impact vegetation and erosion potential in the urban landscape. Tracer-based hydrograph separation also showed that the majority of event streamflow is comprised of pre-event water in both catchments. Although overland flow processes may be affected by development, the rapid mobilization of subsurface water still occurs in SHR. Since processes that convey large amounts of pre-event water to the stream occur near the stream,

this points to the importance of the ravine greenspace for preserving natural streamflow generation of pre-event water.

Baseflow separation and stable water isotopes showed that groundwater is the primary contributor to streamflow in both SHR and GRR. Baseflow separation shows that 95% and 86% of streamflow is baseflow in SHR and GRR. Urban hydrology studies tend to focus on the impacts of urban land use on streamflow during precipitation events due to the implications for flood risk and stormwater management. However, this study highlights the importance of groundwater as the controlling factor on streamflow regime. Stable water isotopes also suggest that groundwater from the shallow overburden is the primary source of discharge for these streams. Shallow groundwater is generally more vulnerable to water quality degradation and to the possible impacts of subsurface urban infrastructure. Although no such impacts were observed in this study, these could be important considerations for urban planning and future development. The average isotopic signature of groundwater recharge in SHR points to the preferential recharge of snowmelt in SHR when compared to GRR. This could be in part due to impervious cover, but also to mixing with groundwater from the regional bedrock aquifer. Therefore, groundwater processes, including recharge, soil storage, and discharge, should be considered in conjunction with runoff processes for maintaining natural streamflow and preserving the ecosystems within the urban greenspaces.

Differential gauging and FDC showed contrasting spatial and temporal streamflow trends in SHR and GRR. SHR demonstrated high spatial variation along the length of the stream, but consistent flows throughout the year, and GRR showed high temporal variation but with consistent flow at each gauging station. The contrast in spatial and temporal streamflow variations were generally associated with the geologic heterogeneity of the glacial overburden, and specifically

with high hydraulic conductivity gravel deposits observed within the SHR catchment. The spatial variability of streamflow within the SHR catchment has important implications for managing streamflow within the ravines. FDCs in SHR show that stable contributions from groundwater discharge occur at SHR-SW5 and SHR-SW2, but in between at SHR-SW3 and SHR-SW4, streamflow is intermittent and dry for portions of the flow season. Although streamflow is lost between SHR-SW2 and SHR-SW4, there is likely still a strong hydraulic connection between the SHR-Springs-2 and upstream portion of the catchment due to groundwater underflow. A strong hydraulic connection between SHR-Springs-2 and upstream streamflow suggests that even though surface flow is lost, alterations to upstream flow could still impact discharge lower in the catchment, further supporting the need to evaluate the connection between surface water and groundwater to appropriately manage streamflow within the ravines. Also, gaining reaches of stream in both catchments were defined by discrete groundwater discharge locations. Identifying the location of groundwater discharge is important because disturbing these areas could have an outsized impact on downstream flow and in turn alter the riparian ecosystems within the ravines. The spatial and temporal variations not only demonstrate the unique conditions of each catchment, but also the variable conditions within each catchment that might respond differently to landscape changes.

## **3.2 Limitations**

A key limitation of this study is the duration of monitoring, and this limitation is two-fold. First, without knowing the pre-developed streamflow regime in an individual catchment, one can only speculate if the streamflow regime has changed since development occurred. Only reasonable explanations can be provided to understand the mechanisms behind the differences in streamflow

observed in the SHR and GRR catchments. Another issue is that some impacts of development may occur over a long period of time and might not be captured by a short-term study such as this one. For example, the rise or fall of baseflow due to urban influences would likely only be captured with a multi-year data set. In addition, the results of this study are only representative of the meteorological conditions of a single year. Streamflow and groundwater characteristics are likely different during “wet” or “dry” years. Having long-term data before, during, and after development would make it possible to compare pre-and post-development conditions within the same catchment and allow for better inferences as to why streamflow regime may or may not have changed without the added complexity of comparing different catchments with different physical properties. However, climate variability over such a long period may introduce a different source of complexity. Preferably, monitoring of pre- and post-development conditions would encompass a variety of climatic scenarios to understand the streamflow response to “wet” or “dry” years. However, streamflow response may be unique from year to year, even during similar climatic conditions. Therefore, separating the impacts due to climatic forcing from impacts of development may be challenging.

The second limitation to a short monitoring duration is that there is a finite amount of precipitation events in a year, most of them being small to medium in size. The event response data for this study was mostly limited to events under 25mm. Including more large event data points would improve the understanding of event response characteristics and may also provide enough information to identify event response threshold behavior.

Although the paired watershed concept was designed to limit the differences in natural characteristics and isolate the effects of urban land use, there were inevitable differences between

the catchments that created additional uncertainties when interpreting the results. Additionally, this study focused on the comparison between two catchments. Although data from WNC was used when possible and relevant, it is possible that the results from this study are unique to these catchments. Comparing multiple pre- and post-developed catchments in northwest Calgary may be useful for identifying more general streamflow and groundwater trends associated with urban development. Furthermore, most of the results and analysis from this study were focused on the downstream stream gauging stations in each catchment: SHR-SW5 and GRR-SW4. However, differential gauging and FDCs suggest that streamflow processes vary spatially throughout the SHR catchment. Using the most downstream gauging station integrates all processes contributing to flow at that station, but some of the nuance that occurs within the catchment may be masked. For example, during an event, the contributions from event and pre-event water could vary if tracer-based hydrograph separation was performed at a station like SHR-SW3 or SHR-SW4. Therefore, the interpretation of runoff processes occurring within the catchment could also vary. Similarly, the seasonal baseflow contributions to streamflow are likely different at stations such as SHR-SW3 and SHR-SW4, which are not directly downstream from a discrete discharge location. Performing hydrograph separation at multiple locations along the length of the stream would provide further insight into the nuance of the hydrologic processes taking place within each catchment.

The delineation of both the surface and subsurface contributing areas is complicated by urban development. In terms of surface catchment boundaries, this study used pre-developed topography to delineate the catchment boundaries with the intent of integrating alterations to the boundaries by development into the analysis. However, due to grading of topography, road building, and stormwater routing, the true catchment boundaries are much more complicated than

those used in this study. Similarly, the groundwater contributing areas of SHR and GRR may not necessarily follow the topographically determined catchment boundaries. If the groundwater contributing areas are larger than the catchment boundaries, then it is necessary to characterize this area to fully understand the recharge processes that control groundwater discharge with the study catchments. Additionally, a groundwater contributing area that is larger than the catchment boundary means that urban land use outside of the catchments could influence groundwater discharge within the catchments.

Inaccessibility to the headwater portion of the study catchments was also a limitation of this study. The gravel extraction operations make up a large portion of both catchments, and the influence they have on streamflow in this area is largely unknown. The headwater portions of the SHR and GRR catchments are important recharge areas, and the groundwater behavior in these parts of the catchments is largely uncharacterized for the study period. Groundwater recharge is thought to increase minimally over the lifespan of the gravel operations; however, without data prior to the operations, it is difficult to determine if groundwater or streamflow has been impacted by these operations. Groundwater characterization is limited to a handful of wells that are centralized within each catchment and close to the streams. It is possible that groundwater fluctuations vary spatially throughout the catchments, especially in the upstream portions of the catchments.

### **3.3 Future Work**

One of the goals of this research project was to lay a foundation for a long-term study to identify the influence of urban development on catchment processes. Aside from being the comparator to SHR, one of the primary reasons the GRR catchment was chosen as a study location

was because the community of Glacier Ridge is slated to be developed similar to that of Sage Hill. The hope, and goal, is that continued data collection in GRR can occur throughout the development, and post-development phases. In addition to continued monitoring of the GRR catchment, there are other undeveloped headwater catchments outside the city limits of Calgary that could provide further comparisons to the data collected in SHR and GRR.

In the meantime, the results of this study raise many questions about the surface water-groundwater dynamics in SHR and GRR. One of the main limitations identified in this study was the limited number of large events used to define the event response characteristics. One of the consequences of this was the inability to define threshold behaviors. An interesting study to characterize event responses differently would be to collect very high-resolution streamflow, EC, and precipitation data for medium to large sized events. Theoretically, inflection points in streamflow and EC data in relation to cumulative precipitation could be used to identify thresholds within the event, instead on data from multiple sized events to characterize streamflow response. Multiple events could then be compared to identify trends in the shape of the curves. In other words, a quality over quantity approach to event response.

Runoff ratios and event water suggest that the effective area of SHR is proportionally smaller than GRR and WNC. Characterizing the effective area of these catchments using GIS tools would be beneficial for understanding both the natural effective areas and the impact of the impervious cover and stormwater systems on the effective area of SHR.

Isotopic signatures of surface water and groundwater showed slight differences in the average recharge composition suggesting the SHR is preferentially recharged by snowmelt compared to GRR. Although it is difficult to prove, preferential recharge by snowmelt in SHR

does fit the hypothesis of the interception of rainfall by impervious cover, but why would snowmelt be preferentially recharged by the same surfaces? Understanding how snow gets distributed and artificially moved throughout the urban catchment could help understand how snow is recharged compared to rainfall in the urban environment. Characterizing the groundwater flow boundaries would also be important for understanding the extent of the groundwater contribution area relative to catchment area defined by topography. A more regional groundwater contributing area would impact the composition of recharge due to recharge contributions from outside the catchment.

In addition to understanding snow distribution and winter recharge, the streamflow and groundwater regimes in SHR and GRR were not characterized during the winter months. Groundwater discharge was observed during the winter in both catchments. Frozen soils combined with mid-winter and spring-melt events present a different dynamic for understanding event runoff characteristics within these catchments.

With spatial and temporal variability within and across catchments attributed primarily to geologic heterogeneity, future work might focus on characterizing the shallow overburden that supports groundwater discharge and influences transmission loss. An interesting study would be to use a geophysical method, such as EM-31, to map the shallow subsurface of the ravine bottoms in detail. Correlating geophysical data to high resolution differential gauging (50-100m) would provide interesting insight into the nature of the substrate leading to transmission losses and to groundwater discharge. An idea that was not explored in this study but could be interesting to investigate using high resolution differential gauging and groundwater monitoring is the potential connection of stormwater ponds near the SHR stream have with groundwater and the influence they might have on adjacent groundwater and streamflow.

The gravel deposits observed in the boreholes of SHR are an important control on groundwater in the catchment and probably throughout the region. A pumping test at the SHR wells would be interesting to further characterize the properties and extent of this geologic unit. Another question revolving around the extent of the gravel found in SHR is what the nature of the hydraulic connection is between upstream stream losses and the groundwater discharge at SHR-Springs-2 is? An artificial tracer test might be useful to determine hydraulic connection and transit time.

Although this study is intended to continue long-term monitoring, in the meantime current hydrometric data from studies like this one can be used to inform and calibrate hydrologic models. Hydrologic models could be used to predict long-term impacts of urban development on processes like baseflow, that might not be captured in a short-term study. Findings from this study such as the spatial and temporal variability of streamflow, and the influence of geologic heterogeneity could be used to inform the conceptualization and boundary conditions of a flow model. Not only would hydrologic models be useful for understanding the current development conditions, but they could also be used to predict the impact of new stormwater design concepts and green stormwater infrastructure. For example, rain gardens have been proposed to promote infiltration and reduce the volume of water from rooftops and paved areas entering the stormwater system. Modelling the large-scale implementation of rain gardens is important for understanding the impact of this green infrastructure on local water tables in both the short- and long-term, as well as assessing risk to adjacent infrastructure.

## References

- Ali G, Oswald CJ, Spence C, Cammeraat E, Mcguire KJ, Meixner T, Reaney SM. 2013. Towards a unified threshold-based hydrological theory: Necessary components and recurring challenges. *Hydrological Processes* **27** (2): 313–318 DOI: 10.1002/hyp.9560
- AltaLIS. 10m DEM 82O. TIF file Available at: <https://libguides.ucalgary.ca/guides/GIS/> [Accessed 4 September 2020]
- Anderson MG, Burt TP. 1978. The Role of Topography in Controlling Throughflow Generation. *Earth Surface Processes* **3** (4): 331–344
- Ariano SS, Oswald CJ. 2022a. Broad scale assessment of key drivers of streamflow generation in urban and urbanizing rivers. *Hydrological Processes* **36** (4): 1–15 DOI: 10.1002/hyp.14579
- Ariano SS, Oswald CJ. 2022b. Rapid mobilization of old water during urban stormflow. *Hydrological Processes* **36** (11) DOI: 10.1002/hyp.14745
- Arnold JG, Allen PM, Muttiah R, Bernhardt G. 1995. Automated Base Flow Separation and Recession Analysis Techniques. *Groundwater* **33** (6): 1010–1018
- Baker DB, Richards RP, Loftus TT, Kramer JW. 2004. A new flashiness index: Characteristics and applications to Midwestern rivers and streams. *Journal of the American Water Resources Association* **40** (2): 503–522 DOI: 10.1111/j.1752-1688.2004.tb01046.x
- Barker AA, Riddell JTF, Slattery SR, Andriashek LD, Moktan H, Wallace S, Lyster S, Jean G, Huff GF, Stewart SA, et al. 2011. *Edmonton–Calgary Corridor Groundwater Atlas*. Energy Resources Conservation Board, ERCB/AGS: Edmonton, AB.
- Bell CD, McMillan SK, Clinton SM, Jefferson AJ. 2016. Hydrologic response to stormwater control measures in urban watersheds. *Journal of Hydrology* **541**: 1488–1500 DOI: 10.1016/j.jhydrol.2016.08.049
- Bhaskar AS, Beesley L, Burns MJ, Fletcher TD, Hamel P, Oldham CE, Roy AH. 2016. Will it rise or will it fall? Managing the complex effects of urbanization on base flow. *Freshwater Science* **35** (1): 293–310 DOI: 10.1086/685084
- Blume T, Zehe E, Bronstert A. 2007. Rainfall-runoff response, event-based runoff coefficients and hydrograph separation. *Hydrological Sciences Journal* **52** (5): 843–862 DOI: 10.1623/hysj.52.5.843
- Bonneau J, Burns MJ, Fletcher TD, Witt R, Drysdale RN, Costelloe JF. 2018. The impact of urbanization on subsurface flow paths – A paired-catchment isotopic study. *Journal of Hydrology* **561**: 413–426 DOI: 10.1016/j.jhydrol.2018.04.022

- Booth DB, Jackson CR. 1997. Urbanization of aquatic systems - Degradation thresholds, stormwater detention, and limits of mitigation. *Journal of the American Water Resources Association* **33** (5): 1077–1090
- Boyd MJ, Bufill MC, Knee RM. 1993. Pervious and impervious runoff in urban catchments. *Hydrological Sciences Journal* **38** (6): 463–478 DOI: 10.1080/02626669309492699
- Brown AE, Western AW, McMahon TA, Zhang L. 2013. Impact of forest cover changes on annual streamflow and flow duration curves. *Journal of Hydrology* **483**: 39–50 DOI: 10.1016/j.jhydrol.2012.12.031
- Brown VA, McDonnell JJ, Burns DA, Kendall C. 1999. The role of event water, a rapid shallow flow component, and catchment size in summer stormflow. *Journal of Hydrology* **217** (3–4): 171–190 DOI: 10.1016/S0022-1694(98)00247-9
- Burton TA. 1997. Effects of Basin-scale Timber Harvest on Water Yield and Peak Streamflow. *Journal of the American Water Resources Association* **33** (6): 1187–1196
- Buttle JM. 1994. Isotope hydrograph separations and rapid delivery of pre-event water from drainage basins. *Progress in Physical Geography* **18** (1): 16–41 DOI: 10.1177/030913339401800102
- Cey EE, Rudolph DL, Parkin GW, Aravena R. 1998. Quantifying groundwater discharge to a small perennial stream in southern Ontario, Canada. *Journal of Hydrology* **210** (1–4): 21–37 DOI: 10.1016/S0022-1694(98)00172-3
- Cheng L, Yaeger M, Viglione A, Coopersmith E, Ye S, Sivapalan M. 2012. Exploring the physical controls of regional patterns of flow duration curves - Part 1: Insights from statistical analyses. *Hydrology and Earth System Sciences* **16** (11): 4435–4446 DOI: 10.5194/hess-16-4435-2012
- City of Calgary. Calgary Imagery Available at: <https://maps.calgary.ca/CalgaryImagery/> [Accessed 3 October 2023]
- City of Calgary. 2023. Impervious Surfaces 2021 Available at: <https://data.calgary.ca/Environment/Impervious-Surface-2021/rgsu-3v7u> [Accessed 11 April 2023]
- Clark ID, Fritz P. 1997. *Environmental Isotopes in Hydrogeology*. CRC Press: Boca Raton, FL, USA.
- Clausen JC, Spooner J. 1993. *Paired Watershed Study Design EPA 841-F-93-009*. U.S. Environmental Protection Agency, Office of Water, Washington, DC.
- Dingman SL. 2002. *Physical Hydrology*. Waveland Press, Inc: Long Grove, IL, USA.
- Donato MM. 1998. *Surface-water/ground-water relations in the Lemhi River Basin, east-central Idaho*. U.S. Geological Survey Water Resources Investigations Report 98-4185: 29 pp.

- EBA. 2003. *Spy Hill Lands Provincial Aggregate Operation Hydrogeological Assessment 33-025-2 W5M*. EBA Engineering Consultants LTD: 34 pp.
- Ehsanzadeh E, van der Kamp G, Spence C. 2016. On the changes in long-term streamflow regimes in the North American Prairies. *Hydrological Sciences Journal* **61** (1): 64–78 DOI: 10.1080/02626667.2014.967249
- Ehsanzadeh E, Spence C, van der Kamp G, McConkey B. 2012. On the behaviour of dynamic contributing areas and flood frequency curves in North American Prairie watersheds. *Journal of Hydrology* **414–415**: 364–373 DOI: 10.1016/j.jhydrol.2011.11.007
- Environment and Climate Change Canada (ECCC). 2023. Adjusted and homogenized Canadian climate data Available at: <https://www.canada.ca/en/environment-climate-change/services/climate-change/science-research-data/climate-trends-variability/adjusted-homogenized-canadian-data.html> [Accessed 31 October 2023]
- ESRI Inc. 2021. ArcGIS Pro 2.9.5. Redlands, CA: ESRI Inc. Software
- Fanelli R, Prestegard K, Palmer M. 2017. Evaluation of infiltration-based stormwater management to restore hydrological processes in urban headwater streams. *Hydrological Processes* **31** (19): 3306–3319 DOI: 10.1002/hyp.11266
- Fang X, Minke A, Pomeroy JW, Brown T, Westbrook C, Guo X, Guangul S. 2007. *A review of Canadian Prairie Hydrology: Principles, Modelling and Response to land Use and Drainage Change*. Centre for Hydrology Report 2, University of Saskatchewan: Saskatoon SK.
- Forgrave R, Elliott EM, Bain DJ. 2022. Event scale hydrograph responses highlight impacts of widespread stream burial and urban infrastructure failures. *Hydrological Processes* **36** (5): 1–13 DOI: 10.1002/hyp.14584
- Freeze RA, Cherry JA. 1979. *Groundwater*. Prentice-Hall: Englewood Cliffs, N.J.
- Gelmini Y, Zuecco G, Zaramella M, Penna D, Borga M. 2022. Hysteresis in streamflow-water table relation provides a new classification system of rainfall-runoff events. *Hydrological Processes* **36** (9): 1–16 DOI: 10.1002/hyp.14685
- Grief LA. 2006. Establishing a groundwater monitoring network using rural wells in the West Nose Creek watershed, Alberta. MSc Thesis, University of Calgary, Calgary, AB, Canada: 125 pp.
- Guillemette F, Plamondon AP, Prévost M, Lévesque D. 2005. Rainfall generated stormflow response to clearcutting a boreal forest: Peak flow comparison with 50 world-wide basin studies. *Journal of Hydrology* **302** (1–4): 137–153 DOI: 10.1016/j.jhydrol.2004.06.043
- Gwenzi W, Nyamadzawo G. 2014. Hydrological Impacts of Urbanization and Urban Roof Water Harvesting in Water-limited Catchments: A Review. *Environmental Processes* **1** (4): 573–593 DOI: 10.1007/s40710-014-0037-3

- Hall FR. 1968. Base-Flow Recessions - A Review. *Water Resources Research* **4** (5): 973–983
- Hamblin AP. 2004. *Paskapoo-Porcupine Hills Formations in Western Alberta: Sythesis of Regional Geology and Resource Potential*. Geological Survey of Canada Open File 4679: 31 pp.
- Hamel P, Daly E, Fletcher TD. 2013. Source-control stormwater management for mitigating the impacts of urbanisation on baseflow: A review. *Journal of Hydrology* **485**: 201–211 DOI: 10.1016/j.jhydrol.2013.01.001
- Hayashi M, Farrow CR. 2014. Watershed-scale response of groundwater recharge to inter-annual and inter-decadal variability in precipitation (Alberta, Canada). *Hydrogeology Journal* **22** (8): 1825–1839 DOI: 10.1007/s10040-014-1176-3
- Hewlett JD, Lull HW, Reinhart KG. 1969. In Defense of Experimental Watersheds. *Water Resources Research* **5** (1): 306–316 DOI: 10.1029/WR005i001p00306
- Hooper RP, Shoemaker CA. 1986. A Comparison of Chemical and Isotopic Hydrograph Separation. *Water Resources Research* **22** (10): 1444–1454 DOI: 10.1029/WR022i010p01444
- Hopkins KG, Morse NB, Bain DJ, Bettez ND, Grimm NB, Morse JL, Palta MM, Shuster WD, Bratt AR, Suchy AK. 2015. Assessment of regional variation in streamflow responses to urbanization and the persistence of physiography. *Environmental Science and Technology* **49** (5): 2724–2732 DOI: 10.1021/es505389y
- Hvorslev MJ. 1951. *Time Lag and Soil Permeability in Ground-Water Observations*. U.S. Army Corps of Engineers, Waterways Experiment Station, Bulletin No. 36: Vicksburg, MS, USA.
- Jefferson AJ, Bell CD, Clinton SM, Mcmillan SK. 2015. Application of isotope hydrograph separation to understand contributions of stormwater control measures to urban headwater streams. *Hydrological Processes* **29** (25): 5290–5306 DOI: 10.1002/hyp.10680
- Jefferson AJ, Hopkins KG, Fanelli R, Avellaneda PM, Mcmillan SK. 2017. Stormwater management network effectiveness and implications for urban watershed function : A critical review. *Hydrological Processes* **31** (23): 4056–4080 DOI: 10.1002/hyp.11347
- Kayembe A, Mitchell CPJ. 2018. Determination of subcatchment and watershed boundaries in a complex and highly urbanized landscape. *Hydrological Processes* **32** (18): 2845–2855 DOI: 10.1002/hyp.13229
- Klaus J, McDonnell JJ. 2013. Hydrograph separation using stable isotopes: Review and evaluation. *Journal of Hydrology* **505**: 47–64 DOI: 10.1016/j.jhydrol.2013.09.006
- Laudon H, Slaymaker O. 1997. Hydrograph separation using stable isotopes, silica and electrical conductivity: An alpine example. *Journal of Hydrology* **201** (1–4): 82–101 DOI: 10.1016/S0022-1694(97)00030-9

- Leopold LB. 1968. *Hydrology for Urban Land Planning - A Guidebook on the Hydrologic Effects of Urban Land Use*. U.S. Geological Survey Circular 554: 18 pp.
- Liu Z, Higgins CW. 2015. Does temperature affect the accuracy of vented pressure transducer in fine-scale water level measurement? *Geoscientific Instrumentation, Methods and Data Systems* **4** (1): 65–73 DOI: 10.5194/gi-4-65-2015
- Maule CP, Chanasyk DS, Muehlenbachs K. 1994. Isotopic determination of snow-water contribution to soil water and groundwater. *Journal of Hydrology* **155** (1–2): 73–91 DOI: 10.1016/0022-1694(94)90159-7
- McDonnell JJ, Stewart MK, Owens IF. 1991. Effect of Catchment-Scale Subsurface Mixing on Stream Isotopic Response. *Water Resources Research* **27** (12): 3065–3073
- McGlynn BL, McDonnell JJ, Seibert J, Kendall C. 2004. Scale effects on headwater catchment runoff timing, flow sources, and groundwater-streamflow relations. *Water Resources Research* **40** (7): 1–14 DOI: 10.1029/2003WR002494
- Mcgrath GS, Hinz C, Sivapalan M. 2007. Temporal dynamics of hydrological threshold events. *Hydrology and Earth System Sciences* **11** (2): 923–938
- McMahon TA, Nathan RJ. 2021. Baseflow and transmission loss: A review. *Wiley Interdisciplinary Reviews: Water* **8** (4): 1–30 DOI: 10.1002/wat2.1527
- McNamara JP, Kane DL, Hinzman LD. 1997. Hydrograph separations in an Arctic watershed using mixing model and graphical techniques. *Water Resources Research* **33** (7): 1707–1719 DOI: 10.1029/97WR01033
- McPhillips LE, Earl SR, Hale RL, Grimm NB. 2019. Urbanization in Arid Central Arizona Watersheds Results in Decreased Stream Flashiness. *Water Resources Research* **55** (11): 9436–9453 DOI: 10.1029/2019WR025835
- Meyer JL, Paul MJ, Taulbee WK. 2005. Stream ecosystem function in urbanizing landscapes. *Journal of the North American Benthological Society* **24** (3): 602–612 DOI: 10.1899/04-021.1
- Moran SR. 1986. *Surficial Geology of the Calgary Urban Area*. Alberta Research Council Bulletin No. 53: Edmonton, AB, Canada.
- Neary DG. 2016. Long-term forest paired catchment studies: What do they tell us that landscape-level monitoring does not? *Forests* **7**: 164 DOI: 10.3390/f7080164
- Oswald CJ, Kelleher C, Ledford SH, Hopkins KG, Sytsma A, Tetzlaff D, Toran L, Voter C. 2023. Integrating urban water fluxes and moving beyond impervious surface cover: A review. *Journal of Hydrology* **618**: 129188 DOI: 10.1016/j.jhydrol.2023.129188

- Paul MJ, Meyer JL. 2001. Streams in the Urban Landscape. *Annual review of Ecology and Systematics* **32** (1): 333–365
- Payn RA, Gooseff MN, McGlynn BL, Bencala KE, Wondzell SM. 2012. Exploring changes in the spatial distribution of stream baseflow generation during a seasonal recession. *Water Resources Research* **48**: W04519 DOI: 10.1029/2011WR011552
- Pearce AJ, Stewart MK, Sklash MG. 1986. Storm Runoff Generation in Humid Headwater Catchments 1. Where Does the Water Come From? *Water Resources Research* **22** (8): 1263–1272
- Pellerin BA, Wollheim WM, Feng X, Vorosmarty CJ. 2008. The application of electrical conductivity as a tracer for hydrograph separation in urban catchments. *Hydrological Processes* **22** (12): 1810–1818 DOI: 10.1002/hyp.6786
- Peng H, Mayer B, Harris S, Krouse HR. 2004. A 10-yr record of stable isotope ratios of hydrogen and oxygen in precipitation at Calgary, Alberta, Canada. *Tellus* **56B**: 147–159 DOI: 10.3402/tellusb.v56i2.16410
- Petrakis RE, Norman LM, Vaughn K, Pritzlaff R, Weaver C, Rader A, Pulliam HR. 2021. Hierarchical Clustering for Paired Watershed Experiments: Case Study in Southeastern Arizona, U.S.A. *Water* **13**: 2955 DOI: 10.3390/w13212955
- Petrucci G, Rodriguez F, Deroubaix JF, Tassin B. 2014. Linking the management of urban watersheds with the impacts on the receiving water bodies: The use of flow duration curves. *Water Science and Technology* **70** (1): 127–135 DOI: 10.2166/wst.2014.206
- Pilgrim DH, Huff DD, Steele TD. 1979. Use of specific conductance and contact time relations for separating flow components in storm runoff. *Water Resources Research* **15** (2): 329–339 DOI: 10.1029/WR015i002p00329
- Price K. 2011. Effects of watershed topography, soils, land use, and climate on baseflow hydrology in humid regions: A review. *Progress in Physical Geography* **35** (4): 465–492 DOI: 10.1177/0309133311402714
- Risley JC, Stonewall A, Haluska TL. 2008. *Estimating flow-duration and low-flow frequency statistics for unregulated streams in Oregon*. U.S. Geological Survey Scientific Investigations Report 2008-5126: 22 pp.
- Roodsari BK, Chandler DG. 2017. Distribution of surface imperviousness in small urban catchments predicts runoff peak flows and stream flashiness. *Hydrological Processes* **31** (17): 2990–3002 DOI: 10.1002/hyp.11230
- Rosenberry DO, LaBaugh JW. 2008. *Field Techniques for Estimating Water Fluxes Between Surface Water and Ground Water*. U.S. Geological Survey Techniques and Methods 4-D2: 128 pp.

- Ross CA, Ali G, Bansah S, Laing JR. 2017. Evaluating the Relative Importance of Shallow Subsurface Flow in a Prairie Landscape. *Vadose Zone Journal* **16** (5) DOI: 10.2136/vzj2016.10.0096
- Ross CA, Ali GA, Spence C, Courchesne F. 2021. Evaluating the Ubiquity of Thresholds in Rainfall-Runoff Response Across Contrasting Environments. *Water Resources Research* **57** (1): 1–22 DOI: 10.1029/2020WR027498
- Ross CA, Ali G, Spence C, Oswald C, Casson N. 2019. Comparison of event-specific rainfall–runoff responses and their controls in contrasting geographic areas. *Hydrological Processes* **33** (14): 1961–1979 DOI: 10.1002/hyp.13460
- Ruehl C, Fisher AT, Hatch C, Huertos ML, Stemler G, Shennan C. 2006. Differential gauging and tracer tests resolve seepage fluxes in a strongly-losing stream. *Journal of Hydrology* **330** (1–2): 235–248 DOI: 10.1016/j.jhydrol.2006.03.025
- Sauer VB, Meyer RW. 1992. *Determination of Error in Individual Discharge Measurements*. U.S. Geological Survey Open-File Report 92-144: 21 pp.
- Searcy JK. 1959. Flow-Duration Curves. In *Manual of Hydrology: Part 2. Low-Flow Techniques* U.S. Geological Survey Water-Supply Paper 1542-A: 33 pp. DOI: 10.3133/wsp1542A
- Shaughnessy AR, Prener CG, Hasenmueller EA. 2019. An R package for correcting continuous water quality monitoring data for drift. *Environmental Monitoring and Assessment* **191** (7): 1–10 DOI: 10.1007/s10661-019-7586-x
- Shaw DA, Pietroniro A, Martz LW. 2013. Topographic analysis for the prairie pothole region of Western Canada. *Hydrological Processes* **27** (22): 3105–3114 DOI: 10.1002/hyp.9409
- Sklash MG, Farvolden RN. 1979. The role of groundwater in storm runoff. *Developments in Water Science* **12** (C): 45–65 DOI: 10.1016/S0167-5648(09)70009-7
- Sklash MG, Stewart MK, Pearce AJ. 1986. Storm Runoff Generation in Humid Headwater Catchments 2. A Case Study of Hillslope and Low-Order Stream Response. *Water Resources Research* **22** (8): 1273–1282
- Smakhtin VU. 2001. Low flow hydrology: a review. *Journal of Hydrology* **240** (3–4): 147–186
- Smith BK, Smith JA, Baeck ML, Villarini G, Wright DB. 2013. Spectrum of storm event hydrologic response in urban watersheds. *Water Resources Research* **49** (5): 2649–2663 DOI: 10.1002/wrcr.20223
- Spence C. 2007. On the relation between dynamic storage and runoff: A discussion on thresholds, efficiency, and function. *Water Resources Research* **43** (12): 1–11 DOI: 10.1029/2006WR005645

- Sulam DJ. 1979. Analysis of changes in ground-water levels in a sewered and an unsewered area of Nassau County, Long Island, New York. *Groundwater* **17** (5): 446–455
- Sultana R, Mroczek M, Sengupta A, Dallman S, Stein ED. 2020. Improving Effective Impervious Estimates to Inform Stormwater Management. *Water Resources Management* **34** (2): 747–762 DOI: 10.1007/s11269-019-02474-7
- Turnipseed DP, Sauer VB. 2010. *Discharge measurements at gaging stations*. U.S. Geological Survey Techniques and Methods book 3, chap. A8: 87 pp.
- van der Kamp G, Hayashi M. 2009. Groundwater-wetland ecosystem interaction in the semiarid glaciated plains of North America. *Hydrogeology Journal* **17** (1): 203–214 DOI: 10.1007/s10040-008-0367-1
- Vogel RM, Fennessey NM. 1994. Flow-Duration Curves I: New Interpretation and Confidence Intervals. *Journal of Water Resources Planning and Management* **120** (4): 485–504
- Vogel RM, Fennessey NM. 1995. Flow Duration Curves II: A Review of Applications in Water Resources Planning. *Water Resources Bulletin* **31** (6): 1029–1039
- von Freyberg J, Studer B, Rinderer M, Kirchner JW. 2018. Studying catchment storm response using event- and pre-event-water volumes as fractions of precipitation rather than discharge. *Hydrology and Earth System Sciences* **22** (11): 5847–5865 DOI: 10.5194/hess-22-5847-2018
- Walsh CJ, Fletcher TD, Burns MJ. 2012. Urban Stormwater Runoff: A New Class of Environmental Flow Problem. *PLoS ONE* **7** (9): e45814 DOI: 10.1371/journal.pone.0045814
- Walsh CJ, Roy AH, Feminella JW, Cottingham PD, Groffman PM, Morgan RP. 2005. The urban stream syndrome: Current knowledge and the search for a cure. *Journal of the North American Benthological Society* **24** (3): 706–723 DOI: 10.1899/04-028.1
- Weiler M, McDonnell J. 2004. Virtual experiments: A new approach for improving process conceptualization in hillslope hydrology. *Journal of Hydrology* **285** (1–4): 3–18 DOI: 10.1016/S0022-1694(03)00271-3
- Weiler M, McDonnell JJ, Tromp-van Meerveld I, Uchida T. 2005. Subsurface Stormflow. *Encyclopedia of Hydrological Sciences*: 1–14 DOI: 10.1002/0470848944.hsa119
- Winter TC. 2007. The role of ground water in generating streamflow in headwater areas and in maintaining base flow. *Journal of the American Water Resources Association* **43** (1): 15–25 DOI: 10.1111/j.1752-1688.2007.00003.x
- Winter TC, Harvey JW, Franke OL, Alley WM. 1998. *Ground Water and Surface Water - A Single Resource*. U.S. Geological Survey Circular 1139: 79 pp. DOI: 10.3133/CIR1139

- Winter TC, Rosenberry DO, Labaugh JW. 2003. Where Does the Ground Water in Small Watersheds Come From? *Groundwater* **41** (7): 989–1000 DOI: 10.1111/j.1745-6584.2003.tb02440.x
- Wittenberg H. 2003. Effects of season and man-made changes on baseflow and flow recession: Case studies. *Hydrological Processes* **17** (11): 2113–2123 DOI: 10.1002/hyp.1324
- Ye S, Yaeger M, Coopersmith E, Cheng L, Sivapalan M. 2012. Exploring the physical controls of regional patterns of flow duration curves - Part 2: Role of seasonality, the regime curve, and associated process controls. *Hydrology and Earth System Sciences* **16** (11): 4447–4465 DOI: 10.5194/hess-16-4447-2012

## Appendix A: Catchment Delineation

Catchment boundaries for this study were delineated using the ‘Watershed’ tool in ArcGIS Pro (ESRI Inc., 2021). The DEM used to delineate the boundaries is 10m resolution and was completed in 1984 (AltaLIS n.d.). The catchment boundaries were then manually corrected and smoothed for pixelation. Table A1 is the culmination of catchment areas determined for each gauging station using this method. Figure A1 is the visual representation of the completed catchments and the contours of the DEM used to delineate the catchments.

Table A1. Summary of catchment areas for each gauging station in this study.

SHR						
Catchment area (km <sup>2</sup> )	SW1	SW2	SW3	SW4	SW5	Total
	4.69	8.54	9.16	9.54	9.94	10.1
GRR						
Catchment area (km <sup>2</sup> )	SW1	SW2	SW3	SW4	Total	
	0.599	1.18	1.37	1.43	2.03	
WNC						
Catchment area (km <sup>2</sup> )	WNC GS					
	244					

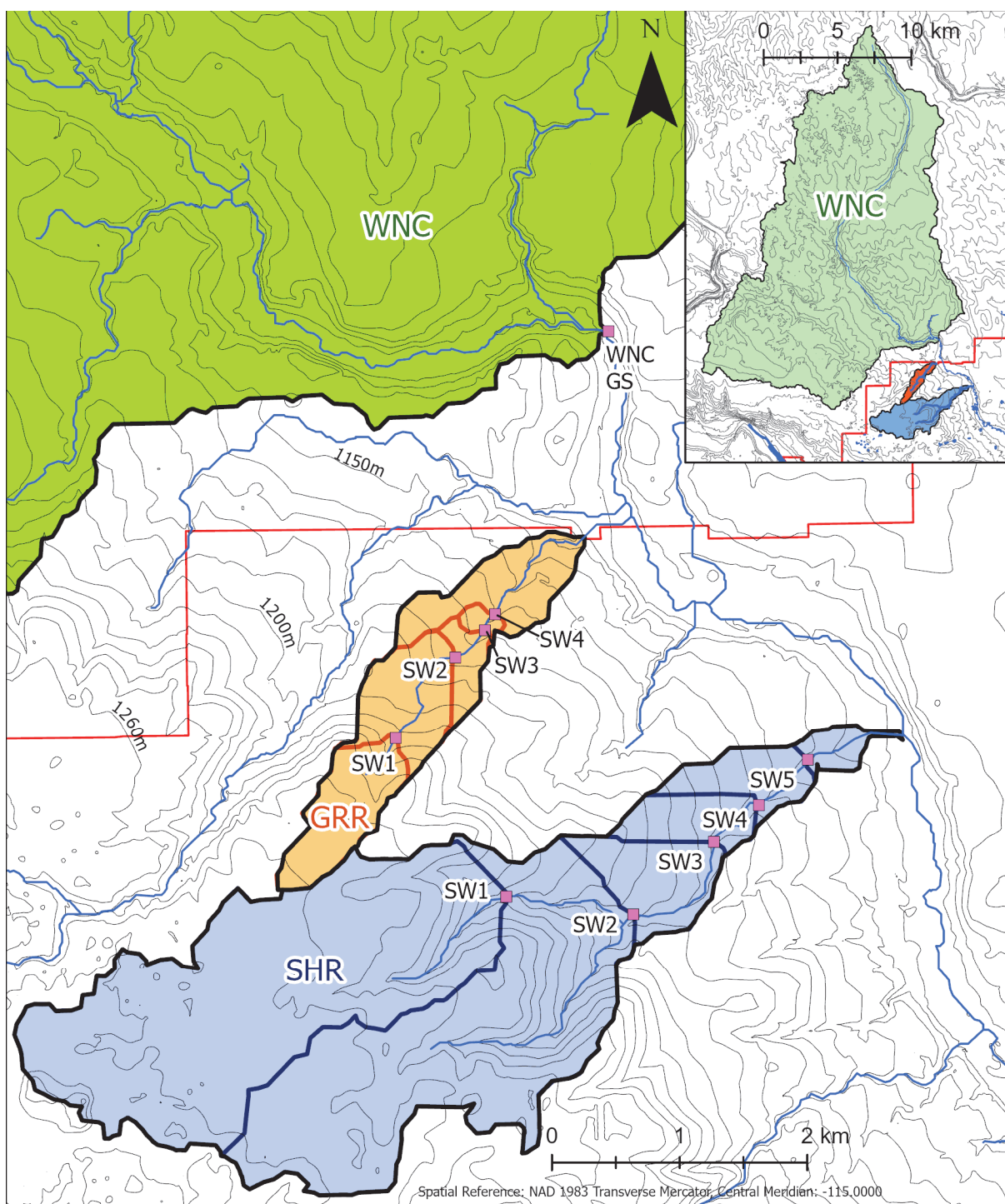


Figure A1. Map of the catchment boundaries for each gauging station with the 10m contour lines of the DEM (AltaLIS n.d.) used to generate the catchment boundaries.

## Appendix B: Site Photographs



Figure B1. Photograph from the south slope of SHR facing downstream near SHR-SW4. Photo taken June 3, 2022.



Figure B2. Photograph from the east slope of GRR facing downstream near GRR-MW1. Photo taken July 7, 2021.



Figure B3. Photograph from north bank of GRR stream facing upstream of the farmed cropland between GRR-SW1 and GRR-SW2. Photo taken May 13, 2021.



Figure B4. Photograph from the north slope of SHR facing downstream of the SHR-Springs-1. Photo taken May 3, 2023.



Figure B5. Photograph of a typical culvert stream gauging station at SHR-SW3 facing downstream. Photo taken July 22, 2021.



Figure B6. Photograph of a v-notch weir stream gauging station at GRR-SW4 facing upstream. Photo taken June 16, 2022.

## Appendix C: Borehole Logs and Well Completions


HOLE ID: SHR20-MW1A			DRILL START/FINISHED: Nov. 9, 2020	
			CONTRACTOR: Earth Drilling	
PROJECT: Paired watershed study			DRILLING METHOD: ODEX	
LOCATION: Sage Hill, Calgary, AB			UTM: E: 699410.52 N: 5673521.98	
FIELD INVESTIGATOR: Sam Johnson			TOC ELEVATION: 1134.411	
Well Completion	Depth (m) (ft)	BH Log	Lithological Description	
<div><div><div><div><div>- Stick up: 1.036m</div><div>- 51mm solid PVC: 0.0 - 8.3 mBGS</div><div>- Bentonite chips: 0.0 - 8.4 mBGS</div><div>- Coated peltonite: 8.4 - 8.9 mBGS</div><div>- 51mm slotted PVC (10-slot): 8.3 - 9.1 mBGS (2.5ft)</div><div>- Sand filter pack: 8.9 - 10.0 mBGS</div><div>- Well installation compromised by bentonite bridging in the drill casing. Well completion rose roughly 2.5ft during the extraction of the drill equipment. It is likely that bentonite is on well screen and in filter pack. End of well screen was measured after well was developed on Dec. 24, 2020.</div></div></div><div><div><div><div><div>0</div><div>0</div></div><div><div>5</div><div>2</div></div><div><div>10</div><div>4</div></div><div><div>15</div><div>6</div></div><div><div>20</div><div>8</div></div><div><div>25</div><div>10</div></div><div><div>30</div><div>12</div></div><div><div>35</div><div>14</div></div><div><div>40</div><div>16</div></div><div><div>45</div><div>18</div></div><div><div>50</div><div>20</div></div></div><div><div><div><div><div>Topsoil - Clay, silt, gravel mixed in</div><div>Gravel - Mostly broken gravel, some smaller rounded pebbles, clay and silt present</div><div>- Smaller gravel mixed with 2cm pebbles and clay, moist</div><div>- 1cm - 2cm gravel with clay matrix</div><div>- 2mm - 2cm gravel with sandy-clay matrix</div><div>- Muddy gravel with clay, gravel is larger ~2cm</div><div>- Coarse gravel with clay matrix</div><div>- Less return, mostly gravel still, but more fine sediment - could be smashed rock though</div><div>- High plasticity clay with 1-2cm pebbles</div><div>Clay - High plasticity, fine grained</div><div>Bedrock (Shale) - Pulverized pieces of shale, wet</div><div>- Tons of water while drilling - probably weathered if it is shale, taking a long time to drill, pieces of oxidized sst.</div><div>Bottom of hole: 32.8 ft</div></div></div></div></div></div></div><div><div>ABBREVIATIONS: mBGS: meters below ground surface TOC: top of casing</div><div>COORDINATE SYSTEM: NAD83 UTM Z11</div><div>PAGE 1 OF 1</div></div></div></div>				



HOLE ID: <b>SHR20-MW2A</b>			DRILL START/FINISHED: Nov. 9, 2020	
			CONTRACTOR: Earth Drilling	
PROJECT: Paired watershed study			DRILLING METHOD: ODEX	
LOCATION: Sage Hill, Calgary, AB			UTM: E: 699428.95 N: 5673581.34	
FIELD INVESTIGATOR: Sam Johnson			TOC ELEVATION: 1138.08	
Well Completion	Depth (m) (ft)	BH Log	Lithological Description	
- Stick up: 0.630m - 51mm solid PVC: 0.0 - 13.3 mBGS	0		Topsoil - Organics, clay, silt, some gravel, dry	
	5		Gravel - Gravel with some silt and clay - Pebbles 1mm - 1cm, Dry	
- Bentonite chips: 0.0 - 5.8 mBGS	10		- Some angular and rounded yellow sst. Pebbles 1cm in size	
	15		- Lots of angular gravels - probably from ODEX, silty clay matrix	
- Slough: 5.8 - 11.7 mBGS	20		- Gravel is cleaner - less fines	
	25		- Mostly gravel still, more fines again though	
- Coated peltonite: 11.7 - 12.8 mBGS	30		- Sand and gravel	
	35		- Sand and gravel, likely hit water table btw. 23-24 ft	
- Sand filter pack: 12.8 - 14.0 mBGS	40		- Water spraying out rig, fully saturated sand and gravel with suspended fines	
	45		- Coarse sand, gravel, and clay globs	
- 51mm slotted PVC (10-slot): 13.3 - 14.0 mBGS (2.5ft)	50		- More silt, still large pebbles	
			Clay - Silty clay, trace gravel	
			- Saturated, clay-rich, stones are angular 1mm - 1cm	
			- Crumbly clay globs with with small gravel, some chunks of bedrock	
			Bedrock (Shale) - Black mudstone, slightly oxidized, mostly pulverized	
			- Mix of bedrock and silty clay with pebbles	
			- Pulverized bedrock	
			Bottom of hole: 46 ft	
ABBREVIATIONS: mBGS: meters below ground surface TOC: top of casing			COORDINATE SYSTEM: NAD83 UTM Z11	



HOLE ID: <b>GRR21-MW1</b>		DRILL START/FINISHED: July 7, 2021	
		CONTRACTOR: Mobile Augers	
PROJECT: Paired watershed study		DRILLING METHOD: Solid Stem	
LOCATION: Glacier Ridge, Calgary, AB		UTM: E: 697227.27 N: 5674825.32	
FIELD INVESTIGATOR: Sam Johnson		TOC ELEVATION: 1167.968	
Well Completion	Depth (m) (ft)	BH Log	Lithological Description
<div> <div> <div>- Stick up: 0.862m</div> <div>- 51mm solid PVC: 0.0 - 10.4 mBGS</div> <div>- Bentonite chips: 0.0 - 3.4 mBGS</div> <div>- Slough and drill cuttings: 3.4 - 8.5 mBGS</div> <div>- Coated peltonite: 8.5 - 9.7 mBGS</div> <div>- Sand filter pack: 9.8 - 11.9 mBGS</div> <div>- 51mm slotted PVC (10-slot): 10.4 - 11.9 mBGS</div> </div> <div> <div>0</div> <div>5</div> <div>10</div> <div>15</div> <div>20</div> <div>25</div> <div>30</div> <div>35</div> <div>40</div> <div>45</div> <div>50</div> </div> <div> <div>0</div> <div>5</div> <div>10</div> <div>15</div> <div>20</div> <div>25</div> <div>30</div> <div>35</div> <div>40</div> <div>45</div> <div>50</div> </div> </div>			
<div> <div>*****</div> <div>*****</div> <div>*****</div> <div>*****</div> </div> <div> <div>Topsoil - organics, poor recovery</div> <div>Silty Clay (Till) - Fine to very fine sand and silt with high clay content, brown, trace gravel</div> <div>- Dry, crumbly, calcite precipitate, small pebbles with some larger stones, very stiff, roots</div> <div>- Oxidation staining, clay clumps, trace pebbles and larger stones</div> <div>- Chunks of coal at 8 ft.</div> <div>- Clay matrix with stones and coal chunks, not coherent yet, mottled, oxidized</div> <div>- Water content appears to be increasing</div> <div>- Clay content appears to be increasing, mottling</div> <div>- Weathered and oxidized still</div> <div>- Saturated btw. 28 and 29 ft., increase in pebble content</div> <div>- Easier drilling, starting to get darker brown, possibly some unoxidized layers, saturated on outside but seems dry on inside</div> <div>- Poor recovery</div> <div>- Rig pause at 38 ft. pieces of thin dry rock on auger at 38 ft., Refusal at 39 ft</div> </div>			
Bottom of hole: 39 ft, slough to 37.5 ft after pulling auger, water is 21.5 ft BGS			
ABBREVIATIONS: mBGS: meters below ground surface TOC: top of casing		COORDINATE SYSTEM: NAD83 UTM Z11	

HOLE ID: GRR21-MW2			DRILL START/FINISHED: July 7, 2021	
			CONTRACTOR: Mobile Augers	
PROJECT: Paired watershed study			DRILLING METHOD: Hollow Stem	
LOCATION: Glacier Ridge, Calgary, AB			UTM: E: 697203.05 N: 5674836.83	
FIELD INVESTIGATOR: Sam Johnson			TOC ELEVATION: 1162.652	
Well Completion	Depth (m) (ft)	BH Log	Lithological Description	
<div><div><div><div>- Stick up: 0.672m</div><div>- 51mm solid PVC: 0.0 - 6.1 mBGS</div><div>- Bentonite chips: 0.0 - 5.8 mBGS</div><div>- Sand filter pack: 5.8 - 7.6 mBGS</div><div>- 51mm slotted PVC (10-slot): 6.1 - 7.6 mBGS</div></div><div></div></div><div><div><div>00</div><div>5</div><div>2</div><div>10</div><div>4</div><div>15</div><div>6</div><div>20</div><div>25</div><div>8</div><div>30</div><div>10</div><div>35</div><div>12</div><div>40</div><div>45</div><div>14</div><div>50</div></div><div><div>*****</div><div>*****</div><div>*****</div><div>Clay (Till) - Brown clay with mottles, trace gravel</div><div>- Organics, clay, poor recovery</div><div>- Brownish, mottled clay with some stones, calcite precipitates, malleable, easily indented with thumb</div><div>- Very malleable, clay-rich, still too stiff to sample with soil ring</div><div>- Stiff, difficult to indent</div><div>- Poor recovery, small coal chunks</div><div>- Lots of small pebbles, roots in middle of core</div><div>- Poor recovery, full push, some sand veins in the end of core</div><div>- Haven't hit bedrock yet</div><div>Bottom of hole: 25 ft, hole is dry at completion</div></div></div></div>				
ABBREVIATIONS: mBGS: meters below ground surface TOC: top of casing			COORDINATE SYSTEM: NAD83 UTM Z11	
			PAGE 1 OF 1	

HOLE ID: <b>GRR21-MW3</b>		DRILL START/FINISHED: July 7, 2021	
		CONTRACTOR: Mobile Augers	
PROJECT: Paired watershed study		DRILLING METHOD: Solid Stem	
LOCATION: Glacier Ridge, Calgary, AB		UTM: E: 697185.12 N: 5674478.15	
FIELD INVESTIGATOR: Sam Johnson		TOC ELEVATION: 1183.176	
Well Completion	Depth (m) (ft)	BH Log	Lithological Description
<div> <div> <div>- Stick up: 0.953m</div> <div>- 51mm solid PVC: 0.0 - 2.7 mBGS</div> <div>- Bentonite chips: 0.0 - 2.4 mBGS</div> <div>- Sand filter pack: 2.4 - 5.2 mBGS</div> <div>- 51mm slotted PVC (10-slot): 2.7 - 5.8 mBGS</div> <div>- Slough: 5.2 - 6.1 mBGS</div> </div> <div> </div> </div>			
	<div> <div>0</div> <div>0</div> <div>5</div> <div>2</div> <div>10</div> <div>4</div> <div>15</div> <div>6</div> <div>20</div> <div>25</div> <div>8</div> <div>30</div> <div>10</div> <div>35</div> <div>12</div> <div>40</div> <div>14</div> <div>45</div> <div>50</div> </div>	<div> <div>***</div> <div>Topsoil</div> <div>Clay (Till) - Brown, mottled, oxidized, trace gravel</div> <div>- Soft</div> <div>- Firmer near bottom of auger section</div> <div>- Clay with larger pebbles and stones</div> <div>- Sand stringer at 9 ft</div> <div>Gravelly Clay - Clay with high gravel content, larger stones</div> <div>- Thin gravel seams at 10 ft and 15 ft</div> <div>Clay (Till) - Stiff brown clay till</div> </div>	<div> <div>Bottom of hole: 20 ft, Slough to 15 ft initially - hole cleaned out, sloughed again to 17 ft, screen driven in 2 ft</div> </div>
ABBREVIATIONS: mBGS: meters below ground surface TOC: top of casing		COORDINATE SYSTEM: NAD83 UTM Z11	

## Appendix D: Hydraulic Conductivity Tests

Hydraulic conductivity values estimated using slug tests were estimated using the Hvorslev (1951) method in Aqtesolv. The underlying equation of the Hvorslev (1951) method is:

$$K = \frac{r^2 \ln\left(\frac{L}{R}\right)}{2L(t_2 - t_1)} \ln\left(\frac{H_1}{H_2}\right) \quad (C1)$$

Table D1. Summary of variables in Hvorslev (1951) equations.

Symbol	Description	Units
r	Casing radius	(m)
L	Screen/Filter pack length	(m)
R	Screen/Borehole radius	(m)
t <sub>i</sub>	time	(s)
H <sub>i</sub>	Displacement at t <sub>i</sub>	(m)

The hydraulic conductivity was estimated by manually fitting the Hvorslev (1951) solution to the time-displacement data on a log-linear plot of normalized displacement versus time in Aqtesolv. Figure D1 is an example output for SHR-MW2A.

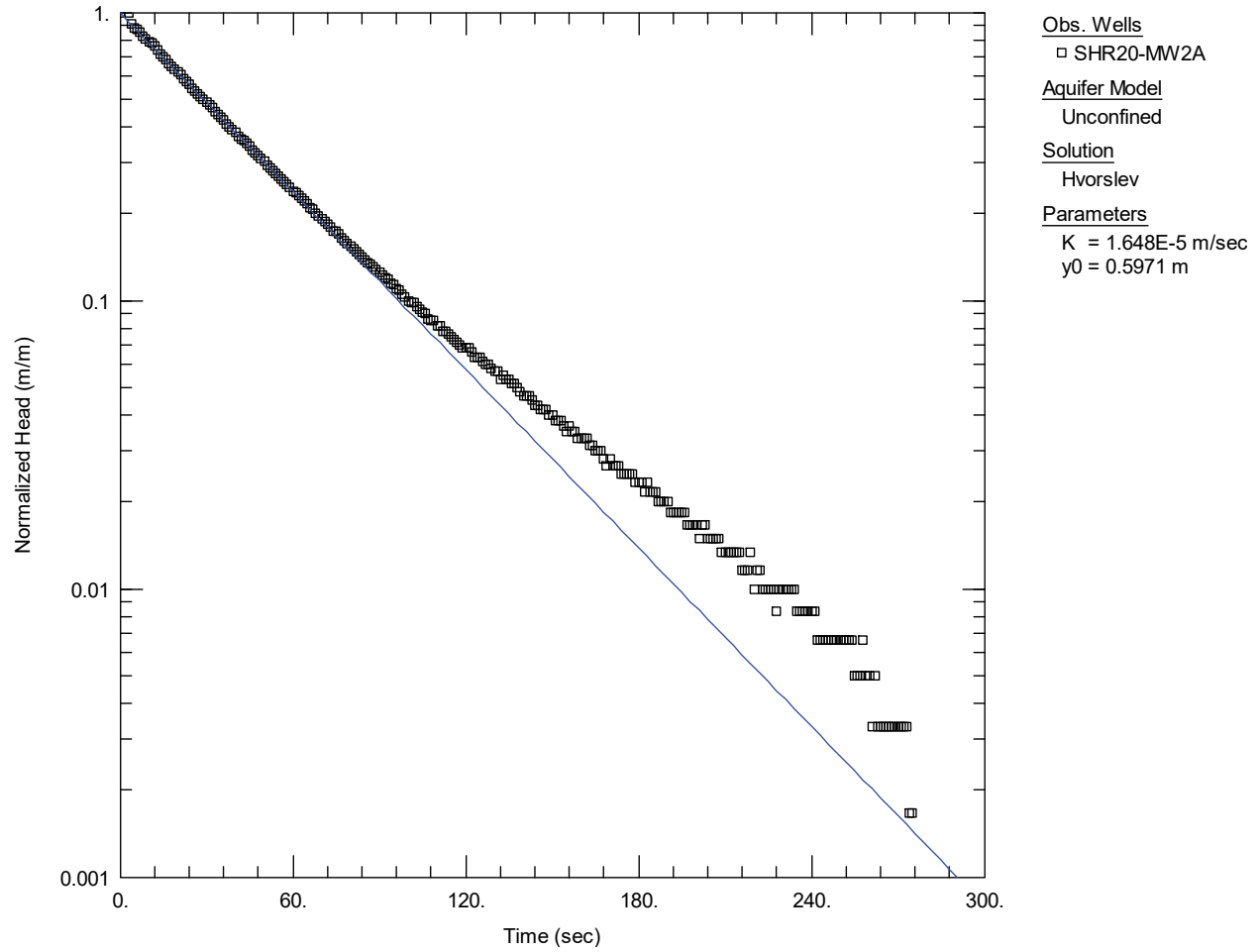


Figure D1. Hydraulic conductivity estimation using the Hvorslev solution in Aqtesolv. Blue line is the manual fit to the pressure transducer data (black squares). The estimated  $K$  for SHR-MW2A is  $2 \times 10^{-5} \text{ m/s}$ .

Hydraulic conductivity determined using constant flow tests were estimated manually using the Hvorslev (1951) steady state flow equation:

$$K = \frac{Q}{FH} \quad (C2)$$

where  $Q$  is the flow rate in ( $\text{m}^3/\text{s}$ ) and  $F$  is the shape factor for the completion interval in (m):

$$F = \frac{2\pi L}{\ln\left(\frac{L}{R}\right)} \quad (C3)$$

Flow rate was calculated by pumping the well and timing how long it took to fill a calibrated bucket. Displacement was calculated by measuring the water level before the test and after the last bucket was filled. Table D2 is an example calculation for SHR-MW1B.

Table D2: Data for constant flow test with example calculation for SHR-MW1B.

		Water level before test (mBTOC) =	2.699
		End of test water level (mBTOC) =	2.728
		End of test drawdown (m) =	0.029
Bucket #	Time to fill 4L (s)	Q (L/min)	Q (m <sup>3</sup> /s)
1	-	-	-
2	56.11	4.28	7.1E-05
3	57.48	4.18	7.0E-05
4	56.49	4.25	7.1E-05
5	58.28	4.12	6.9E-05
6	57.13	4.20	7.0E-05
7	57.55	4.17	7.0E-05
		Q <sub>avg</sub> (m <sup>3</sup> /s) =	7.0E-05
		H (m) =	0.029
		L (m) =	0.762
		R (m) =	0.03
		F (m) =	1.48
		<b>K (m/s) =</b>	<b>2E-03</b>

All hydraulic conductivity test data and calculations can be found in the supplementary data folder under: “**HydraulicConductivityTests.xlsx**”.

## Appendix E: Rating Curves

Stage-discharge relationships for each gauging station were determined using the equation:

$$Q_s = C(h - a)^n \quad (D1)$$

where  $Q_s$  (L/s) is the stream discharge,  $h$  (m) is the stream stage, and  $C$ ,  $a$  (m) and  $n$  are constants. The constants were calculated using the least squares method to minimize the error between manual discharge measurements and the calculated discharge (Eq. D1) for the corresponding stage measurement. The least squares error was then used to calculate the root mean squared error (RMS) for each gauging station. Stream stage for all SHR and GRR stream gauging stations was calibrated to a fixed point where  $Q_s = 0$  L/s when  $h = 0.000$ m. Therefore, the stage offset for all SHR and GRR gauging stations is  $a = 0.000$ m. The constants and RMS for all gauging stations used in this study are summarized in Table E1. The stage-discharge rating curves for gauging stations are summarized in Figures E1, E2, and E3. Due to sediment build up in the GRR-SW1 culvert after precipitation events, the rating curve was adjusted periodically in an attempt to account for changes in the stage-discharge relationship (Figure E1).

Table E1. Summary of constants and root mean squared error (RMS) for all stream gauging stations used in this study.

Gauging Station	C	a (m)	n	RMS (L/s)
GRR-SW1	7125	0.000	3.1	0.4
GRR-SW1 <sup>a</sup>	17866	0.000	3.8	0.0
GRR-SW1 <sup>b</sup>	32767	0.000	4.2	0.5
GRR-SW2	498	0.000	2.4	0.1
GRR-SW3	676	0.000	2.6	0.1
GRR-SW4	965	0.000	2.4	0.1
SHR-SW1	2073	0.000	2.0	0.6
SHR-SW2	4215	0.000	2.3	1.5
SHR-SW3	2040	0.000	2.3	1.0
SHR-SW4	859	0.000	2.2	2.2
SHR-SW5	1293	0.000	2.0	2.2
WNC GS	2195	0.306	1.1	25

<sup>a</sup> GRR-SW1 rating curve adjusted after sediment build up in culvert from event on 2022-07-07.

<sup>b</sup> GRR-SW1 rating curve adjusted after further sediment build up in culvert from event on 2022-07-30

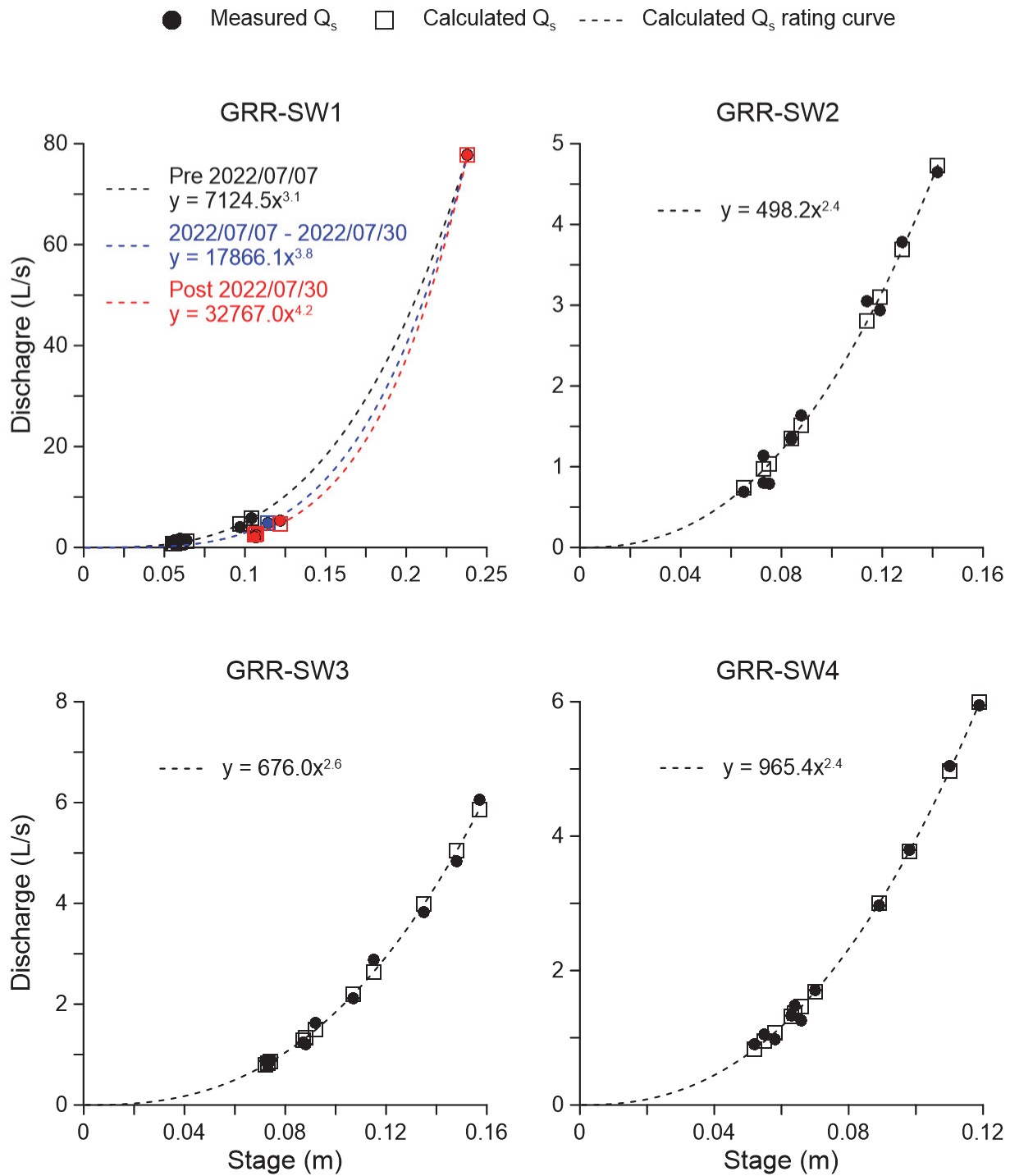


Figure E1. Summary of stage-discharge rating curves for GRR-SW1, GRR-SW2, GRR-SW3, and GRR-SW4. Note the adjusted rating curves (blue and red) for GRR-SW1 that account for sediment build-up in the culvert after precipitation events.

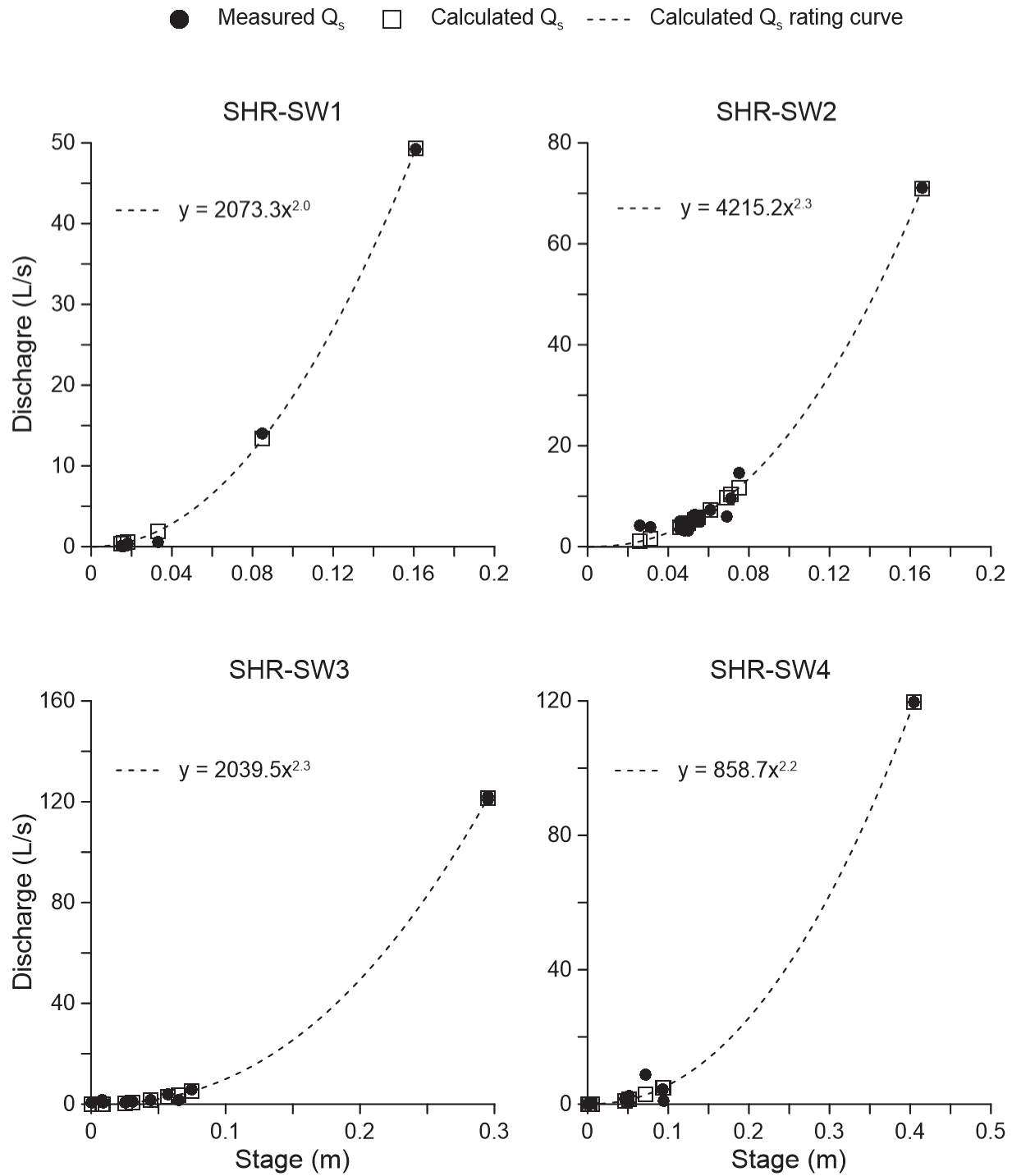


Figure E2. Summary of stage-discharge relationships for SHR-SW1, SHR-SW2, SHR-SW3, and SHR-SW4.

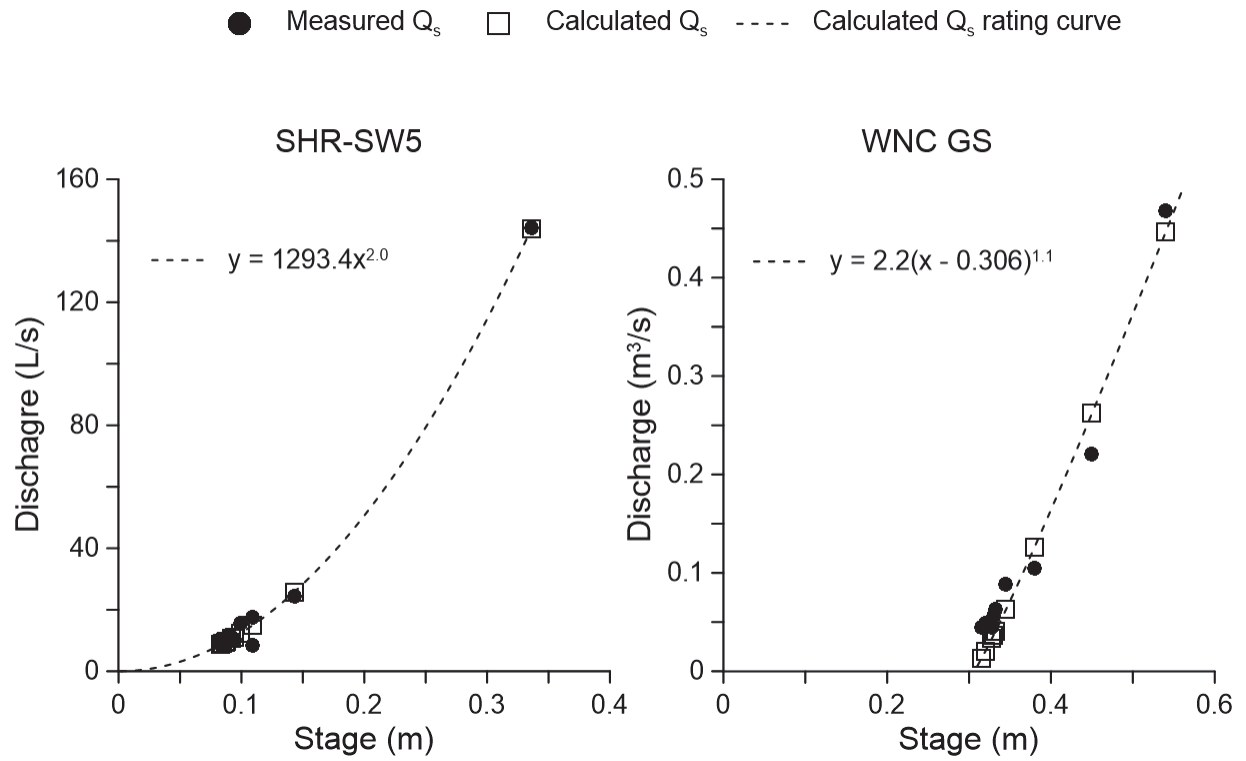


Figure E3. Summary of stage-discharge rating curves for SHR-SW5 and WNC GS. Note the WNC GS unit of discharge are in  $m^3/s$ .

## Appendix F: Stable Water Isotope Sampling

Water sampling sessions in SHR and GRR took place every 4-6 weeks between February 2022 and October 2022, with sampling sessions in June 2021 and November 2021 as well. Water sampling for surface water (SW) and groundwater (GW) took place during baseflow conditions. At least one duplicate sample was taken during 9 of the 10 sampling sessions, which equates to 10 duplicates out of 141 total samples. A full suite of surface water and groundwater samples was 15, however, the number of samples taken during a sampling session varied because of the absence of flow at some stream gauging stations during the season. Three  $\delta^{18}\text{O}$  analyses differed from the original by more than the analytical error of 0.2‰. These three  $\delta^{18}\text{O}$  duplicates were outside the analytical error by 0.01‰, 0.11‰, and 0.02‰. Zero  $\delta^2\text{H}$  analyses differed from the original by more than the analytical error of 1.0‰.  $\delta^{18}\text{O}$  duplicate analyses had an average difference of 0.11‰ and  $\delta^2\text{H}$  duplicate analyses had an average difference 0.3‰ when compared to the originals. A full list of the surface water, groundwater, and precipitation stable isotope samples and results can be found in the supplementary data folder under: **“StableWaterIsotopeData\_QAQC.xlsx”**

## Appendix G: Event Breakdown 2022

Two types of hydrograph separation were applied in this study: graphical hydrograph separation and tracer-based hydrograph separation. Graphical hydrograph separation was applied to all events identified during the 2022 flow season in the SHR, GRR, and WNC catchments (Table G1). A straight line was used to graphically separate quick flow from baseflow. The following steps were taken to delineate the beginning and end of hydrograph events and to define the straight line separating quick flow from baseflow:

- a) The onset of precipitation defined the beginning of an event.
- b) The beginning of quick flow was the lowest value of  $Q_s$  before the rising limb of the hydrograph.
- c) The end of the event was defined when the falling limb of the hydrograph reached 95% recovered.
  - i.  $Q_{peak} - (\Delta Q \times 0.95) = 95\% \text{ recovered}$ .
  - ii. If the falling limb did not reach 95% of the  $\Delta Q$ , then the recovery fraction value was scaled back in 5% intervals until intersection with the hydrograph occurred.
- d) A straight line was then drawn connecting the beginning of quick flow to the end of the event.
- e) Quick flow was then determined by subtracting cumulative baseflow ( $V_b$ ) from the cumulative streamflow ( $V_s$ ) during the runoff response.

Tracer-based hydrograph separation was used on all events in the SHR and GRR catchments during the 2022 flow season that had sufficient EC data (Table E1). Continuous EC data was not available for WNC; therefore, tracer-based hydrograph was not used for events in WNC. The following parameters were used to delineate the beginning and end of an event:

- a) The onset of precipitation defined the beginning of the event.

- b) The end of the event was determined using the straight line graphical hydrograph separation technique described above.
- c) If  $Q_p/Q_s$  was above 1.00 at the end of the event, then a baseline shift of the EC during the event is performed using linear interpolation.

Table G1. Summary of 2022 event parameters for SHR-SW5, GRR-SW4, and WNC. Blank spaces indicate that data was insufficient to determine the event parameter due missing data, data loss, unavailable data. Tracer data was not available for WNC in 2022.  $T$ : Event duration, RF: Recovery fraction,  $P_E$ : Total event precipitation,  $AP_5$ : 5-day antecedent precipitation,  $V_s$ : Cumulative stream discharge,  $Q_{peak}$ : Peak flow discharge,  $RR$ : Runoff ratio,  $MEF$ : Maximum event water fraction,  $V_e/V_s$ : Cumulative event water fraction.

SHR-SW5										
Event #	Start time	$T$	RF	$P_E$	$AP_5$	$V_s$	$Q_{peak}$	$RR$	$MEF$	$V_e/V_s$
		(hrs)		(mm)	(mm)	(mm)	(mm/day)	(%)	(%)	(%)
1	2022-04-15 10:00	10.50	0.95	2.2	0.4	0.04	0.11	0.13		
2	2022-04-19 12:00	1.00	0.95	6.4	2.2	0.00	0.10	0.00		
3	2022-04-20 09:00	21.25	0.75	9.2	8.6	0.08	0.11	0.18		
4	2022-04-22 10:00	11.50	0.90	9.8	15.6	0.04	0.09	0.08		
5	2022-04-26 19:00	1.50	0.95	1.4	9.8	0.01	0.11	0.01		
6	2022-05-08 20:00	24.25	0.95	9.6	0.8	0.10	0.14	0.37		
7	2022-05-10 14:00	5.00	0.95	2.8	10.4	0.02	0.09	0.02		
8	2022-05-17 14:00	6.50	0.95	3.2	0.2	0.03	0.12	0.10		
9	2022-05-19 11:00	17.75	0.95	7.4	4.2	0.06	0.10	0.07		
10	2022-06-04 18:00	37.50	0.85	18.8	0.0	0.14	0.12	0.14	4.4	-0.8
11	2022-06-06 15:00	29.25	0.95	24.0	18.8	0.14	0.17	0.14	9.8	4.0
12	2022-06-11 18:00	4.25	0.60	1.8	21.0	0.01	0.07	0.03	0.7	0.2
13	2022-06-12 19:00	3.25	0.25	0.8	2.0	0.01	0.07	0.01	0.0	-0.1
14	2022-06-13 13:00	56.50	0.95	78.0	2.8	0.72	1.25	0.63	51.1	38.8
15	2022-06-17 20:00	43.75	0.95	11.6	79.0	0.21	0.15	0.13	8.4	1.5
16	2022-06-23 08:00	8.75	0.95	11.8	9.2	0.05	0.22	0.06	17.3	7.0
17	2022-06-24 01:00	16.25	0.95	2.8	11.8	0.08	0.12	0.09	0.0	-0.4
18	2022-06-28 19:00	3.00	0.95	1.6	2.8	0.01	0.11	0.03	0.3	0.1
19	2022-06-29 04:00	16.50	0.95	5.8	4.2	0.08	0.14	0.27	3.4	1.6
20	2022-06-29 22:00	5.00	0.40	1.4	7.4	0.02	0.10	0.05	0.7	0.2
21	2022-07-02 17:00	1.75	0.95	1.8	9.2	0.01	0.13	0.00	1.3	0.7
22	2022-07-03 18:00	53.00	0.95	18.8	11.0	0.26	0.22	0.29	20.5	3.3
23	2022-07-07 16:00	13.00	0.95	12.2	20.6	0.15	0.71	0.63	38.7	25.8
24	2022-07-18 12:00	11.75	0.95	2.4	0.0	0.05	0.10	0.09	1.5	0.8
25	2022-07-22 16:00	3.75	0.95	1.6	2.6	0.01	0.10	0.02	0.3	-0.1
26	2022-07-25 01:00	4.50	0.95	2.0	2.2	0.02	0.10	0.02	0.5	0.2
27	2022-07-29 18:00	7.25	0.95	12.8	2.0	0.03	0.15	0.04	8.4	2.9
28	2022-07-30 19:00	3.50	0.95	14.2	12.8	0.02	0.21	0.04	18.6	8.8
29	2022-08-04 14:00			4.6	14.2				5.9	
30	2022-08-12 20:00	32.50	0.80	1.0	0.0	0.12	0.09	1.02	1.1	-0.3
31	2022-08-16 21:00	5.00	0.75	3.2	1.0	0.02	0.09	0.03	0.6	-0.2
32	2022-08-21 19:00	4.25	0.95	4.2	3.6	0.02	0.10	0.02	0.1	-0.5
33	2022-08-22 22:00	23.75	0.95	12.8	4.8	0.10	0.13	0.06	6.2	1.3
34	2022-08-27 13:00	11.25	0.95	19.2	12.8	0.05	0.16	0.04	13.3	5.8

35	2022-09-08 23:00	14.75	0.95	5.2	0.0	0.07	0.13	0.07	0.7	-0.1
36	2022-09-19 09:00	13.50	0.95	6.2	0.0	0.05	0.11	0.05	1.1	0.5
37	2022-10-05 23:00	5.25	0.95	0.8	0.0	0.02	0.10	0.05	0.0	-0.5
38	2022-10-10 21:00	8.50	0.85	5.2	1.0	0.04	0.12	0.06	0.7	-0.2
39	2022-10-21 21:00	21.75	0.95	14.2	0.2	0.08	0.09	0.01	0.6	0.0
40	2022-10-23 11:00	5.50	0.95	11.0	14.6	0.02	0.09	0.00	0.8	0.4
41	2022-10-24 13:00	3.00	0.95	2.4	25.6	0.01	0.09	0.00	1.2	0.7

GRR-SW4										
Event #	Start time	$T$	RF	$P_E$	$AP_5$	$V_s$	$Q_{peak}$	RR	MEF	$V_e/V_s$
		(hrs)		(mm)	(mm)	(mm)	(mm/day)	(%)	(%)	(%)
1	2022-04-15 10:00			2.4	0.0					
2	2022-04-19 11:00			8.0	2.4					
3	2022-04-20 09:00			3.0	10.4					
4	2022-04-22 11:00			7.6	11.0					
5	2022-04-26 19:00			1.2	7.6					
6	2022-05-08 20:00	30.00	0.95	4.6	1.0	0.10	0.16	0.80		
7	2022-05-10 14:00	6.75	0.95	2.8	5.6	0.02	0.11	0.26		
8	2022-05-17 14:00	5.25	0.95	2.6	0.0	0.02	0.14	0.15		
9	2022-05-19 11:00	19.75	0.75	6.8	3.4	0.07	0.15	0.37		
10	2022-06-04 18:00	38.25	0.90	19.0	0.0	0.11	0.39	0.31	32.2	8.9
11	2022-06-06 13:00	33.25	0.95	17.0	19.0	0.21	0.40	0.79	28.4	13.9
12	2022-06-11 18:00	5.75	0.85	3.6	16.8	0.03	0.29	0.36		
13	2022-06-12 19:00	12.50	0.90	2.0	3.6	0.07	0.37	1.01		
14	2022-06-13 13:00			65.0	5.6					
15	2022-06-17 20:00	39.50	0.95	11.2	68.0	0.60	0.76	0.94		
16	2022-06-23 07:00	11.75	0.95	8.2	10.0	0.19	0.70	0.86		
17	2022-06-24 01:00	17.50	0.95	2.8	9.0	0.19	0.29	0.50		
18	2022-06-28 19:00	3.00	0.95	1.0	2.8	0.04	0.28	0.08	1.3	0.3
19	2022-06-29 08:00	12.75	0.95	7.6	2.2	0.19	0.56	0.73	16.4	9.0
20	2022-06-29 23:00	6.25	0.95	1.6	8.6	0.07	0.29	0.37	2.4	0.6
21	2022-07-02 17:00	3.50	0.95	1.8	10.4	0.04	0.28	0.11	2.1	0.9
22	2022-07-03 23:00	44.00	0.95	13.8	11.2	0.63	0.93	1.22	33.9	3.4
23	2022-07-07 16:00	14.75	0.95	13.0	15.8	0.37	1.60	1.63	46.3	18.5
24	2022-07-18 14:00	8.75	0.95	0.8	0.0	0.08	0.24	1.59	2.4	1.9
25	2022-07-22 16:00	11.75	0.85	2.4	1.0	0.08	0.18	0.21	1.5	0.6
26	2022-07-25 01:00	5.50	0.65	1.8	2.6	0.03	0.16	0.11	0.5	0.3
27	2022-07-29 18:00	10.00	0.85	5.8	1.8	0.07	0.36	0.53	25.7	14.9
28	2022-07-30 19:00	6.75	0.90	6.8	5.8	0.06	0.39	0.38	25.0	13.2
29	2022-08-04 14:00			0.2	7.0				1.8	
30	2022-08-12 20:00	23.75	0.95	0.8	0.0	0.10	0.12	2.78	6.9	3.9
31	2022-08-16 21:00	6.00	0.95	0.8	0.8	0.02	0.09	0.29	3.8	1.8

32	2022-08-21 17:00	8.75	0.85	3.8	1.0	0.03	0.12	0.20	10.6	5.9
33	2022-08-22 22:00	23.75	0.90	11.4	3.8	0.11	0.33	0.36	30.8	12.6
34	2022-08-27 14:00	16.00	0.95	4.2	11.8	0.07	0.15	0.28	11.7	3.8
35	2022-09-08 23:00	8.75	0.85	3.8	0.0	0.03	0.11	0.19	14.5	6.8
36	2022-09-19 09:00	11.00	0.95	5.6	0.0	0.03	0.10	0.10	8.2	4.1
37	2022-10-05 22:00	4.25	0.70	0.6	0.0	0.01	0.03	0.04	0.0	-0.2
38	2022-10-10 21:00	9.50	0.90	5.4	0.6	0.02	0.07	0.10	2.2	-0.1
39	2022-10-21 20:00	38.00	0.95	5.6	0.0	0.16	0.09	1.26	15.7	4.6
40	2022-10-23 12:00	7.25	0.95	7.4	5.6	0.02	0.07	0.02	4.4	2.2
41	2022-10-24 11:00	2.50	0.95	0.6	13.0	0.01	0.08	0.02	1.2	0.5

WNC										
Event #	Start time	$T$	RF	$P_E$	$AP_5$	$V_s$	$Q_{peak}$	$RR$		
		(hrs)		(mm)	(mm)	(mm)	(mm/day)	(%)		
1	2022-04-15 10:00			2.2	0.0					
2	2022-04-19 11:00			3.4	2.2					
3	2022-04-20 09:00			0.3	5.6					
4	2022-04-22 10:00			3.9	3.7					
5	2022-04-26 19:00			1.0	4.0					
6	2022-05-08 20:00			8.0	1.4					
7	2022-05-10 14:00			1.5	9.4					
(8, 9)	2022-05-17 14:00	119.50	0.95	15.2	0.0	0.25	0.08	0.71		
(10, 11)	2022-06-04 23:00	158.00	0.95	38.0	0.0	0.56	0.18	1.01		
12	2022-06-11 18:00	19.00	0.95	3.1	19.7	0.03	0.04	0.18		
13	2022-06-12 16:00	11.50	0.95	4.7	3.3	0.01	0.03	0.03		
(14, 15)	2022-06-13 13:00	188.00	0.85	76.1	8.1	1.73	0.55	1.83		
(16, 17)	2022-06-23 07:00	75.00	0.95	13.3	6.8	0.28	0.11	0.73		
(18, 19, 20)	2022-06-28 18:00	64.50	0.80	13.7	3.2	0.15	0.07	0.41		
21	2022-07-02 17:00	18.00	0.95	1.8	15.7	0.04	0.06	0.20		
22	2022-07-03 16:00	90.00	0.95	10.0	17.5	0.25	0.09	0.62		
23	2022-07-07 16:00	18.00	0.95	17.3	11.8	0.04	0.07	0.05		
24	2022-07-18 14:00	4.50	0.65	0.8	0.0	0.00	0.02	0.11		
(25, 26)	2022-07-22 16:00	115.50	0.90	3.8	0.8	0.15	0.08	2.23		
(27, 28)	2022-07-29 18:00	111.00	0.95	7.7	1.6	0.10	0.03	0.71		
29										
30	2022-08-12 20:00	2.00	0.95	4.1	0.1	0.00	0.01	0.00		
31	2022-08-16 21:00	2.00	0.95	2.9	4.1	0.00	0.01	0.00		
(32, 33)	2022-08-21 17:00	117.00	0.90	16.0	2.9	0.08	0.03	0.31		
34	2022-08-27 14:00	51.50	0.95	4.7	12.3	0.04	0.03	0.31		
35	2022-09-08 22:00			3.4	0.1					
36	2022-09-19 07:00			6.5	0.0					
37	2022-10-05 21:00			0.2	0.1					

38	2022-10-10 21:00	3.7	0.2
39	2022-10-21 20:00	6.5	0.1
40	2022-10-23 12:00	7.2	6.6
41	2022-10-24 09:00	0.8	13.8

---

## Appendix H: Hydrograph separation tracer comparison

Stable water isotope samples were collected using an automated sampler during Events 22 and 33 to compare the 2-component hydrograph separation results of  $\delta^{18}\text{O}$ ,  $\delta^2\text{H}$ , to EC. The  $\delta^{18}\text{O}$ ,  $\delta^2\text{H}$ , and EC concentrations along with corresponding hydrograph separation results are shown in figures H1 and H2. The cumulative pre-event water fractions using  $\delta^{18}\text{O}$ ,  $\delta^2\text{H}$ , and EC are compared in Table H1, and the instantaneous pre-event water fractions using  $\delta^{18}\text{O}$ ,  $\delta^2\text{H}$ , and EC are compared in Table H2. Due to the erratic nature of the  $\delta^{18}\text{O}$  at the end of SHR-E22, the last three data points of the SHR event hydrograph were omitted from the uncertainty analysis.

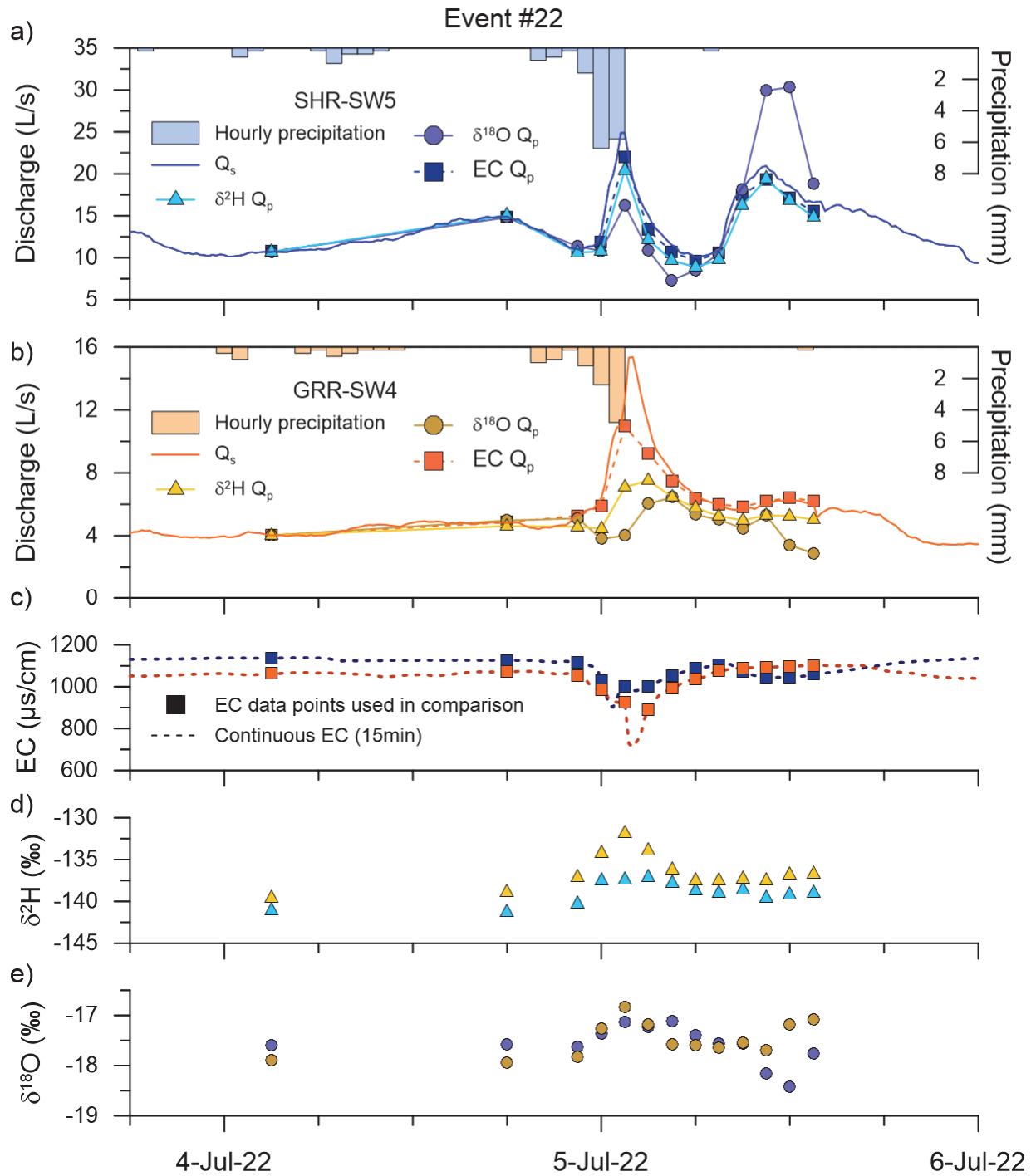


Figure H1. Two-component hydrograph separation comparison for Event 22. a) Total stream discharge of SHR-SW5 and the corresponding pre-event water discharge for each tracer  $\delta^{18}\text{O}$ ,  $\delta^2\text{H}$ , and EC. b) Total stream discharge of GRR-SW4 and the corresponding pre-event water discharge for each tracer  $\delta^{18}\text{O}$ ,  $\delta^2\text{H}$ , and EC. c) EC values used for E22 comparison (squares) and the 15-minute continuous EC (dotted line). d)  $\delta^2\text{H}$  values used for the E22 comparison. e)  $\delta^{18}\text{O}$  values used for the E22 comparison.

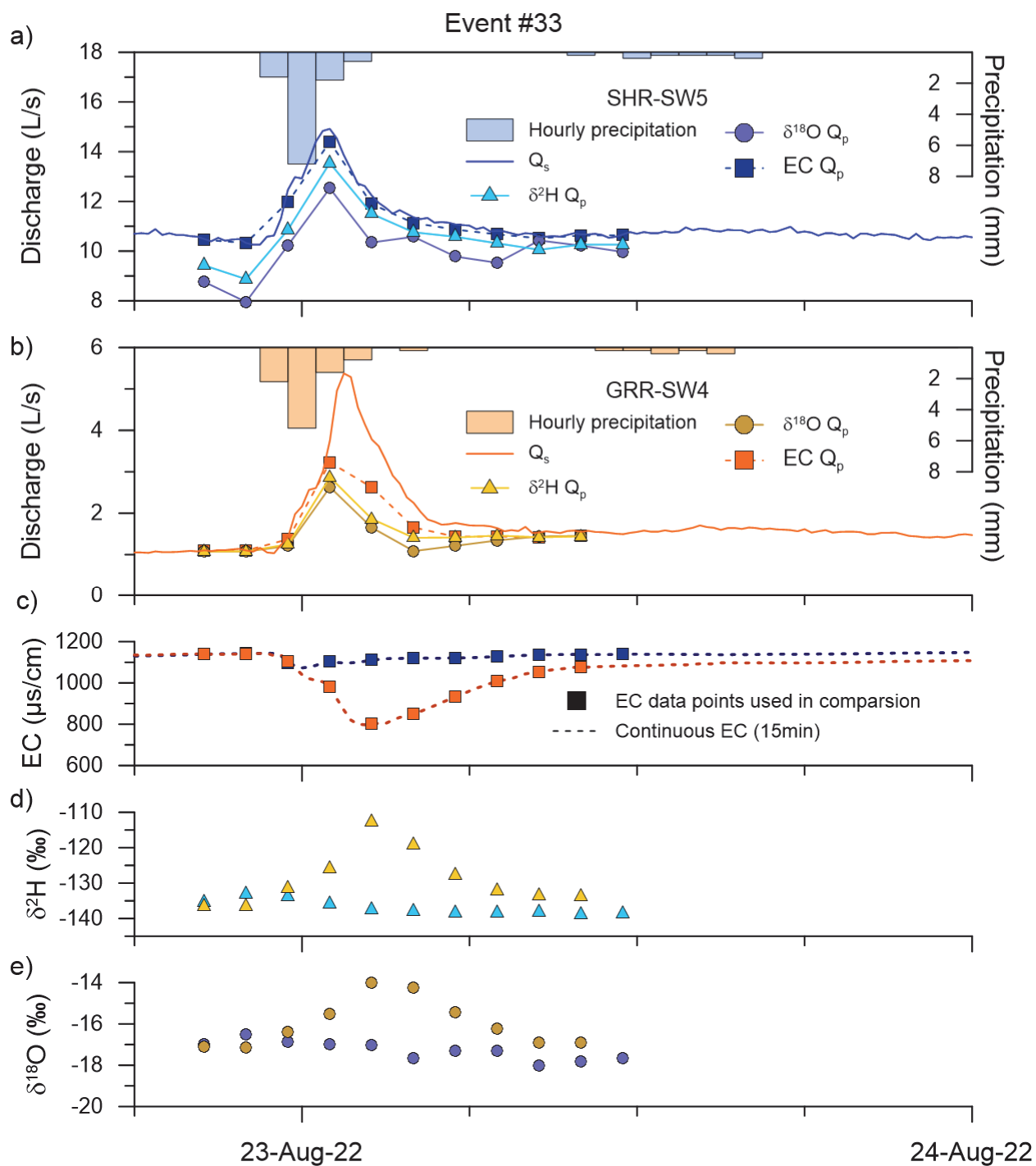


Figure H2. Two-component hydrograph separation comparison for Event 33. a) Total stream discharge of SHR-SW5 and the corresponding pre-event water discharge for each tracer  $\delta^{18}O$ ,  $\delta^2H$ , and EC. b) Total stream discharge of GRR-SW4 and the corresponding pre-event water discharge for each tracer  $\delta^{18}O$ ,  $\delta^2H$ , and EC. c) EC values used for E33 comparison (squares) and the 15-minute continuous EC (dotted line). d)  $\delta^2H$  values used for the E33 comparison. e)  $\delta^{18}O$  values used for the E33 comparison.

Table H1. Summary of cumulative pre-event water fractions for Events 22 and 33.

Event 22	$\delta^{18}\text{O} (V_p/V_s)$	$\delta^2\text{H} (V_p/V_s)$	EC ( $V_p/V_s$ )
SHR-SW5	0.92	0.95	0.97
GRR-SW4	0.81	0.85	0.97
Event 33			
SHR-SW5	0.88	0.93	0.98
GRR-SW4	0.70	0.75	0.84

Table H2. Summary of pre-event fractions for individual samples for events 22 and 33. \*Data points that were omitted from the uncertainty analysis.

Event 22 - SHR-SW5							
Date and time	$Q_s$	$\delta^{18}\text{O}$ ( $Q_p/Q_s$ )	$\delta^2\text{H}$ ( $Q_p/Q_s$ )	EC ( $Q_p/Q_s$ )	$\delta^2\text{H}(Q_p/Q_s) -$ $\delta^{18}\text{O}(Q_p/Q_s)$	EC( $Q_p/Q_s$ ) - $\delta^{18}\text{O}(Q_p/Q_s)$	EC( $Q_p/Q_s$ ) - $\delta^2\text{H}(Q_p/Q_s)$
	(L/s)						
2022-07-04 03:00	10.7	1.00	1.00	1.00	0.00	0.00	0.00
2022-07-04 18:00	14.9	0.99	1.01	0.99	0.02	0.00	-0.02
2022-07-04 22:30	11.0	1.03	0.96	0.99	-0.07	-0.04	0.03
2022-07-05 00:00	13.1	0.83	0.83	0.91	0.00	0.08	0.08
2022-07-05 01:30	24.9	0.65	0.82	0.88	0.17	0.23	0.06
2022-07-05 03:00	15.1	0.72	0.81	0.88	0.09	0.16	0.08
2022-07-05 04:30	11.5	0.64	0.84	0.93	0.20	0.29	0.09
2022-07-05 06:00	10.0	0.85	0.89	0.96	0.04	0.11	0.07
2022-07-05 07:30	10.8	0.97	0.90	0.98	-0.07	0.00	0.07
2022-07-05 09:00	18.5	0.98	0.88	0.95	-0.10	-0.03	0.07
*2022-07-05 10:30	20.9	1.43	0.93	0.92	-0.50	-0.50	0.00
*2022-07-05 12:00	18.6	1.63	0.91	0.92	-0.72	-0.71	0.01
*2022-07-05 13:30	16.6	1.13	0.90	0.94	-0.24	-0.20	0.04
Average difference =					0.03	0.08	0.05
Min EC ( $Q_p/Q_s$ ) difference =					0.17	0.23	0.06
Peak $Q_p$ difference =					0.17	0.23	0.06
Event 22 - GRR-SW4							
2022-07-04 03:00	4.0	1.00	1.00	1.00	0.00	0.00	0.00
2022-07-04 18:00	4.8	1.03	0.96	1.01	-0.07	-0.02	0.05
2022-07-04 22:30	5.3	0.96	0.86	0.99	-0.10	0.03	0.13
2022-07-05 00:00	6.4	0.59	0.70	0.92	0.10	0.33	0.23
2022-07-05 01:30	12.6	0.32	0.56	0.87	0.24	0.55	0.31
2022-07-05 03:00	11.1	0.54	0.68	0.83	0.13	0.29	0.15
2022-07-05 04:30	8.0	0.80	0.81	0.93	0.00	0.13	0.12
2022-07-05 06:00	6.6	0.81	0.88	0.97	0.07	0.16	0.09
2022-07-05 07:30	6.0	0.84	0.88	1.01	0.04	0.16	0.13

2022-07-05 09:00	5.7	0.78	0.87	1.02	0.09	0.24	0.15
2022-07-05 10:30	6.1	0.87	0.88	1.02	0.01	0.15	0.15
2022-07-05 12:00	6.2	0.55	0.84	1.03	0.30	0.48	0.19
2022-07-05 13:30	6.0	0.48	0.84	1.03	0.36	0.55	0.20
Average difference =					0.09	0.23	0.15
Min EC ( $Q_p/Q_s$ ) difference =					0.13	0.29	0.15
Peak $Q_p$ difference =					0.24	0.55	0.31
Event 33 - SHR-SW5							
2022-08-22 20:30	10.5	0.84	0.90	1.00	0.06	0.16	0.10
2022-08-22 22:00	10.3	0.77	0.86	1.00	0.09	0.23	0.14
2022-08-22 23:30	12.5	0.82	0.87	0.96	0.05	0.14	0.09
2022-08-23 01:00	14.9	0.84	0.91	0.96	0.07	0.12	0.06
2022-08-23 02:30	12.2	0.85	0.94	0.97	0.09	0.13	0.03
2022-08-23 04:00	11.4	0.93	0.95	0.98	0.02	0.05	0.03
2022-08-23 05:30	11.1	0.88	0.96	0.98	0.07	0.10	0.03
2022-08-23 07:00	10.8	0.88	0.95	0.99	0.07	0.11	0.03
2022-08-23 08:30	10.6	0.99	0.95	0.99	-0.04	0.01	0.04
2022-08-23 10:00	10.7	0.96	0.96	1.00	0.00	0.04	0.03
2022-08-23 11:30	10.7	0.93	0.96	1.00	0.03	0.06	0.04
Average difference =					0.05	0.10	0.06
Min EC ( $Q_p/Q_s$ ) difference =					0.05	0.14	0.09
Peak $Q_p$ difference =					0.07	0.12	0.06
Event 33 - GRR-SW4							
2022-08-22 20:30	1.1	0.98	0.98	1.00	0.01	0.02	0.02
2022-08-22 22:00	1.1	0.98	0.98	1.00	0.01	0.02	0.02
2022-08-22 23:30	1.4	0.85	0.88	0.97	0.03	0.11	0.09
2022-08-23 01:00	3.8	0.70	0.76	0.86	0.06	0.16	0.09
2022-08-23 02:30	3.8	0.44	0.49	0.69	0.06	0.26	0.20
2022-08-23 04:00	2.2	0.48	0.63	0.74	0.14	0.25	0.11
2022-08-23 05:30	1.8	0.69	0.80	0.81	0.11	0.12	0.01
2022-08-23 07:00	1.6	0.82	0.89	0.88	0.07	0.06	-0.01
2022-08-23 08:30	1.5	0.94	0.92	0.92	-0.01	-0.02	0.00
2022-08-23 10:00	1.6	0.94	0.93	0.94	-0.01	0.01	0.01
Average difference =					0.05	0.10	0.05
Min EC ( $Q_p/Q_s$ ) difference =					0.06	0.26	0.20
Peak $Q_p$ difference =					0.06	0.16	0.09
Average difference for SHR points =					0.04	0.09	0.06
Average difference for GRR points =					0.07	0.18	0.11
Average difference for all points =					0.05	0.14	0.08
Total count =					44	44	44